BIOLOGICAL RESPONSE OF INNOVATIVE BIOMATERIALS FOR BONE TISSUE ENGINEERING APPLICATIONS

BY

ANTHIE GEORGOPOULOU

PhD DISSERTATION

DEPARTMENT OF MATERIALS SCIENCE AND TECHNOLOGY

UNIVERSITY OF CRETE

HERAKLION GREECE

MAY 2018

Supervisor: Prof. Maria Chatzinikolaidou
Co-supervisors: Prof. Maria Vamvakaki, Prof. Charalampos Pontikoglou

BIOLOGICAL RESPONSE OF INNOVATIVE BIOMATERIALS FOR BONE TISSUE ENGINEERING APPLICATIONS

This dissertation is submitted to the

UNIVERSITY OF CRETE

for the degree of

DOCTOR OF PHILOSOPHY

Thesis author	Anthie Georgopoulou
Supervisor	Prof. Maria Chatzinikolaidou
Thesis committee	Prof. Maria Chatzinikolaidou
	Prof. Maria Vamvakaki
	Prof. Charalampos Pontikoglou
	Prof. Anna Mitraki
	Prof. Maria Venihaki
	Prof. Aristides Eliopoulos
	Prof. Athina Bakopoulou

Department of Materials Science and Technology

Heraklion, Greece

Summary

Bone is a multi-scale, hierarchically structured composite tissue with the ability to regenerate when damaged. However, when bone defects are large enough or critical-sized, they cannot regenerate and the intervention in the form of bone grafts is required [1]. Due to the large economic impact of bone grafts and their companion materials, the investigation of suitable alternatives is a major clinical challenge in medicine. Bone tissue engineering strategies guide tissue regeneration via osteoconductive and highly porous scaffolds. Different classes of materials have been utilized for scaffold fabrication including a variety of ceramics and polymers. Polymers, either natural or chemically synthesized, should be biodegradable with great design flexibility molecules. Chitosan is a natural, biocompatible and biodegradable polymer derived from alkaline deacetylation of chitin. It's an important biomaterial as it evokes minimal foreign body response and fibrous encapsulation as well as it promotes the wound healing. Moreover, as a cationic polymer, chitosan possesses antibacterial properties and supports the adhesion and proliferation of osteogenic cells due to its hydrophilicity.

Taking into consideration all the above advantages of this natural polymer, the **main objective during this thesis** was to combine chitosan with other synthetic (section 3.1) or natural (section 3.2) polymers and **examine their biocompatibility and their potential to promote osteogenesis**.

In section 3.1, the results on the biocompatibility and osteogenic assessment of a chitosan-*graft*-polycaprolactone (CS-*g*-PCL) copolymer are presented, and in section 4.1 these results are discussed. These copolymers were synthesized via a multi-step process and were evaluated as a potential biomaterial for the adhesion, proliferation and differentiation of MC3T3-E1 pre-osteoblastic cells. CS-*g*-PCL material surfaces were synthesized and characterized by the research group of Prof. Vamvakaki. PCL is a synthetic, biocompatible, biodegradable and non-toxic polyester with good mechanical properties and high plasticity. Previous studies have included CS/PCL blends in skin and osteochondral tissue engineering, by combining the biocompatibility and biological

properties of chitosan with the suitable mechanical properties of PCL [2]. Moreover, our group has shown that CS-*g*-PCL copolymers promote the viability and proliferation of Wharton's jelly mesenchymal stromal cells and could potentially be used in myocardium regeneration.

Our results indicated a strong adhesion of MC3T3-E1 pre-osteoblastic cells with a characteristic spindle-shaped morphology from the first day of culture onto the copolymer surfaces. The viability and proliferation of the cells on the CS-*g*-PCL surfaces, after 3 and 7 days in culture, were significantly higher compared to the cells cultured on the tissue culture treated polystyrene (TCPS) control. The osteogenic potential of the pre-osteoblastic cells cultured on CS-*g*-PCL surfaces was evaluated by determining various osteogenic differentiation markers. Specifically, alkaline phosphatase activity levels show significantly higher values at both time points compared to TCPS, while secreted collagen into the extracellular matrix was found to be higher on day 7. Calcium biomineralization deposited into the matrix was significantly higher for the CS-*g*-PCL copolymer after 14 days in culture, while intracellular osteopontin expression was increased in cells grown on CS-*g*-PCL surfaces compared to TCPS. The expression levels of alkaline phosphatase *(alp),* collagen type I *(collaI)* and bone sialoprotein *(bsp) genes* were found to be similar for cells cultured either on CS-*g*-PCL or on TCPS.

In section 3.2, the results on the fabrication of 3D porous scaffolds combining chitosan with another natural polymer, gelatin, as well as their biocompatibility and osteogenic potential are presented, and these results are discussed in section 4.2. Gelatin is a biocompatible and biodegradable polymer that promotes cell adhesion, proliferation, migration and differentiation as it retains the Arg-Gly-Asp [RGD] motif, an important sequence found in collagen, well known for mediating cell attachment [3]. The produced chitosan/gelatin scaffolds (CS:Gel) were tested for their capacity to promote osteogenic response. CS:Gel scaffolds have also been used in many tissue engineering applications such as skin [4], cartilage [5] and bone [6] regeneration. CS:Gel scaffolds were fabricated by chemical crosslinking using either glutaraldehyde or genipin as a crosslinker. In both cases the scaffolds were produced by freeze-drying. Our results suggested that CS:Gel

scaffolds crosslinked with either glutaraldehyde or genipin elicit a similar structure morphology with a small difference in the pore size ranging between 40-120 μm and 70-170 μm respectively. Due to the more efficient cell adhesion and infiltration that was observed for the glutaraldehyde crosslinked CS:Gel scaffolds, a more detailed *in vitro* evaluation was set. Among the four different ratios of CS:Gel scaffolds (20%-80% CS:Gel, 80%-20% CS:Gel, 40%-60% CS:Gel and 60%-40% CS:Gel), the viability and proliferation was significantly increased for cells cultured on 40%-60% CS:Gel scaffolds for 5 and 7 days. Moreover, 40%-60% CS:Gel scaffolds crosslinked with two different concentrations of glutaraldehyde (0.1% v/v and 1% v/v) were used to examine the biological response of MC3T3-E1 pre-osteoblastic cells. These scaffolds show significant cell viability and proliferation increase of MC3T3-E1 pre-osteoblastic cells after 7 days in culture compared to 2D CS:Gel substrates. Collagen secreted into the extracellular matrix by the pre-osteoblasts cultured for 4 and 7 days on the CS:Gel scaffolds, indicate a significant increase when compared to TCPS control surface. Moreover in order to test the stability of these scaffolds, degradation assay showed that the degradation rate of 40%-60% CS:Gel scaffolds crosslinked with 0.1% v/v or 1% v/v glutaraldehyde was 48% and 18% of weight loss after 21 days, respectively.

CS:Gel scaffolds crosslinked with 0.1% glutaraldehyde were also tested for their ability in sustaining viability, proliferation and extracellular matrix formation of primary cells. Human bone marrow (hBM) derived mesenchymal stem cells (MSCs), abbreviated as hBM-MSCs, were cultured on these scaffolds and were able to adequately grow, proliferate and secrete collagen in our conditions. The above observations extend also to co-culture setups. Co-culture of hBM-MSCs with human umbilical vein endothelial cells (HUVECs) on CS:Gel scaffolds resulted in increased proliferation rates for both cell types compared to monocultures, which is attributed to the availability of secreted signal molecules that promote their proliferative behaviour.

This PhD thesis focuses on the potential of chitosan-based biomaterials, through their investigation in appropriate cell systems *in vitro*, to be used in bone repair as biocompatible and biodegradable scaffolds. Both CS-g-PCL and CS:Gel material surfaces

support the viability, proliferation and differentiation of MC3T3-E1 pre-osteoblastic cells and hBM-MSCs, demonstrating their potential use in cancellous bone tissue regeneration.

This thesis is structured as follows: Section 1 provides an introduction to this thesis, comprising background, related work, and a short summary of thesis contributions. Section 2 describes the materials and methods used for the investigation of both chitosan-based biomaterials. Section 3 describes the main thesis results, including the data obtained from the in vitro biocompatibility and osteogenic differentiation capacity of both biomaterials. Section 4 discusses the results of this study. Section 5 outlines the thesis conclusions, and Section 6 discusses some perspectives and future work, with focus on preliminary results on nanohydroxyapatite containing chitosan/gelatin scaffolds (appendix, section 7).

Acknowledgements

Firstly, I would like to express my sincere gratitude to my advisor Prof. Maria Chatzinikolaidou for the continuous support of my PhD study on the field of bone biomaterials and osteogenesis research. Her guidance was important during experimental setting and writing of this thesis.

Then I would like to thank Prof. Maria Vamvakaki and Prof. Charalampos Pontikoglou, my co-supervisors, for their support and valuable advice throughout this thesis. I also greatly acknowledge Prof. Anna Mitraki, Prof. Maria Venihaki, Prof. Athina Bakopoulou and Prof. Aristides G. Eliopoulos, who accepted to be members of my thesis committee.

It would be impossible not to thank Dr. Maria Kaliva from the group of Prof. Vamvakaki for providing and characterizing the CS-*g*-PCL co-polymers and for the many hours we spent together discussing results and troubleshooting experiments.

I also greatly acknowledge Prof. Ioannis Vondas and Prof. Kritonas Kalantidis and their groups at Biology Department, University of Crete, for the use of several of their instruments, as well as all members of SEM facility of the Biology Department, and especially Mrs. Alexandra Siakouli for expert assistance with SEM.

Special thanks to all members of Biomaterials Lab for all the scientific and non-scientific discussions and the time we spent together.

Last but not the least, I would like to thank Ioannis, my friends and my parents for supporting me spiritually throughout my PhD thesis and my life in general.

Table of contents

Table of Figures

List of tables

1 Introduction

1.1 Structure of bones

The human skeleton is a metabolically active organ, which is composed of 206 bones in adulthood. The maximum density of bone mass is reached around age 21. The bones of human skeleton can be divided into two major groups, the axial and the appendicular skeleton, which consists of approximately 74 and 126 bones, respectively [7]. According their shape bones are classified into four categories, long, short, flat and irregular. Long bones have a shaft plus two ends which are often expanded, whereas short bones are roughly cube shaped. Moreover, flat bones are usually thin, flattened and curved in contrast to complicated shapes of irregular bones. The bones of the skeleton have multiple functions as they provide structural support to the body, protect vital internal organs, facilitate movement with their cooperation with muscles and tendons and create an ideal environment for marrow. Bone marrow is responsible for the production of all blood cells. In addition, bones are responsible for mineral storage, such as calcium and phosphorus, as well as for fat, growth factors and cytokines storage and play a key role in acid-base balance by absorbing or releasing alkaline salts [8]. Bones also produce a hormone called osteocalcin, which acts in pancreas and fat cells in order to regulate insulin levels in the body [9].

Bones are highly vascularized organs characterized by rigidity and hardness and have the capacity to regenerate and repair. Bones are made up of bone tissue, bone marrow, epithelium, nerves and other small blood vessels. Bone tissue is the specific bone mineral matrix which forms the rigid parts of the organ and the bone cells within it [10]. There are two types of bone tissue, the cortical and the cancellous bone (Figure 1). Both cortical and trabecular bone are composed of osteons, the multiple microscopic columns, in which osteoblasts and osteocytes are deposited in layers around a central haversian canal. Cortical or compact bone has dense, white and solid appearance and

accounts for 80% of the total bone mass of an adult human skeleton. The outer surface of cortical bone called periosteum and the inner surface called endosteum. Periosteum is a fibrous connective tissue, which surrounds with the outer cortical surface of bone and contains blood vessels, osteoblasts, osteoclasts and nerves. This structure plays an important role in bone formation and fracture repair. On the other hand endosteum is the boundary between the cortical and the cancellous bone. Cancellous or trabecular or spongy bone is a honeycomb-like network with porous appearance, which is scattered located in the marrow space of the bone. Trabeculae is an irregular network of spaces which created by thin formations of osteoblasts covered in endosteum [11]. Within this porous structure are bone marrow stem cells which can be differentiated into bones, tendons, cartilage and muscles and hematopoietic stem cells that give rise to white blood cells, red blood cells and platelets [12]. Despite the fact that cancellous bone has ten times the surface area of cortical bone, it accounts only for the remaining 20% of total bone mass. Different ratios of cortical to trabecular bone are observed in different bones and skeletal sites within bones. For example radial diaphysis is composed of cortical to trabecular bone in a ratio of 95:5 in contrast to 25:75 observed in vertebra [7].

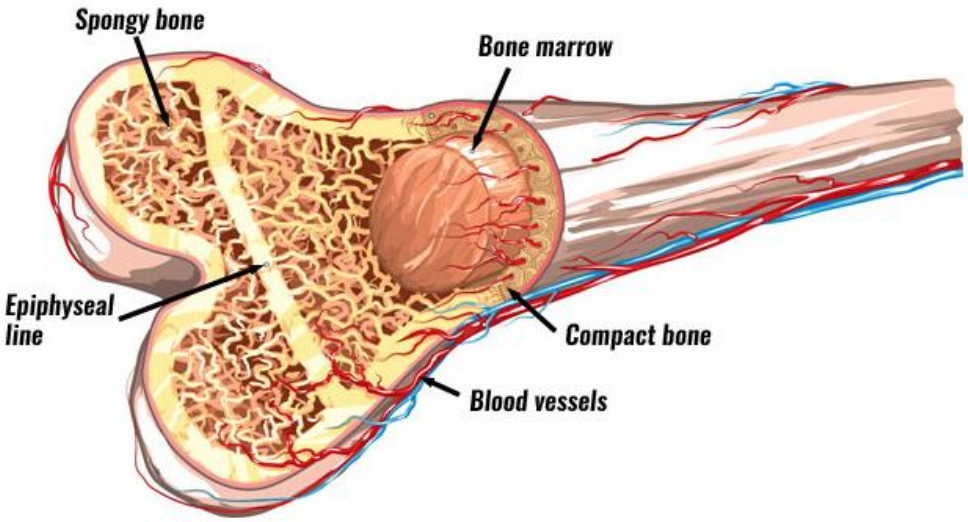

Figure 1.1: Schematic representation of bone structure
Retrieved from: https://www.easynotecards.com/notecard_set/18419

1.2 Chemical composition of bones

The skeletal organ system is a metabolically active organ, which is composed of different types of embedded cells in a mineralized extracellular matrix. The extracellular matrix (ECM) of bone is a composite of an organic phase reinforced by an inorganic phase [8]. The role of bone matrix is important as it provides mechanical support, plays key role in bone homeostasis and supports and regulates the activity of bone cells, through adhesion molecules. The most common category of adhesion molecules is integrins, which are involved in the interaction between bone cells and bone matrix [13]. The structure of bone matrix is constituted by an inorganic or mineral phase (69%), an organic phase (22%) and water (10%).

The mineral phase of bone consists mainly of hydroxyapatite (Ca_{10} $(PO_4)_6(OH)_2$) (99%) and small amounts of carbonate, magnesium and acid phosphate, with missing hydroxyl groups that are normally present [7]. Hydroxyapatite is a crystalline complex of calcium and phosphate, which are derived from nutritional sources and transported through blood circulation. The presence of mineral salts in the osteoid matrix is the reason that all bones are hard and rigid. Bone hydroxyapatite crystals are smaller, more soluble with poorly crystalline in contrast to geologic hydroxyapatite crystals, thereby allowing them to support mineral metabolism. These crystals are deposited along or in close relation to bone collagen fibrils [14]. Alkaline phosphatase and some other non-collagenous proteins such as osteocalcin, osteopontin and bone sialoprotein regulate matrix mineralization by regulating the size and amount of these hydroxyapatite crystals.

On the other hand, the organic phase of bone is composed of 85 to 90% collagen. Collagen I is the predominant protein which constitutes 90-95% of the bone matrix [15]. The precursors of collagen I are synthesized by osteoblasts. Moreover, noncollagenous proteins compose 10 to 15% of total bone proteins [16]. This complex of molecules arise from local or exogenous sources. The main categories of noncollagenous proteins are

proteoglycans, glycosylated proteins, glycosylated proteins with potential cell-attachment activities and γ-carboxylated (gla) proteins. The appropriate role of these proteins is not clear but may involved in regulation of mineral deposition and bone cell activity [17].

1.3 Bone formation and bone remodeling

Bone formation or ossification or osteogenesis is the process by which new bone is produced. This process begins about the third month of fetal life in humans and continues throughout adulthood. Even after bone development continues for repair of fractures and for remodeling to meet changing lifestyles. Ossification is carried out by two important processes, the intramembranous and endochondral ossification. Intramembranous ossification mainly occurs during the formation of flat bones and it is also an essential process during the natural healing of bone fractures. In this process, bone is formed mainly from connective tissue rather than from cartilage. However, endochondral ossification usually occurs during the formation of long bones and it is also an essential process during the natural healing of bone fractures [18].

Bone remodeling is a continuous process which involves the removal of old bone, the replacement with newly synthesized matrix and the mineralization of this proteinaceous matrix to form new bone. This process is necessary for the maintenance of structural integrity of skeleton and mineral homeostasis. The bone remodeling cycle depends on the interaction of two cell lineages, the osteoblastic (derived from the mesenchymal) and the hematopoietic lineage [19]. Osteoblasts and osteoclasts are the main cell types, responsible for the balance between bone resorption and bone deposition. Bone balance is the difference between the old bone resorbed and new bone formed.

1.4 Remodeling Phases

Bone remodeling occurs continually throughout our lives during growth and after microfractures, breaks and mechanical stress and usually takes about 4 to 8 months. About 20% of all bones are replaced annually by the remodeling process. This process

can be divided into the following four phases: activation, resorption, reversal and formation (Figure 2) [20].

- ***Activation phase***: The activation phase begins when different inputs, such as a micro fracture or an alteration of mechanical loading sensed by the osteocytes or some released factors (insulin growth factor (IGFI), tumor necrosis factor-α (TNF-α), parathyroid hormone (PTH) and interleukin-6 (IL-6)) and activate the lining cells [21]. The bone lining cells are elongated mature osteoblasts existing on the endosteal surface. These cells give the stimulus for the recruitment and activation of mononuclear monocyte-macrophage osteoclast precursors from the circulation via the expression of RANKL (Receptor Activator of Nuclear κB Ligand). The interaction between RANKL with its receptor, RANK, expressed by pre-osteoclasts, leads to differentiation, migration and fusion of the large multinucleated osteoclasts [22].
- ***Resorption phase***: This process takes approximately 2-4 weeks during each remodeling cycle. Once osteoclasts differentiated, they adhere to the bone surface and they start to dissolve its organic and inorganic components via the secretion of hydrogen ions, matrix metalloproteinase-9 (MMP-9) and lysosomal enzymes, such as cathepsin K. Macrophages are responsible for the completion of the resorption phase and osteoclasts undergo to apoptosis in order to avoid the excess bone resorption.
- ***Reversal phase***: During this phase bone resorption transitions to bone formation. Reverse cells are macrophage-like cells responsible for the removal of debris produced during matrix degradation.
- ***Formation phase***: Once osteoclasts have resorbed the bone matrix they recruit osteoblasts which initiate bone formation. The release of growth factors, usually stored in the bone matrix, such as bone morphogenetic proteins (BMPs) transforming growth factor-β (TGF-β), platelet-derived growth factor (PDGF) and insulin-like growth factor I and II (IGF-I and II), are responsible for the recruitment of osteoblasts to the resorbed area. When pre-osteoblasts are

differentiated into mature osteoblasts via the expression of growth factors, they start to synthesize the osteoid matrix and promote its mineralization, until they eventually stop and cover the newly formed bone surface.

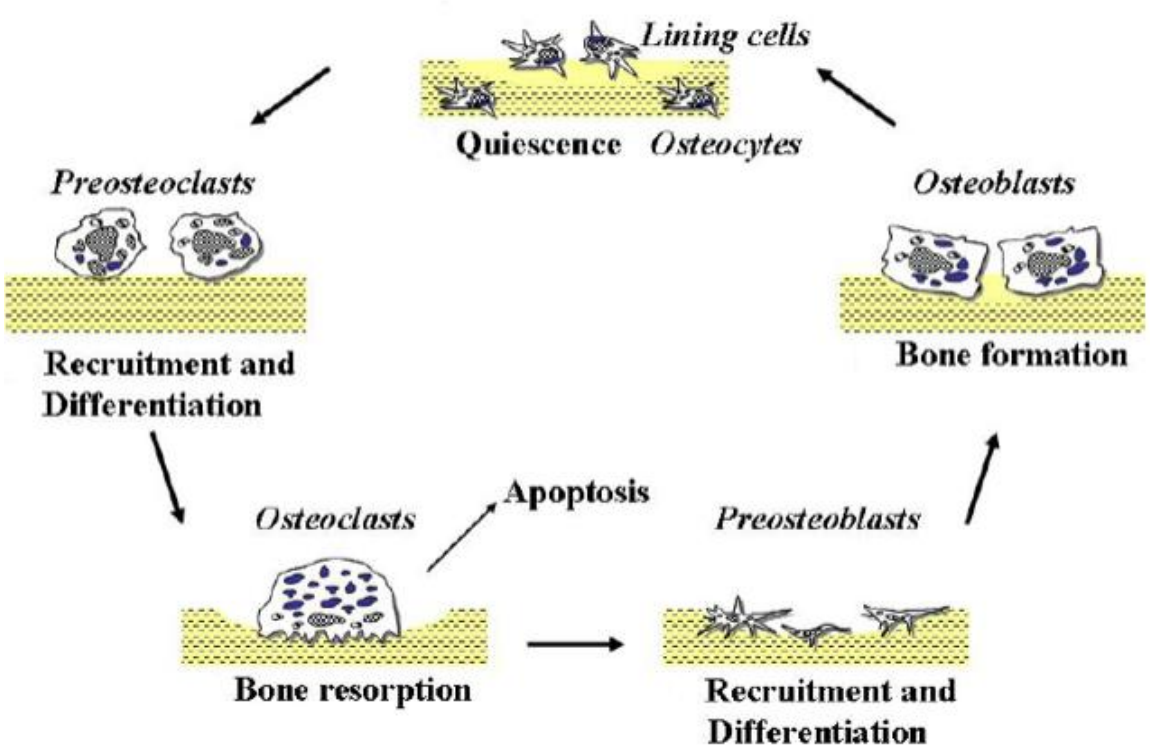

Figure 1.2: Schematic representation of four phases of bone remodeling process
Bone remodeling process starts with activation of the lining cells which trigger osteoclast differentiation. Osteoclasts start to resorb the bone matrix and recruit osteoblasts to the resorbed area through the release of growth factors, usually stored in the bone matrix. Osteoblasts in their turn start to produce the new bone matrix and promote its mineralization. Image retrieved from Marquis *et al.* 2009 [23].

1.5 Bone cells

Cortical and cancellous bone consist of four different types of cells, the osteoblasts, the osteoclasts, the osteocytes and the lining cells.

1.5.1 Osteoblasts: Osteoblasts are one of the three cell types found on the surface in vertebrate bones. They are cuboidal and flat in morphology cells with a single nucleous, derived from mesenchymal stem cells [24]. Osteoblasts function in groups of connected cells and are responsible for bone formation. During bone formation, osteoblasts firstly secrete collagen fibrils and other extracellular matrix components forming the osteoid, which they then mineralize with hydroxyapatite crystals [25]. Osteoblasts are also responsible for the regulation of osteoclasts [26]. Hormones, growth factors, physical activity and other stimuli bring about their effect on bone through osteoblasts [27].

1.5.2 Osteoclasts: Osteoclasts are bone cells responsible for the dissolution and absorption of mineralized bone, dentine and calcified cartilage. Osteoclasts are large multinucleated cells formed through fusion of mononuclear precursors of the hematopoietic lineage [28]. Macrophage colony stimulating factor (M-CSF) stimulates the proliferation of osteoclasts while RANKL pathway is mandatory for osteoclast differentiation [21]. Osteoclasts lie in a small cavity, called Howship's lacunae, and produce a number of enzymes. One of these enzymes is acid phosphatase that dissolves the organic collagen and the inorganic calcium and phosphorus of the bone.

1.5.3 Osteocytes: Osteocytes are differentiated osteoblasts commonly found in the mature bone tissue. These single nucleus cells are star-shaped and derived for osteoprogenitors [29]. Human skeleton has about 42 billion osteocytes, which have an average half time of 25 years [30]. They are not capable of mitotic division and they have reduced synthetic activity. On the other hand, they involved in the turnover of bone matrix through mechanosensory mechanisms.

1.5.4 Lining cells: Lining cells are inactive flattened osteoblasts that cover all surfaces of the bone. They are responsible for the protection of bone from harmful chemicals and the release of calcium in the bone if it is too low in the blood. Moreover, they are responsible for the maintenance of the bone fluids [31].

1.6 Osteoblast differentiation

As previously described, osteoblasts and osteoclasts actively attend the bone remodelling. Bone formation depends on the recruitment of a sufficient number of osteoblasts on the bone surface. Osteoblasts arise from a subgroup of mesenchymal stem cells (MSCs) with an osteogenic differentiation capacity [32]. The first step of osteoblastogenesis is the commitment of MCSs towards an osteo/chodro-progenitor. In these early events, Wingless-int (Wnt) pathway and Bone morphogenic proteins (BMPs) play a key role. More specifically, Wnt10b promotes the commitment towards an osteo/chondro progenitor and inhibits pre-adipocyte commitment, through the induction of Runt-related transcription factor2 (Runx2). Runx2 is a necessary for osteoblast differentiation as well as for endochondral and intramembranous ossification. Previous studies demonstrate that Runx2 knock out mice are lacking of osteoblasts and they do not form mineralized bone. During pre-osteoblastic commitment, Alkaline Phosphatase (ALP) is highly expressed, as it is one of the earliest markers of osteoblast phenotype [33].

On the other hand, Parathyroid hormone-related protein (PTHrp) and Insulin-like growth factor 1 (IGF-1) are necessary during the latter stages of osteoblastic differentiation. Mature osteoblasts are highly enriched in ALP and secrete bone matrix proteins such as collagen I and other non-collagenous proteins including osteopontin, osteocalcin, osteonectin and bone sialoprotein II (BSPII) [21].

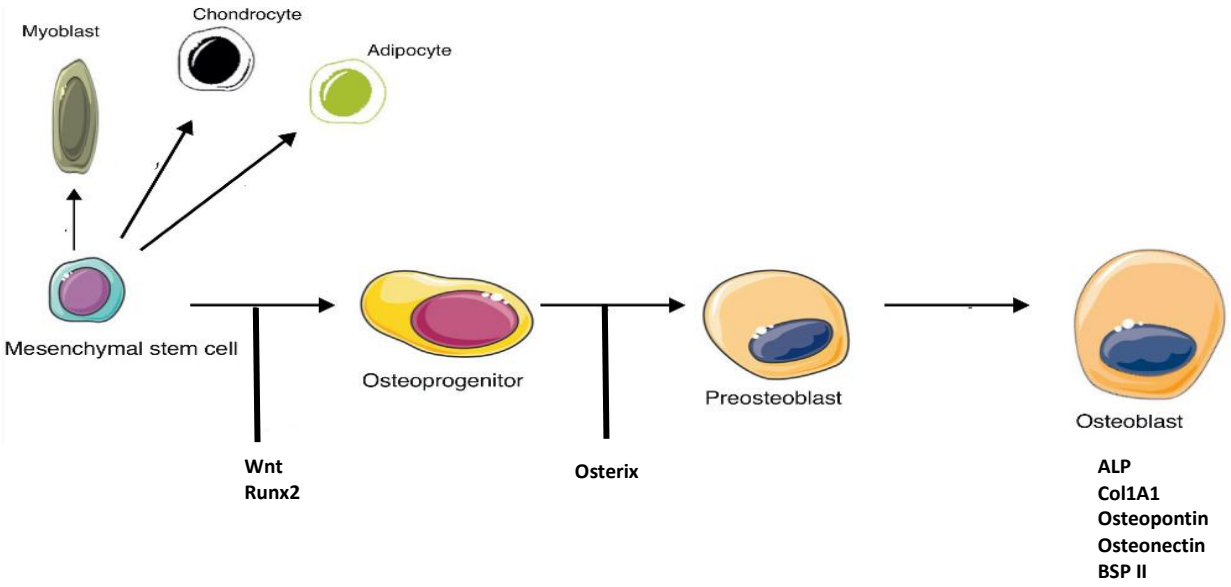

Figure 1.3: Schematic representation of osteoblast differentiation.
Image retrieved from Arboleya et al. 2013 [34].

1.7 Markers of bone formation

Biochemical markers of bone metabolism provide important information about the turnover of osseous tissue and can be classified into bone formation and bone resorption markers [35]. Bone formation markers produced by osteoblasts during osteoblast differentiation and they reflect different aspects of osteoblast function and of bone for bone formation.

1.7.1 Alkaline Phosphatase

Alkaline phosphatase (ALP) is a metalloenzyme that found in many organisms from bacteria to human. More specifically, ALP is a homodimeric enzyme and each catalytic site contains three metal ions, two Zn^{2+} and one Mg^{2+}, necessary for enzymatic activity. This enzyme catalyzes the hydrolysis of monoesters of phosphoric acid at a high pH with

release of inorganic phosphate [36]. ALP exists as several tissue-specific isoenzymes encoded by separate genes. Humans have four Alp genes corresponding to Intestinal alkaline phospahatase (IALP), placental alkaline phosphatase (PLALP), germ cell alkaline phosphatase (GCALP) and liver/bone/kidney alkaline phosphatase (L/B/K ALP) or tissue nonspecific (TNSALP). TNALP is encoded as a single genetic locus, mapped to the short arm of chromosome 1. Deficiency in TNSALP leads to hypophosphatasia (HPP), a rare inborn disease that characterized by defective bone mineralization.

ALPs are membrane bound glycoproteins expressed on the cell membrane of hypertrophic chondrocytes, osteoblasts, and odontoblasts and of the membrane of matrix vesicles. They are linked to the membrane via glycosylphosphatidylinositol (GPI). Little is known regarding the physiological functions of ALPs in most tissues except that the bone isoenzyme has long been thought to play a role in bone mineralization [37]. Mineralization process starts with the formation of hydroxyapatite crystals in matrix vesicles and continue with propagation of hydroxyapatite into the extracellular matrix and its deposition between collagen fibrils. It is thought that ALP may have two different roles in bone mineralization, to increase the local concentration of inorganic phosphate and to decrease the concentration of extracellular pyrophosphate, an inhibitor of mineral formation [38].

1.7.2 Extracellular matrix collagen

Collagen is the most abundant, insoluble, fibrous protein in the body, making up from 25% to 35% of the whole-body protein content. The vertebrate collagen superfamily includes over 50 collagens and collagen-like proteins. Collagen is found mostly in fibrous tissues such as tendons, ligaments and skin, but it is also abundant in corneas, cartilage, bones, blood vessels and the dentin in teeth. It is synthesized intracellularly in fibroblasts, osteoblasts and chondroblasts as a large precursor molecule, called preprocollagen, and it is then secreted in the extracellular matrix. After enzymatic modification, the mature collagen monomers aggregate and become cross linked to form collagen fibrils [39] (Figure 4). Collagen is a family of structurally related proteins

and the different types of collagen are characterized by different polypeptide compositions. Each collagen is composed of three polypeptide chains, two identical chains (α_1) and an additional chain that differs slightly in its chemical composition (α_2). The most common motifs in the amino acid sequence of collagen are [Glycine-Proline-X]n and [Glycine-X-Hydroxyproline]n, where X is any amino acid other than glycine, proline or hydroxyproline [40]. Based on their relative abundance in connective tissues, collagens can be classified into major (types I, II and III) and minor (types V and XI). Types I, II and III accounts 80-90% of the collagen in the body and appear a rope like structure. Among these, collagen type I, is present in tendons, ligaments, the endomysium of myofibrils, the organic part of bone, the dermis and the dentin. Collagen type I, contains two α_1 and one α_2 chains, forming fibrils 300nm in length [41].

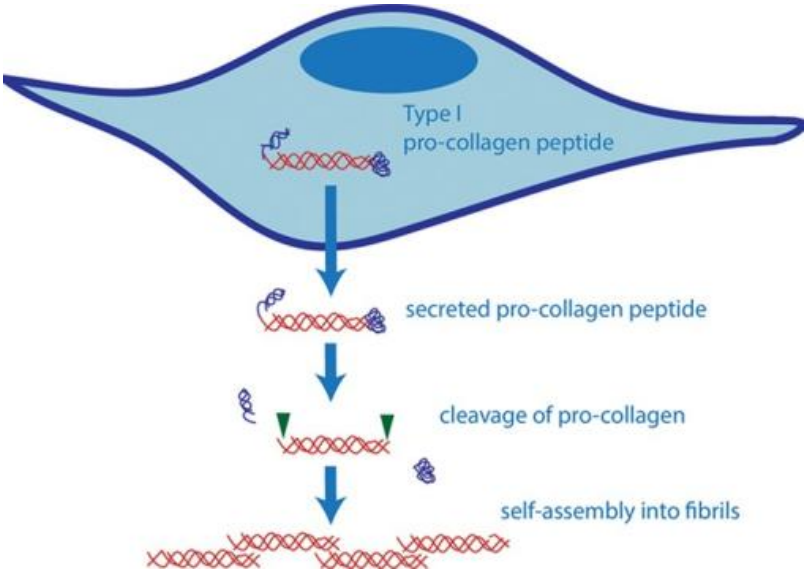

Figure 1.4: Schematic representation of collagen synthesis pathway
Image from Ireton et al. 2013 [42].

1.7.3 Osteopontin (OPN) or Bone sialoprotein I (BSP-1)

Osteopontin is a secreted phosphorylated glycoprotein that expressed in bones, kidneys and epithelial linings as well as is secreted in bodily fluids including milk, blood and

urine. It is encoded by the *SSP1* gene, located on the long arm of chromosome 4, and its synthesis is stimulated by calcitriol (1, 25-dihydroxy-vitamin D_3).

OPN is synthesized as an approximately 32 kDa protein, but due to extensive post-translational modifications its apparent molecular mass ranges from 45 to 75 kDa [43] It is also a member of the Small Integrin-Binding Ligand N-linked Glycoprotein family (SIBLING). OPN appears to be involved in bone mineralization, regulate the immune cell function, inhibit the calcification, control the tumor cell phenotype and control cell activation. OPN expression in bone predominantly occurs by osteoblasts and osteocytes as well as osteoclasts and plays a role in anchoring osteoclasts to the mineral matrix of bones [44].

1.7.4 Bone sialoprotein (BSP)

Bone sialoprotein 2 (BSP) or cell binding sialoprotein or integrin-binding sialoprotein is a highly glycosylated and sulphated phosphoprotein, a necessary component of the bone extracellular matrix that constitute approximately 8% of total non-collagenous of bone. Except of bone tissue, BSP is also expressed in dentin, cementum, and calcified cartilage and encoded by the *IBSP* gene [45]. Specific hormones and cytokines that promote bone formation stimulate the expression of BSP in newly formed osteoblasts [46]. BSP plays a key role during the mineralization process and maybe acts as a nucleus for the formation of the first apatite crystals, which then help to direct and inhibit the crystal growth. This is due to the presence of an RGD (arginine-glycine-aspartic acid) cell attachment sequence and two glutamic acid (glu)-rich regions [47]. Moreover, it has been reported that BSP involved in angiogenic pathways and in protection from complement-mediated cell lysis [48].

1.8 Bone defects and economic impact

It is known that bone fractures usually caused by trauma or bone diseases such as osteoporosis, arthritis and cancer. Bone healing or fracture healing is a physiological

process in which the body facilitates the repair of bone fracture. This process occurs in three distinct phases: the reactive phase, the reparative phase and the remodeling phase. During the reactive phase, the injury site is covered with blood cells forming a blood clot, called hematoma [49].These cells also release cytokines and increase blood capillary permeability. After this, blood cells within the blood clot degenerate and die and fibroblasts form a loose aggregate of cells, called granulation tissue. Days after fracture, fibroblasts within the granulation tissue develop into chondrocytes and form a hyaline cartilage. Moreover, periosteal cells develop into chondrocytes and osteoblasts and produce hyaline cartilage and woven bone respectively. These processes form a heterogeneous tissue called fracture callus [50].The next step of the reparative phase is the replacement of fracture callus with lamellar bone. The lamellar bone begins forming soon after the collagen matrix of either tissue becomes mineralized. After this, the mineralized matrix is penetrated by osteoblasts and vascular channels which lay down stronger trabecular bone. The final phase of bone healing is bone remodeling that is previously described [51].

In most clinical situations bone healing can be easily managed without a scar formation [52]. Nevertheless, in pathological fractures or large and massive bone defects, bone healing and repair fail. Insufficient blood supply, infection of the bone or the surrounding tissues, and systemic diseases can negatively influence bone healing, resulting in delayed unions or non-unions [53, 54]. These problems in bone healing directly affects functional status. Many individuals suffer from pain and height loss and may face problems in everyday life, as well as they are at risk of complications such as pressure sores, pneumonia and urinary tract infections [55]. Moreover, previous studies have shown that over one million factures occur each year in the United Kingdom and 5% to 10% of them have problems in healing [56]. Hence, caring of all these non-union fractures is expensive. Studies show that annual direct care expenditures for osteoporotic fractures range from $12 to $18 billion per year in 2002 dollars. Indirect costs (e.g., lost productivity for patients and caregivers) likely add billions of dollars to this figure. These costs could double or triple in the coming decades. In addition, except

of economic impact, problems in bone healing have negative impact in body image and mood which may lead to psychological problems. Individuals who suffer fractures may be immobilized by a fear of falling and suffering additional fractures. Not surprisingly, they may begin to feel isolated and helpless [57].

1.9 Therapeutic approaches of bone defects

As previously described, bone defects constitute a major health problem in developed countries with major socioeconomic effects. Per conventional definition, if a fracture is not healed after 6 months, it can be considered as nonunion [58]. Long treatments are associated not only with economic effects on the patient and society, but also with permanent disabilities related to manulation, joint stiffness, muscular atrophy and reflex sympathetic dystrophy. Bone substitute materials can be either biological or synthetic. The current therapeutic approaches to restore bone defects include autologous and allogenic transplantations [59-61].

Autografts are considered to be the gold standard in orthopedics. A patient's bone from one site is removed with a surgical procedure and used to fill up the defect. Autografts are histocompatible, non-immunogenic and they promote osteoinduction and osteogenesis as they include osteoprogenitor cells and growth factors, necessary for bone reconstruction. However, autologous transplantations are very expensive procedures and they are associated with bleeding, inflammation, infection and chronic pain as a second surgery is necessary. Furthermore, this approach is limited where the defect site requires larger volumes of bone than is feasible or available [62].

One other conventional treatment is the use of allografts which are removed from one donor and used to fill up the defect of a patient. Depending on the host's requirements, allogenic bones have many forms including, demineralized bone matrix (DBM), cortico-cancellous and cortical grafts, osteochondral and whole-bone segments. Despite allografts are likely histocompatible, their use is limited due to the high risk of disease

transmission [63]. Moreover, in contrast to autografts, they do not have osteoinductive properties as they are removed via irradiation or freeze-drying.

Other commonly used bone repair techniques may involve distraction osteogenesis, bone cement fillers, and bone morphogenic proteins [64]. Because of all these disadvantages, none of the above therapeutic approaches possess all of the ideal characteristics such as, high osteoinductive and angiogenic potentials, biological safety, low patient morbidity, no size restrictions, ready access to surgeons, long shelf life, and reasonable cost.

Tissue engineering (TE) is an alternative strategy for bone grafting that combines cells, materials and suitable biochemical and physicochemical factors to improve or replace tissues. This term was first used in 1988 as 'the application of principles and methods of engineering and life sciences toward the fundamental understanding of structure-function relationships in normal and pathological mammalian tissues and the development of biological substitutes to restore, maintain or improve tissue function' [65].

1.10 Novel therapeutic approach: Tissue Engineering (TE)

In our days, there are three therapeutic approaches associated with tissue damage, transplants, mechanical devices and surgical reconstruction. These medical therapies have saved and improved countless patients' lives, but they present associated problems. Therefore, there is need for more definitive solutions for tissue repair and the goal of TE is the development of in vitro devices that would repair in vivo damaged tissue. TE is an interdisciplinary field addressed to create functional three-dimensional (3D) tissues combining scaffolds, cells and bioactive molecules (Figure 4) [66]. TE leads to engineered tissues, which allow us to study human physiology in vitro, as 3D cultures better mimic the in vivo microenvironment of a tissue in contrast to 2D cultured [67]. However, the appropriate combination of scaffolds, cells and biomolecules is crucial for each desired application. There are two main approaches to produce engineered

tissues. In the first case, cells were seeded on a scaffold and then encouraged to produce the foundations of a tissue for transplantation. During the second approach, scaffolds were combined with growth factors and implanted into the body, where cells are recruited to the scaffold area and form tissue [68].

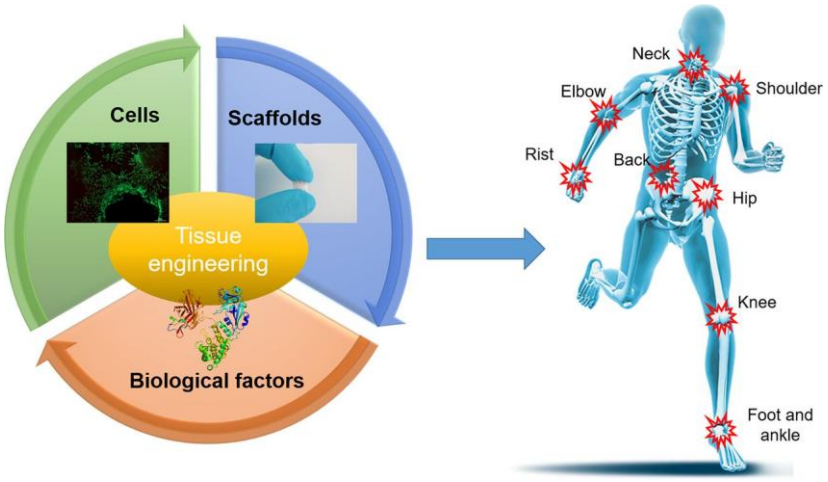

Figure 1.5: Schematic diagram of tissue engineering (TE) principle
TE is an interdisciplinary field that combines 3D scaffolds, cells and bioactive molecules to create *in vitro* devices that would repair the damaged tissue *in vivo*. Image from Brochhausen *et el.* [69].

1.11 Sources of cells for tissue engineering strategies

Cell source selection is a critical issue in tissue engineering applications. The production of an engineered tissue requires the use of capable cells to proliferate and migrate onto the scaffold surface, to secret growth factors and cytokines that activate the endogenous tissue regeneration and produce matrix similar to the native tissue [68]. Many studies demonstrate that the use of primary cells, taken from the patient, cultured on scaffold's surface and implanted again to the body is the best choice for tissue engineering applications. However, some cell types are difficult to be collected and cultured and may be in a diseased state. Therefore, attention has focused on the use of stem cells, including embryonic stem cells (ESCs) and adult stem cells (ASCs) [70].

ESCs are pluripotent cells that are obtained from 'embryos' which are formed following fertilization up until the ninth week of gestation. They are able to differentiate into any lineages but their use is highly restricted due to ethical controversies and their potentiality to produce teratomas. To overcome ethical debates regarding their usage, ESCs are usually obtained from embryos developed by in vitro fertilization techniques. ESCs have been successfully used in bone, vascular and nerve degeneration [71].

On the other hand, ASCs are multipotent cells, so they have more limited capacity to differentiate than ESCs. ASCs overcome some problems associated with ESCs and they are more appropriate for tissue engineering applications [72]. ASCs and tissues derived from them are currently believed less likely to initiate rejection after transplantation. Research on ASCs is progressing rapidly and up today, they have been isolated from different tissues including bone marrow, muscle and adipose tissue [73] and umbilical cord [74, 75], peripheral blood and tooth-derived. In our study, we used bone marrow Mesenchymal Stem Cells (BM-MSCs) which will be analyzed below.

More specifically, cellular-based approaches in BTE were focused on the early stages of bone repair when the recruitment of skeletal progenitors may be impaired. There are two major proposed mechanisms to enhance bone regeneration, the release of osteogenic and vasculogenic growth factors and the formation of a template to recruit host osteogenic and vasculogenic cells. Several studies have used mesenchymal stem cells (MSCs), embryonic stem cells (ESCs), adipose derived stem cells (ADSCs) and stem cells from human exfoliated deciduous teeth (SHED) to explore their capacity to promote bone formation [76]. For successful clinical application in the regeneration of bone, the properties of choice include isolation and expansion efficiency, expression and stability of osteogenic markers, capacity to promote bone formation, and long-term safety (immunorejection, graft-versus-host disease, tumorigenicity). In our study, we used bone marrow Mesenchymal Stem Cells (BM-MSCs) that will be analyzed below.

1.12 Mesenchymal Stem Cells (MSCs)

Mesenchymal Stem Cells (MSCs) are multipotent, non-haematopoietic stromal cells that can differentiate into a variety of cell types, including osteoblasts, chondrocytes, adipocytes and myocytes. They are adherent cells with characteristic fibroblastic-like morphology. Despite bone marrow is the most important source, MSCs have successfully been isolated from skeletal muscle, adipose tissue, umbilical cord, synovium, the circulatory system, dental pulp, amniotic fluid, liver and lung [77]. MSC populations obtained from most tissues commonly express a number of surface receptors including CD29, CD44, CD49a-f, CD51, CD73, CD105, CD106, CD166, and Stro1 and lack expression of definitive hematopoietic lineage markers including CD11b, CD14, and CD45. Many clinical trials demonstrate that MSC therapy is a promising tool in the treatment of bone and cartilage diseases, cardiovascular diseases, neurodegenerative diseases, autoimmune and liver diseases [78], as well as diabetes and graft versus host disease. This happens due to their ability to differentiate into various cell types and secrete specific molecules for the recovery of injured cells and the inhibition of inflammation. Moreover, MSCs lack immunogenicity and have the capacity to home to the site of inflammation when injected intravenously after a tissue injury [79].

1.13 Biomolecules in tissue engineering

Except of cell source selection, signaling molecules are very important in TE applications as they modulate several aspects of cell biology, from proliferation capacity to specific phenotypic features of fully differentiated cells [80]. Growth factors, hormones and cytokines are the main signaling molecules involved in biological phenomena such as chemotaxis, morphogenesis and wound healing. These signals are tightly controlled and unique to each organ [81]. In vivo studies demonstrate that they are secreted locally in the areas undergoing bone remodeling or at the injury sites, cause the migration of inflammatory and precursor cells and/or the activation of osteoblasts and osteoclasts [82]. However, in TE applications these molecules were usually added to the culture medium as soluble factors or attached to the scaffold by covalent and non-covalent interactions. The direct delivery of these molecules in the culture medium is usually

used to evaluate their effect in vitro. This approach has limitations due to rapid degradation and deactivation of these biomolecules by cell-secreted enzymes. For this reason, bounding factors to the matrix helps to protect them from degradation. Consequently, the controlled release of different factors from scaffolds allows their constant renewal, having a great potential to direct tissue regeneration and formation [83]. Moreover, growth factors must be utilized in specific concentrations at the range of nanograms per milliliter because of their adverse effects such as ectopic bone formation, antibody development and carcinogenesis [84].

1.14 Scaffolds in Tissue engineering (TE)

A major challenge in TE applications is the design of 3D scaffolds capable to provide the appropriate environment for the regeneration of tissues and organs. These structures provide the appropriate biophysical, biomechanical and biochemical cues in order to guide the proliferation, migration and differentiation of cells [85]. In vivo, ECM provide them a proper 3D microenvironment and imparts biochemical signaling through two mechanisms: (i) the binding of a wide variety of soluble Growth Factors (GF), enzymes and other effector molecules, controlling their diffusion and local concentrations and (ii) the exposure of specific motifs that are recognized by cellular adhesion receptors. Moreover, ECM is integrated with the intracellular signaling pathways that regulate gene expression and participate in cell phenotype determination [86].

Over the last three decades, numerous scaffolds manufactured with a variety of fabrication techniques, have been used to regenerate different tissues and organs *in vivo*. In TE applications, a number of key considerations are important when designing or determining the suitability of a scaffold for use in tissue engineering:

- ***Biocompatibility***: This criterion is very important is TE applications in order to provide support for cells to adhere, grow, proliferate and migrate on the material surface prior to the implantation into the body. Moreover, the implanted tissue engineered construct must elicit a negligible immune reaction

to prevent a severe inflammatory response that might reduce healing or cause rejection by the body. Hence, the biomaterials used to fabricate the scaffolds must be compatible with the cellular components of the engineered tissues [87].

- ***Bioactivity***: Scaffolds must interact with cells cultured on their surface in order to facilitate and regulate their activities. Scaffolds usually include biological or physical cues such as cell-adhesion molecules and topography respectively to enhance their attachment and influence their morphology and alignment. Moreover, sometimes scaffolds serve as a delivery vehicle for growth factors in order to enhance tissue regeneration. Hence, biomaterials need to be compatible with the biomolecules and amenable to an encapsulation technique for controlled release of the biomolecules with retained bioactivity [88].
- ***Biodegradability***: Scaffolds and constructs are not intended as permanent implants. One of the goals of TE is to allow body's cells to replace the implanted scaffold. Scaffolds must be biodegradable in order to allow cells to produce their own extracellular matrix. Moreover, by-products of this degradation must be non-toxic and able to exit the body without interference with other organs. In order to allow degradation, an inflammatory response combined with controlled infusion of macrophages is required [89].
- ***Scaffold architecture***: The architecture of scaffolds used for tissue engineering is of critical importance. Scaffolds should provide void volume for vascularization, new tissue formation and remodeling so as to facilitate host tissue integration upon implantation. Thus, high porosity with interconnected pore structure is necessary in order to ensure cellular penetration and avoid the diffusion of nutrients to cells within the construct and to the extracellular matrix [90, 91]. Moreover, the mean pore size plays a key role in tissue engineering applications. Generally, the interaction between cells and scaffolds is achieved via chemical groups (ligands) such as Arg-Gly-Asp (RGD) binding sequences. Thus, pores should be large enough to facilitate cell migration into the structure, where they eventually become bound to the ligands within the scaffold, but small enough to

allow efficient binding of a critical number of cells to the scaffold [92]. Therefore, the appropriate pore size depends on the cell type and the tissue being engineered.

- ***Mechanical properties***: Scaffolds provide mechanical and shape stability to the tissue defect. The mechanical properties of the scaffolds used in tissue engineering applications should match that of the host tissue. Moreover, scaffolds should be strong enough to allow surgical handling during implantation. Producing scaffolds with the appropriate mechanical properties for bone and cartilage regeneration is a major challenge in tissue engineering. For these tissues, the implanted scaffold should have sufficient mechanical integrity to function from the time of implantation to the completion of the remodeling process [93]. Moreover, the fact that healing varies with age should be also taken into account when designing scaffolds for orthopedic applications. Many studies suggest that the success of a scaffold depends on the balance between mechanical properties and porous architecture.

1.15 Biomaterials for bone repair

During the past decades, the market for biomaterials-based treatments in orthopedics is growing at a rapid rate. In 1960s, the evolution of biomaterials began with the first generation, generally termed as 'bioinert' materials. There are three types of first generation biomaterials: metals (such as titanium or titanium alloys), synthetic polymers (such as poly(methyl methacrylate), Teflon-type) and ceramics (such as alumina and zirconia) [94, 95]. These materials resulted in the formation of fibrous tissue that may lead to aseptic loosening in the future. This occurs as a non-specific immune response to a material that cannot be phagocytosed, in which an inflammatory response persists until the foreign body becomes encapsulated by fibrotic connective tissue, protecting it from the immune system and isolating it from the surrounding tissues [96].

To avoid this non-specific immune response, the development of the second generation

biomaterials took place in the past decade and focused on the modification of the first generation biomaterials with coatings that are bioactive or biodegradable. These bone substitute materials include synthetic and naturally-derived biodegradable polymers (e.g. collagen, polyesters), calcium phosphates (synthetic or derived from natural materials such as corals, algae, bovine bone), calcium carbonate (natural or synthetic), calcium sulfates, and bioactive glasses (silica or non-silica based) [97, 98].

Third generation bone graft substitutes try to get closer to the autograft standard by using biomaterials capable of inducing specific cellular responses at the molecular level, by integrating the bioactivity and biodegradability of the second generation devices [99]. For this reason, biomaterials that successfully aid bone regeneration should include the following characteristics:

- ***Bioactivity***: The ability of a scaffold to enhance bone formation
- ***Biocompatibility***: The ability of a scaffold to not be toxic and not cause immunological rejection
- ***Osteoconduction***: The ability of a material to promote bone growth
- ***Osteoinduction***: The ability to provide signals in order to induce osteogenic differentiations of local stem cells
- ***Osteointegration***: The direct structural and functional connection between living bone and the surface of a load-bearing implant

In our study, we used natural and synthetic biodegradable polymers, fabricated using different techniques, and examined their ability to promote the adhesion, proliferation and differentiation of cells. More details about the natural and synthetic polymers will be given below.

1.16 Polymers in BTE

As previously described, the basic concept in TE is that the substitute biomaterial acts as

a scaffold for the surrounding cells/tissue to invade, grow, and thus guide tissue regeneration towards new bone formation. A variety of materials have been used for the replacement of damaged bone tissues [100]. The main disadvantages of metals and ceramics are the lack of degradability in a biological environment and their limited process ability. These are the main reasons why polymers are attractive candidates from the past decade in many bone tissue engineering applications. Polymers are large molecules or macromolecules, composed of many repeated subunits that play essential role in everyday life [101]. These molecules have great design flexibility because their composition and structure can be tailored to the specific needs. Moreover, biodegradability is achieved through molecular design. More specifically, some polymers contain chemical bonds that undergo hydrolysis upon exposure to the body's aqueous environment, and some others can degrade by cellular or enzymatic pathways [102]. One other remarkable property of polymers is their ability to support mechanical needs for a wide variety of applications such and screws and fixation devices in orthopedics. Polymers are categorized as naturally derived materials such as collagen and fibrin and synthetic polymers such as polyesters (poly(lactic acid) (PLA), poly(glycolic acid) (PGA) and their copolymers).

Natural polymers are considered as the first biodegradable biomaterials used clinically. Natural polymers interact better with the cells supporting cell adhesion and function. However, these materials probably exhibit immunogenicity, contain pathogenic impurities and we have less control over their mechanical properties, biodegradability and batch-to-batch consistency. Natural polymers can be classified to proteins (silk, collagen, gelatin, fibrinogen, elastin, keratin, actin, and myosin), polysaccharides (cellulose, amylose, dextran, chitin, and glycosaminoglycans) and polynucleotides (DNA, RNA) [103].

In contrast to natural polymers, the main advantages of synthetic polymers is their reproducible largescale production with controlled properties and strength, degradation rate and microstructure. A wide variety of synthetic polymers are available with

variations in the main chain as well as the side chains. Synthetic biodegradable polymers have been widely used as vehicles for cell transplantation and scaffolds for tissue engineering [104]. In our study we used chitosan, gelatin and poly(ε-caprolactone) that will be analyzed below.

1.17 Properties of polymers

- ***Molecular weight (Mn) of polymers:*** Polymers are large covalent-bound chains, with molecular weights between 10,000 and 1,000,000 [105]. In polymers, the molecular weight is commonly represented as an average value since all chains aren't equally sized. The most commonly used is the number average molecular weight (Mn), which is defined as the total weight of the polymer molecules in a sample divided by the total number of polymer molecules.
- ***Cristallinity:*** Depending on their crystallinity, polymers are characterized as amorphous or semi-crystalline materials. Amorphous polymers are composed of randomly configured chains, with no long-range order in contrast to highly anisotropic crystallites of semi-crystalline polymers. The molecular weight as well as the fabrication technique of polymers directly affects the size and distribution of these crystals. A polymer is never fully crystalline as the crystallinization starts at multiple locations in the scaffold. Therefore, the mechanical properties of a polymer are improved with the presence of more crystalline regions [106].
- ***Thermal degradation***: Thermal degradation of polymers is molecular deterioration as a result of overheating. Both amorphous and semi-crystalline polymers have a limited temperature-related application range. Thermal degradation generally involves changes to the molecular weight (and molecular weight distribution) of the polymer and typical property changes include reduced ductility and embrittlement, chalking, color changes, cracking, general

reduction in most other desirable physical properties.

- ***Co-polymers***: The above polymer properties change when different monomers are co-polymerized. Co-polymers retain the best properties of each individual polymer. Depending on the type of co-polymerization used, combining two semicrystalline polymers can result in either a highly amorphous co-polymer or a semi-crystalline polymer. The combination of two different polymers directly affects the molecular weight, the crystallinity, the glass transition temperature (T_g) and the degradation rate of the co-polymer [107].

1.18 Chitosan

Chitosan is a natural polycationic linear polysaccharide derived from partial deacetylation of chitin. Chitin is the second most abundant natural polysaccharide commonly found in the shells of marine crustaceans, cell walls of fungi and arthropod exoskeleton [108]. Chitosan is composed of β-(1-4)-linked d-glucosamine and N-acetyl-d-glucosamine randomly distributed within the polymer (Figure 5). It's cationic nature allows chitosan to form electrostatic complexes with other negatively charged natural or synthetic polymers [109]. The biocompatibility, biodegradability, non-toxicity, low allergenicity, it's anti-microbial [110] and absorption properties and the capacity to stimulate microphages [111] are the main reasons that chitosan has been used in various applications. All these properties of chitosan were affected by the degree of deacetylation and the molecular weight. Moreover, chitosan has superior physical properties such as high surface area, porosity, tensile strength, conductivity and can be easily modified into different shapes and forms such as films, fibers, sponges, beads, powder, gel and solutions [112].

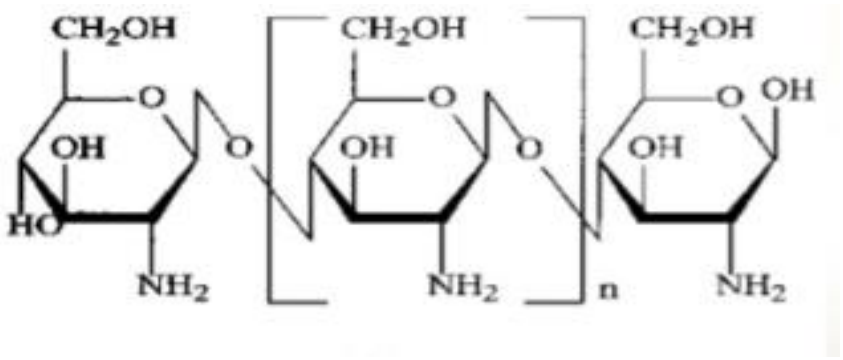

Figure 1.6: Chemical structure of chitosan
Image retrieved from Garcia *et al.* 2014 [113].

1.19 Applications of chitosan

The quality of chitosan depends on the source of chitin and the method of isolation. Therefore, the applications of chitosan depend on the characteristics, such as appearance of polymer, turbidity of polymer solution, degree of deacetylation and molecular weight [114].

1.19.1 Tissue engineering

Due to its properties, chitosan is an excellent polymer to consider as a material for the construction of 3D scaffolds for many tissue engineering applications. Pure chitosan or its combination with other polymers have been used for bone, cartilage, blood vessels, bladder, skin and muscle regeneration. Moreover, previous studies suggest that the combination of chitosan with gelatin improve the biological response compared to pure chitosan [115], demonstrating positive results in skin [4], cartilage [116] and bone regeneration [6].

1.19.2 Drug delivery system

Chitosan and its derivatives have been used in the pharmaceutical industry in drug

delivery systems in different forms, like tablets, microspheres, micelles, vaccines, nucleic acids, hydrogels, nanoparticles and conjugates. Moreover, it can be used in drug delivery systems in both implantable and injectable forms through oral, nasal and ocular routes, as well as in tablet formulation for oral medication [112].

1.19.3 Wound healing

Previous studies have used chitosan as a biomaterial for wound healing due to its biodegradability, biocompatibility, low immunogenicity and antimicrobial activity. Moreover, chitosan has the ability to activate polymorphonuclear leukocytes, macrophages and fibroblasts, which are cells responsible for the granulation and organization of repaired tissues [117]. Its degradation derivate, N-acetyl-β-D-glycosamine, stimulates fibroblast proliferation, aids regular collagen deposition and stimulates hyaluronic acid synthesis at the wound site, accelerating the healing progress as well as preventing scar formation [118].

1.19.4 Obesity treatment

Chitosan has been used as a dietary supplement for lowering serum cholesterol and controlling obesity by giving the feeling of satiety in the stomach. Moreover, chitosan can reduce the absorption of fat in intestines via inhibition of pancreatic lipase activation [119].

1.19.5 Other applications

Chitosan has been widely used in the food industry for wrapping foods and especially meat in order to avoid the growth of microorganisms, molds and yeasts. Moreover, many studies used chitosan and its derivatives in cardiovascular disease treatment, in dry mouth syndrome treatment and in the treatment of age-related diseases [112].

1.20 Gelatin

Gelatin is another natural polymer that has long been used in foods, cosmetics, pharmaceuticals and medical fields. It contains 19 amino acids linked in a partially ordered fashion. Glycine, proline, alanine and hydroxyproline are the predominant amino groups in gelatin molecule. The representation (GlycineX-Proline)n is responsible for the triple helical structure of gelatin, where X represents the amino acids mostly lysine, arginine, methionine and valine. Gelatin is derived either by partial acid or alkaline hydrolysis of animal collagen from skin, bones and tendons, forming gelatin type A and B, respectively (Figure 6). The structure of gelatin appears variable physical properties and chemical heterogeneity due to different collagen sources and preparation techniques [120]. Therefore, gelatin scaffolds fabricated by different techniques have been widely used in many tissue engineering applications including skin, bone and cartilage regeneration due to its properties :

- It's a biodegradable and biocompatible natural polymer with low antigenicity
- It's commercially available at low cost
- Does not produce harmful byproducts upon it's enzymatic degradation
- Retain Arginine-Glycine-Aspartic sequences that enhance cell adhesion
- Contain functional groups for modification (such as crosslinking) and targeting ligands (such as drug delivery vehicles)

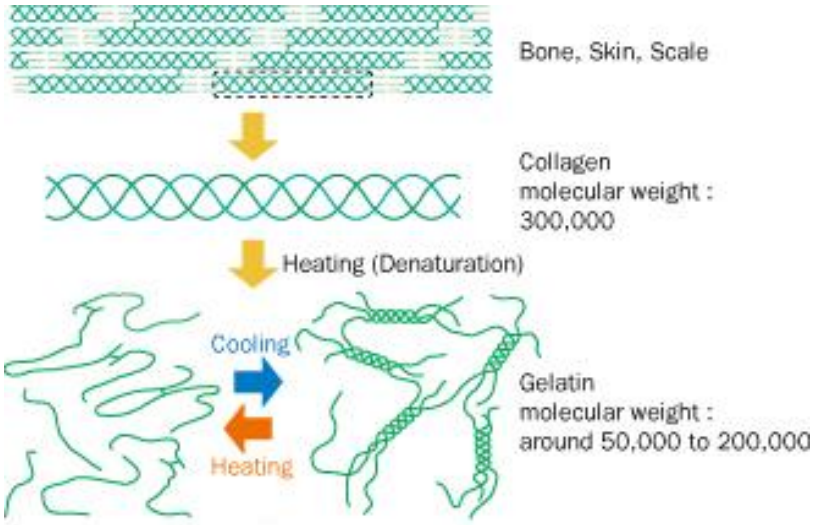

Figure 1.7: Schematic diagram of gelatin production.
Image retrieved from Wang *et al.* 2013 [121].

1.21 Polycaprolactone (PCL)

PCL is a synthetic polymer first synthesized by the Carothers group in 1930. It's a hydrophobic, semicrystalline with long-term degradation polymer. PCL can be synthesized by two main methods, the ring opening polymerization of ε-caprolactone using a catalyst and the polycondensation of a hydroxycarboxylic acid. The rheological and viscoelastic characteristics of PCL makes it easy to manufacture and produce compared to other aliphatic polymers for similar applications. PCL has been used in many tissue engineering applications including bone, cartilage, tendon, cardiovascular, skin and nerve regeneration due to its low production costs and its ability to be modified via copolymerization. Moreover, relevant applications of PCL include: various drug delivery systems, medical devices such as sutures, contraceptive devices, wound dressings, and dental implants [97].

1.22 Fabrication of three-dimensional scaffolds

Several fabrication processes have been utilized to manufacture 3D scaffolds that mimic the natural bone structure. These processes include: salt leaching, gas forming, phase separation, freeze-drying and rapid prototyping techniques.

1.22.1 Salt leaching

This method has been widely used to fabricate porous scaffolds for many tissue engineering applications [122]. In this method, salt crystals, such as sodium chloride are placed into a mold and the polymer is added on top to fill in the remaining spaces. Then the polymer is hardened and the salt is removed via dissolution. The main advantages of this technique is the ability to control the pore size of scaffolds by varying the amount and size of salt crystals as well as the use of small amounts of polymer. However, the interpore and pore shape of these scaffolds are not controllable [123].

1.22.2 Gas forming

In this technique, gas is used as a porogen. First, polymeric discs are formed using compression molding at high temperatures prior to the application of high-pressure carbon dioxide gas through the discs for a few days. Despite this technique is easy and fast, it is difficult to control the pore sizes of the scaffolds. Scaffolds that are fabricated with this technique, have a porosity up to 93% and pore sizes up to 100 μm [124].

1.22.3 Phase separation

In this technique, polymer is dissolved in a specific solvent and then placed in a mold that will be rapidly cooled until the solvent freezes. Finally, the solvent is removed by freeze-drying. The main limitation of this technique is the small pore sizes of the scaffolds [125].

1.22.4 Freeze-drying

The freeze-drying technique or lyophilization has been widely used in the last two decades for the fabrication of 3D porous scaffolds [126]. In this technique, samples are cooled at −70°C to −80°C and then they are located in a chamber in which the pressure is reduced through a partial vacuum, in which ice from the material is removed by direct sublimation. Except of 3D scaffolds, freeze-drying was also used in other applications such as food science, pharmaceuticals and enzyme stabilization [127].

1.22.5 Rapid Prototyping (RP) techniques

Rapid prototyping is a group of techniques in which the object is scanned using a computed tomography (CT) scanner or modeled in a Computer-Aided Design (CAD) software package. The ability to control the geometry and the material composition are the main advantages of RP technologies in contrast to conventional scaffold fabrication techniques. The common RP techniques include stereolithography, laser sintering, 3D printing and fusion deposition modeling. These techniques have been used in many applications including the manufacturing of medical devices, controlled drug delivery systems and engineered tissues [128].

2 Materials and Methods

2.1 Synthesis of CS-*g*-PCL films

In this study, we investigated the *in vitro* biological response of MC3T3-E1 pre-osteoblastic cells on chitosan-*graft*-poly(ε-caprolactone) (CS-*g*-PCL) copolymer surfaces. The copolymeric material was synthesized and characterized in the research group of Prof. Maria Vamvakaki at the University of Crete [129]. Briefly, for the synthesis of the CS-*g*-PCL graft copolymer, low molecular weight chitosan (Sigma-Aldrich, St. Louis, MO, USA) with degree of deacetylation (DD) of ~85%, was used. Poly(ε-caprolactone) bearing

a carboxylic acid end-group (PCL-COOH), with a degree of polymerization of 45, was synthesized by ring opening polymerization using stannous octoate as the catalyst and glycolic acid as the initiator, and was chemically grafted along the chitosan backbone via the primary amino groups. CS-*g*-PCL surfaces on glass substrates were prepared by spin coating using a SPS spin coater (model Spin 150). 140 µl of a 1 %w/v copolymer solution in H_2O/CF_3COOH 50 %v/v was spun at 2000 rpm for 160 seconds. The coatings were dried under high vacuum at 60 °C for 24 h before being neutralized by rinsing with 0.1 M NaOH solution for several minutes, washed with water and dried under a N_2 flow.

For the biological evaluation in a cell culture system, a CS-*g*-PCL co-polymer with 78 wt% CS content was used to coat 15 mm diameter glass coverslips.

2.2 Fabrication of CS:Gel scaffolds

CS:Gel scaffolds were prepared based on a modified protocol [130] by dissolving 2 %w/v chitosan (CS) (Sigma-Aldrich, St. Louis, MO, USA) in 1 %v/v acetic acid (Sigma-Aldrich, St. Louis, MO, USA) and 2 %w/v gelatin (Gel) (Sigma-Aldrich, St. Louis, MO, USA) in ultrapure demineralized water at 50 °C. The two solutions were poured together with the ratio of 2:3 chitosan/gelatin respectively and stirred for 2 h at 50 °C. We then added 0.1 %v/v of the crosslinker, glutaraldehyde (Sigma-Aldrich, St. Louis, MO, USA) or genipin (Sigma-Aldrich, St. Louis, MO, USA) in water to the above mixture and 400 µl/well were casted into the wells of a 24 well plate to produce 40:60% CS:Gel scaffolds crosslinked with glutaraldehyde or genipin. Well plates were kept for 10 min at 50 °C until gel started to form, then transferred to freeze at -20 °C overnight and lyophilized for 24 h at -40 °C. Lyophilized scaffolds were neutralized by using 0.1 N NaOH (Merck Millipore), rinsed thoroughly with ultrapure water until pH was neutral and finally with phosphate buffer saline (PBS) (Sigma-Aldrich, St. Louis, MO, USA) overnight prior to placing in a vented oven for 24 h at 37 °C.

2.3 Degradation and swelling of CS:Gel scaffolds

For the *in vitro* degradation study, CS:Gel scaffolds crosslinked with different concentrations of glutaraldehyde were used. Samples were placed in 10 ml PBS (pH 7.4) and incubated at 37 °C. Every five to six days, samples were taken from the medium, freeze-dried, and the weight loss was examined using the following formula: $D = (W_o - W_1)/ W_o$, where W_o is the weight of dried scaffolds, while W_1 is the weight of scaffolds at different time points after freeze-drying. The values were expressed as the mean +/- standard error (n=5).

The ability of lyophilized CS:Gel scaffolds, crosslinked with glutaraldehyde and genipin, to absorb water was determined by swelling in PBS (pH 7.4). The dry samples were weighted and then placed in PBS for 30 min. The excess of water was removed with paper and their weight was measured directly. The percentage water uptake was examined using the following formula: $W = W_w - W_0/W_0$, where W_0 is the weight of dried scaffolds, while W_w is the weight of wet scaffolds after 30 min in PBS. The values were expressed as the mean +/- standard error (n=5).

2.4 FTIR analysis

The Fourier transform infrared spectroscopy analysis (FTIR) of the 40-60% CS:Gel scaffolds crosslinked with 0.1 % and 1 %v/v glutaraldehyde was recorded using a Nicolet 6700 optical spectrometer within the region 400–4000 cm^{-1}. The spectral data were collected and the numerical values were transferred to Origin software for graphical representation.

2.5 Maintenance of MC3T3-E1 cell line

The pre-osteoblastic cell line MC3T3-E1 was used as a model system for the *in vitro* investigation of cell adhesion, viability, proliferation and differentiation on the CS-*g*-PCL and CS:Gel material surfaces. The undifferentiated pre-osteoblastic cell line MC3T3-E1 was obtained from DSMZ GmbH (Germany; DSMZ no: ACC 210) and derived from a

C57BL/6 mouse calvaria. Cells appear fibroblastic-like morphology (Figure 2.1) and have the capacity to differentiate into osteoblasts and osteocytes as well as to form calcified bone *in vitro*. Moreover, mineral deposits have been identified as hydroxyapatite. It is known that the presence of ascorbic acid (Sigma-Aldrich, St. Louis, MO, USA) and β-glycerol phosphate (Sigma-Aldrich, St. Louis, MO, USA) is necessary for the expression of the osteoblast phenotype. MC3T3-E1 cells secrete also collagen and express high levels of alkaline phosphatase (ALP). Prostaglandin F2a has been reported to stimulate DNA synthesis and proliferation by up-regulation of insulin-like growth factor I receptors.

MC3T3-E1 cells were cultured on tissue culture polystyrene (TCPS) plates (Corning, NY, USA) and placed in an incubator that supplies gases (CO_2) and regulates the physicochemical environment. Cells were cultured in Minimum essential Eagle's medium (α-MEM) (Sigma-Aldrich, St. Louis, MO, USA) supplemented with 10 %v/v fetal bovine serum (FBS) (Sigma-Aldrich, St. Louis, MO, USA), 2% v/v L-glutamine (Sigma-Aldrich, St. Louis, MO, USA) and 1% v/v penicillin-streptomycin (Sigma-Aldrich, St. Louis, MO, USA). 3 x 10^5 cells in 5-6 mL culture medium and 6 x 10^5 cells in 10-11 mL culture medium were seeded in 25 cm^2 and 50 cm^2 TCPS flasks respectively and maintained at 37 ^oC in a humidified atmosphere of 5% CO2 in air. Once a week, when cells reached confluence, they were sub-cultured using trypsin/EDTA (Sigma-Aldrich, St. Louis, MO, USA) and after centrifugation at 1500 rpm for 3 min, they were re-suspended in fresh culture medium.

For long term storage, cultured cells are cryopreserved in highly concentrated, low passage seed stocks. Stocks of 5 x 10^5 – 10^6 cells at early passages between 2 to 16 were prepared in 1 mL freezing medium, containing α-MEM with 20% v/v FBS and 5% v/v dimethyl sulfoxide (DMSO) (Sigma-Aldrich, St. Louis, MO, USA), and placed immediately in liquid nitrogen. Before use, cells were re-suspended immediately in fresh medium (α-MEM with 10 % FBS) and seeded into culture flasks.

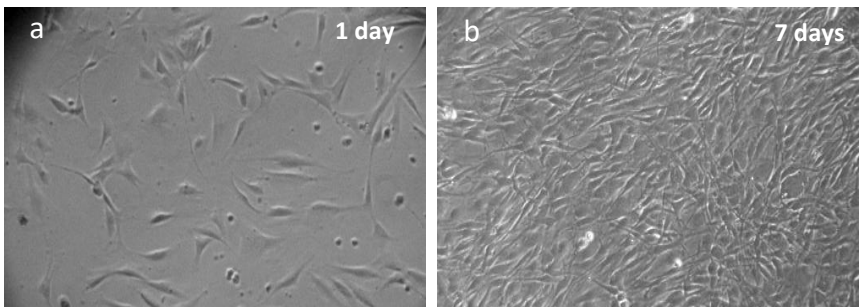

Figure 2.1: Characteristic morphology of MC3T3-E1 pre-osteoblastic cells
Phase contrast microscopy images showing the characteristic fibroblastic morphology of MC3T3-E1 pre-osteoblastic cells (a) 1 day and (b) 7 days after seeding on TCPS surface. Magnification at x10.

2.6 Isolation and maintenance of human bone marrow mesenchymal stem cells (hBM-MSCs)

hBM-MSCs were isolated from the posterior iliac crest of hematologically healthy individuals undergoing hip replacement surgery. The study has been approved by the Ethics Committee of the Heraklion University Hospital (license number: 26-05-2010/3910) and informed consent has been provided by all subjects, according to the Helsinki Protocol. More specifically, BM aspirate was mixed with 3000 units of preservative-free heparin, diluted at 1:1 with phosphate buffered saline (PBS) and layered over Histopaque-1077 (Sigma-Aldrich, St. Louis, MO, USA). Isolated BM mononuclear cells were subsequently seeded and cultured in alpha-modified Eagle's medium (α-MEM) supplemented with 2 mM L-glutamine, 100 U/ml penicillin/streptomycin and 10 % fetal bovine serum (FBS), hereafter referred to as proliferation medium, at 37 °C/5% CO_2 fully humidified atmosphere. Culture medium was replaced twice per week and on 70-90% confluency hBM-MSCs were detached, using 0.25% Trypsin-EDTA and replated at 75 cm^2 Corning flasks. The isolation and culture of the hBM-MSCs as well as the differentiation experiments on the CS:Gel scaffolds were performed at the Hematology Lab under the supervisor of Prof. Pontikoglou and Prof. Papadaki.

2.7 Immunophenotypic characterization of hBM-MSCs

To characterize the hBM-MSCs, cell surface phenotyping was performed on trypsinized cells from P2. More specifically, cells were labeled with phycoerythrin (PE)-conjugated mouse anti-human monoclonal antibodies (mAbs) against CD73 (RMO52; Immunotech/Coulter), CD90 (F15.42; Immunotech/Coulter), CD105 (SN6; Caltag, Burlingame, CA, USA), CD34 (QBend10; Beckman-Coulter) or with fluorescein isothiocyanate (FITC)-conjugated mouse anti-human mAb against CD45 (IMMU19.2; Immunotech/Coulter). Mouse isotype antibodies served as control (Immunotech/Coulter, Caltag, Beckman-Coulter). Acquisition and analysis were performed in a Cytomics FC 500 flow cytometer (Beckman Coulter, Brea, CA, USA) on a minimum of 100000 events.

2.8 Differentiation potential of hBM-MSCs

Trypsinized hBM-MSCs at P2 were induced to differentiate into adipocytes and osteocytes as previously described [131, 132]. More specifically, to promote osteoblastic differentiation in monolayer cultures 1 x 10^4 cells/cm^2 hBM-MSCs were cultured for 21 days in osteogenic medium (α-MEM medium supplemented with 3 mM NaH_2PO_4, 25 mg/l L-ascorbic acid and 0.1 μM dexamethasone). This medium was changed every two days. To assess mineralization, cells were fixed with 4% formaldehyde and stained with 5% Alizarin-red S solution (Sigma-Aldrich, St. Louis, MO, USA) for 5 min. In addition, mineralized matrix was visualized after staining with von Kossa (Sigma-Aldrich, St. Louis, MO, USA) using 5% silver nitrate. Cells were subsequently stained with 5% sodium thiosulfate solution for 5 min.

To promote adipogenic differentiation in monolayer cultures, 1 x 10^4 cells/cm^2 hBM-MSCs were cultured for 15 days in adipogenic medium consisting of low-glucose Dulbecco's modified Eagle's medium supplemented with 10% FBS, 0.5 mM isobutyl methyl xanthine, 6x10^{-6} M indomethacin and 10^{-6} M dexamethasone. The adipogenic medium was changed every two days. To detect lipid droplets, cells were fixed with 4% formaldehyde and stained for 30 min with Oil Red O.

2.9 Culture of human umbilical vein endothelial cells (HUVECs)

Primary human umbilical vein endothelial cells (HUVECs) were purchased from Lonza Walkersville, Inc. (MD, USA). HUVECs are isolated form the vein of the umbilical cord and are commonly used as a laboratory model system for the study of physiological and pharmacological investigations, such as macromolecule transport, blood coagulation, angiogenesis, and fibrinolysis. Moreover, they were first isolated and cultured in vitro and in vivo by Jaffe *et al.* in 1970s, and they usually used due to their low cost and the simple techniques for isolating them. Like human umbilical artery endothelial cells they exhibit a cobblestone phenotype when lining vessel walls.

HUVECs were cultured in Endothelial basal medium (Gibco, ThermoFisher Scientific) supplemented with LSGS Kit (2% v/v fetal bovine serum, 1 μg/ml hydrocortisone, 10 ng/ml human epidermal growth factor, 3 ng/ml basic fibroblast growth factor, 10 μg/ml heparin). 3 x 10^5 cells in 5-6 mL culture medium and 6 x 10^5 cells in 10-11 mL culture medium were seeded in 25 cm^2 and 75 cm^2 Corning flasks, coated with 1% gelatin solution and placed in a humidified atmosphere of 5% CO2 in air. Once a week, when cells reached confluence, they were sub-cultured using 0.25% trypsin/EDTA and after centrifugation at 1500 rpm for 3 min, they were re-suspended in fresh culture medium.

2.10 Culture of cells on different material surfaces

2.10.1 Culture of MC3T3-E1 cells on CS-g-PCL substrates

CS-*g*-PCL films were rinsed twice with PBS, sterilized in 70% ethanol for 30 min and dried for another 30 min under a fume hood. Films were then placed in 24 well plates until cells were seeded on the material surface. TCPS was also used as control substrate. 3 x 10^4 cells/ well and 10^5 cells/well were used for adhesion/proliferation and differentiation assays respectively. Plates were incubated in standard culture conditions (37 ^oC and 5% CO_2) for 1h to allow for initial cell adhesion and then 400 μL of fresh

medium was added into each well. For the differentiation experiments, 24h after seeding of cells on CS-*g*-PCL films, the primary culture medium was replaced with medium supplemented with ascorbic acid, β-glycerol phosphate and dexamethasone (50 μg/ml, 0.1 μM and 10 nM, respectively). Medium was replaced with fresh medium every 2 days. All experiments were carried out using cells between passages 8 to 15.

2.10.2 Culture of MC3T3-E1 and hBM-MSCs on CS:Gel crosslinked scaffolds

Lyophilized scaffolds were rinsed with PBS and culture medium prior cell seeding. Pre-osteoblastic cells (6×10^4 cells/sample for the proliferation assay and 10^5 cells/sample for the extracellular matrix collagen) and hBM-MSCs (3×10^4 cells/sample for the proliferation assay and 10^5 for osteogenic differentiation experiments) were seeded into CS:Gel scaffolds in a 100 μl cell suspension in primary medium and after 1 h additional culture medium was added to each sample. The medium was replaced twice a week. For the differentiation experiments, 24 h for pre-osteoblastic cells and 72 h for hBM-MSCs after seeding of cells on the CS:Gel scaffolds, the primary culture medium was replaced with medium supplemented with 50 μg/ml ascorbic acid, 0.1 μM sodium glycerophosphate and 10 nM dexamethasone for MC3T3-E1 cells and 3 mM NaH_2PO_4, 25 mg/l L-ascorbic acid and 10 nM dexamethasone for hBM-MSCs. For all experiments, unseeded scaffolds were used as controls.

2.10.3 Co-culture of hBM-MSCs and HUVECs on CS:Gel crosslinked scaffolds

It is known that the use of hBM-MSCs have limitations due to their low percentage in adult bone marrow and the vast numbers required for therapeutic approaches [133]. MSCs fate decision can be regulated by exogenous soluble growth factors, cytokines, hormones and chemicals and by external mechanical forces [134]. Another approach to guide MSCs fate is the coculturing with other mature cell populations such as endothelial cells (ECs). Previous studies have shown that these cells express several

factors such as BMP-2 that induce osteogenic differentiation in vitro, when in direct contact with bone marrow mesenchymal stem cells [135]. In our study, hBM-MSCs were cultured with HUVECs on CS:Gel scaffolds in order to examine if cells are capable to growth and proliferate together. Specifically, 6 x 10^4 cells/sample were seeded on the material surface in three different ratios (1:1 BM-MSCs/HUVECS, 1:5 BM-MSCs/HUVECs, 5:1 BM-MSCs/HUVECs) and cultured in EBM-2/a-MEM mixture medium (1:1) for 5 and 10 days. Monocultures of hBM-MSCs and HUVECs were also seeded on CS:Gel surfaces and used as controls. At each time point, the viability and proliferation of the cells was examined using the PrestoBlue® assay, as will be described in paragraph 2.13. Moreover, the morphology of monocultured and co-cultured cells on the material surface was observed using confocal laser fluorescence microscope (CLFM) after 5 days of culture, as will be described in paragraph 2.12. The DAPI dihydrochloride solution (1/100) was used to stain the cell nuclei of HUVECs and hBM-MSCs and an anti-human CD31 antibody (1/1000) was used to stain HUVECs.

2.11 Scanning electron microscopy (SEM)

The morphology of pre-osteoblasts on the CS-*g*-PCL substrates, the porous morphologies of the CS:Gel (crosslinked with glutaraldehyde and genipin) and the adhesion and morphology of pre-osteoblastic cells and hBM-MSCs, cultured on the CS:Gel scaffolds, were monitored using Scanning Electron Microscopy (SEM) (JEOL JSM-6390 LV). Scanning electron microscopy (SEM) scans the surface with a focused beam of electrons and produces images of a sample. These electrons produce in their turn various signals that contain information about the surface topography and composition, by interacting with atoms in the sample. SEM magnification can be controlled over a range of up to 6 orders of magnitude from about 10 to 500,000 times. Resolution can be better than 1 nm with SEM.

3 x 10^4 cells/well MC3T3-E1 were seeded on CS-*g*-PCL substrates whereas 6 x 10^4 cells/well MC3T3-E1 and 10^4 cells/well hBM-MSCs were also seeded on the CS:Gel scaffolds and placed in the CO_2 incubator at 37 °C. At each time point, cells were rinsed

twice with 1 M PBS buffer and fixed with 2% v/v para-formaldehyde and 2% v/v glutaraldehyde for 15 minutes at room temperature. Samples were then dehydrated in increasing concentrations (30% v/v-100% v/v) of ethanol. Because air-drying causes collapse and shrinkage, dehydration was achieved by replacement of water in the cells with ethanol as an organic solvent, followed by replacement of ethanol in turn with liquid carbon dioxide by a critical point drier (Baltec CPD 030). Samples were finally sputter-coated with a 20 nm thick layer of gold (Baltec SCD 050) and were observed under an accelerating voltage of 15 KV (JEOL JSM-6390 LV).

2.12 Confocal laser fluorescence microscope (CLFM)

The CLSM is an optical technique for increasing optical resolution with depth selectivity which allows to do optical sectioning. This means that we can view sections of tiny structures. The CLSM functions by passing a laser beam through a light source aperture, which is then focused by an objective lens into a small area on the surface of the sample and an image is built up pixel-by-pixel by collecting the emitted photons from the fluorophore in the sample.

2.12.1 Adhesion and morphology of MC3T3-E1 cells on CS-g-PCL and CS:Gel material surfaces

Actin distribution and focal adhesion points between cells and material surface, were observed using confocal laser fluorescence microscope (CLFM). In our experiments, a suspension of 2×10^4 and 6×10^4 pre-osteoblastic cells were cultured on CS-*g*-PCL and CS:Gel material surfaces respectively for 2 or 3 days. At each time point, the medium was removed and the samples were washed twice with PBS. Cells were fixed with 4% para-formaldehyde for 15 min and permeabilized with 0.1% Triton X-100 (Sigma-Aldrich (St. Louis, MO, USA)) in PBS. The non-specific binding sites were blocked with 2% BSA solution in PBS for 30 minutes. Samples were stained using fluorescein 1 mg/ml isothiocyanate-conjugated anti-vinculin antibody (1/100) (Sigma-Aldrich (St. Louis, MO, USA)) and 1 mg/ml tetramethyl rhodamine isothiocyanate-conjugated phaloidin (1/40)

(Sigma-Aldrich (St. Louis, MO, USA)) for 50 and 30 min respectively. For cell nuclei staining 0.5 mg/ml of DAPI dihydrochloride solution (1/100) (Invitrogen Life Technologies (Carlsbad, CA, USA) were added on top for another 10 min. Samples were rinsed twice with PBS and observed under a Leica DM IRBE laser scanning confocal microscope using a 40-fold magnification objective lens.

2.12.2 Endogenous expression of osteopontin

The endogenous expression of osteopontin from MC3T3-E1 pre-osteoblastic cells cultured on CS-*g*-PCL films for 7 days, in the presence of osteogenic medium, was also observed using confocal laser fluorescence microscopy (CLFM). At this time point, cells were fixed with 4% paraformaldehyde for 15 min, before permeabilization with 0.1% v/v Triton and blocking with 2% w/v bovine serum albumin (BSA) (Sigma-Aldrich (St. Louis, MO, USA)) for 1h at room temperature. Samples were incubated with anti-osteopontin primary antibody (1/1000) (Abcam, Cambridge, USA) in 2% BSA/PBS for 2h at 4^0C. A FITC-conjugated anti-rabbit IgG H&L (1/1000) (Abcam (ab6717), Cambridge, USA) was used as secondary antibody. For this experiment, cells cultured on cover slips for 7 days were used as control.

2.13 Viability and proliferation assay

2.13.1 Viability and proliferation of MC3T3-E1 cells on CS-g-PCL material surfaces

The viability and proliferation of MC3T3-E1 pre-osteoblastic cells on CS-*g*-PCL films were assessed using the PrestoBlue® assay (Invitrogen Life Technologies (Carlsbad, CA, USA)). It is known that viable cells maintain a reducing environment within their cytosol. PrestoBlue® reagent uses this ability of cells to measure cell viability and proliferation and can be used to establish the relative viability of various reagents across many different cell types. It's a resazurin-based indicator containing a blue, nonfluorescent

cell-permeable compound, which is modified by the reducing environment of viable cells and becomes red and highly fluorescent (Figure 2.2). This change can be detected using fluorescence or absorbance measurements. This assay is fast and highly sensitive and is used for the determination of cell viability and cytotoxicity. Moreover, PrestoBlue® is a live assay and has the advantage of avoiding the destruction of cells at each time point in contrast to 3-[4, 5-dimethylthiazol-2-yl]-2, 5-diphenyl tetrazonium bromide (MTT) assay.

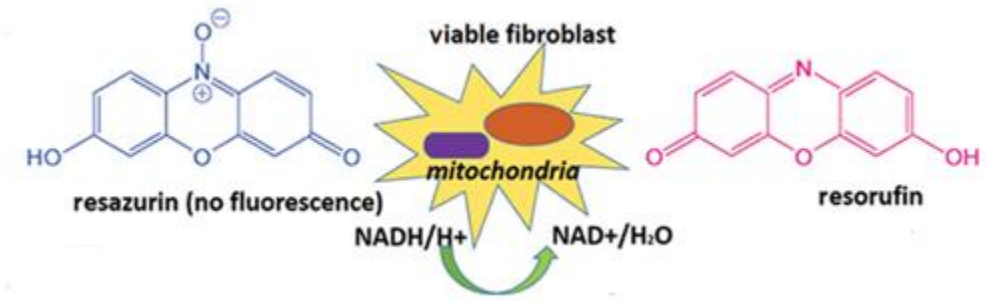

Figure 2.2: The PrestoBlue® reagent
Reduction of resazurin to resorufin in living cells. Resazurin–based dye is blue and weakly fluorescent and becomes pink and highly fluorescent, upon its uptake into viable cells.
Image from http://www.uniscience.com/analises-de-viabilidade-e-citotoxidade/resazurincell-viability-assay-kit-biotium

Before assessing if the CS-*g*-PCL films promotes the viability and proliferation of cells, we performed tests on MC3T3-E1 cells seeded on TCPS in order to identify the required incubation time without longer exposure of live cells to the reagent. For these experiments cells were seeded on 24, 48 and 96 well plates and incubated at 37 ^{o}C. After 24 h, seeded well plates were removed from the incubator and PrestoBlue® reagent diluted in primary culture medium (α-MEM) (1:10) was added. Plates were placed back in the incubator for color development and after 30 min, 1 h and 1 ½ h, the absorbance was measured using a spectrophotometer. Figure 2.3 demonstrates that down to 2.500 cells/well and up to 300.000 cells/well cultured on 24 and 48 well plate

respectively, can be detected after 30 min of incubation. This time of incubation was used to determine the viability and proliferation of MC3T3-E1 cells on CS-*g*-PCL films.

More specifically, 3 x 10^4 cells/well were seeded on the material surface and TCPS for viability and proliferation assay and placed at 37 ^{o}C. At each time point (1, 3 and 7 days of culture), 400 µl PrestoBlue® reagent diluted in primary culture medium (a-MEM) (1:10) was added directly to each well and incubated at 37 °C for 30 min. The supernatants of the samples were transferred to another 24-well plate and the absorbance (570 nm and 600 nm) was measured using a spectrophotometer (Synergy HTX Multi-Mode Microplate Reader). Absorbance units were translated to cell number after using the above calibration curves. For each experiment, three replicates were used (n=3).

a.

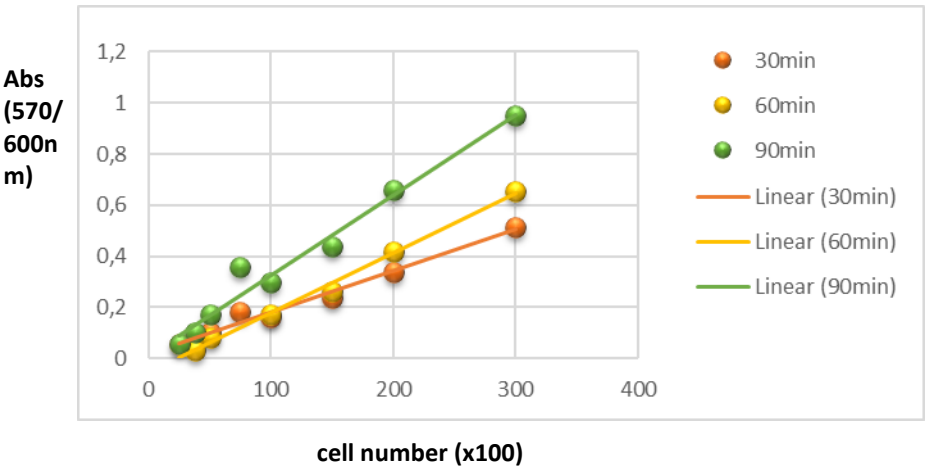

b.

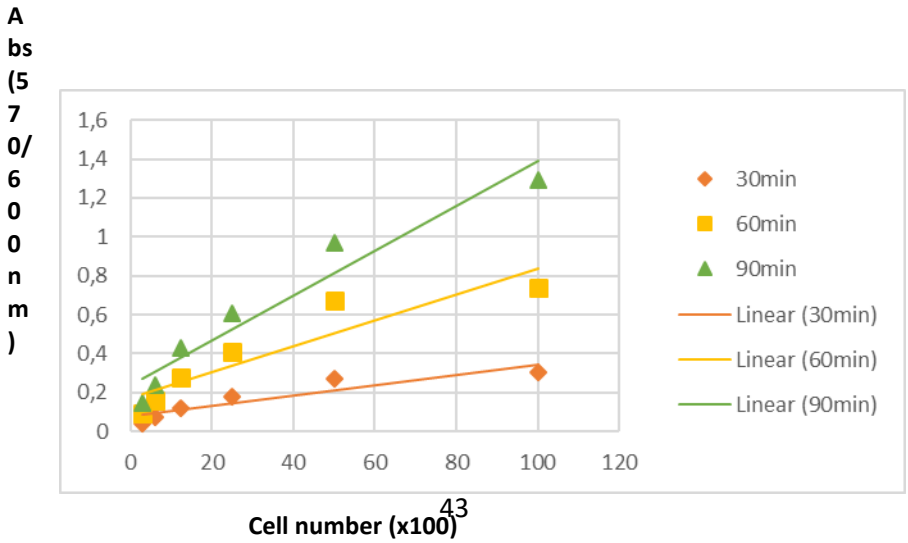

Figure 2.3: Effect of PrestoBlue® incubation time on different dilutions of MC3T3-E1 cells
Different dilutions of MC3T3-E1 cells seeded on (a) 24 well plate and (b) 48 well plate and absorbance (570/600 nm) was measured after 30 min, 1 h and 1 ½ h of incubation. The viability and proliferation experiments of MC3T3-E1 cells cultured on CS-*g*-PCL films were performed after 30 min of incubation and this calibration curve was also used to translate the absorbance units to cell number.

2.13.2 Viability and proliferation of MC3T3-E1 and hBM-MSCs on CS:Gel scaffolds

PrestoBlue® assay was also used to determine the viability and proliferation of MC3T3-E1 pre-osteoblastic cells and hBM-MSCs cultured on CS:Gel porous scaffolds. Briefly, at each time point, at day 2, 4 and 7 in culture of MC3T3-E1 cells, and at day 4, 8 and 12 in culture of hBM-MSCs, 400 µl PrestoBlue® reagent diluted in α-MEM (1:10) was added directly to each well and incubated at 37 °C for 60 min. The supernatants of the samples were transferred to another 24-well plate and the absorbance was measured at 570 nm and 600 nm in a spectrophotometer. The seeded scaffolds were rinsed twice with PBS and placed in fresh culture medium. 2D CS:Gel surfaces and TCPS were used as controls. All samples were analyzed in triplicates of two independent experiments.

2.14 Alkaline phosphatase (ALP) activity assay

As previously described, alkaline phosphatase is a metalloenzyme that catalyze the hydrolysis of phosphate esters. It is highly expressed in osteoblasts and plays a key role in mineralization by increasing the extracellular concentration of inorganic phosphate. ALP levels, expressed from pre-osteoblastic cells cultured on CS-*g*-PCL material surface, were measured using a colorimetric assay. This method utilizes *p*-nitrophenyl phosphate (pNPP) as a substrate, which is hydrolyzed by ALP into a yellow colored product at 37 ^{o}C. More specifically, phosphatases catalyze the hydrolysis of pNPP liberating inorganic

phosphate and para-nitrophenol (pNP). pNP can be detected photometrically at 405 nm (Figure 2.4).

In our experiments, 10^5 pre-osteoblastic cells were cultured on CS-*g*-PCL material and TCPS control surfaces for 7 and 14 days, and at each time point, they were harvested by trypsin-EDTA and collected by centrifugation. Pellets were dissolved in 100 µl lysis buffer (0.1% Triton X-100 in 50 mM Tris-HCl pH=10.5) and subjected to two freeze cycles at -80 °C room temperature. Then, 100 µl of 2 mg/ml *p*-nitrophenyl phosphate substrate solution (Sigma-Aldrich (St. Louis, MO, USA)) was added to each sample and incubated at 37 °C for 60 min. Absorbance was measured using a Synergy HTX plate reader at 405 nm and correlated to equivalent amounts of p-nitrophenol by using a calibration curve. Alkaline phosphatase activity was normalized to cellular protein levels, measured by Bradford assay (Invitrogen Life Technologies (Carlsbad, CA, USA)).

Bradford is a colorimetric assay to determine the protein concentration of a sample. It is based on an absorbance shift of the dye Coomassie Brilliant Blue G-250, which is converted to a blue product when the dye binds to proteins. According to manufacturer's instructions, 200 µL of was added to 100 µL of cell lysate and the absorbance was measured using a Synergy HTX plate reader at 595 nm. Absorbance units were correlated to protein concentration according to a standard curve.

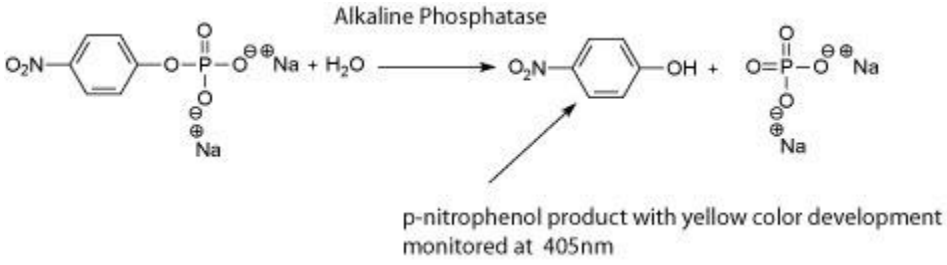

Figure 2.4: Catalysis of *p*-nitrophenyl phosphate (pNPP)
Phosphatases catalyze the hydrolysis of pNNP liberating inorganic phosphate and para-nitrophenol (pNP). pNP is a yellow product that can be detected photometrically at 405 nm. Image from www.public.asu.edu/laserweb/woodbury/classes/chm467/Enzkin/alkphosphat.html

2.15 Collagen production in the ECM

As previously described, collagen is a fibrous secreted protein expressed in cornea, cartilage, bones, blood vessels, glut, intervertebral discs and the dentin in teeth. Collagen type I is highly expressed by osteoblasts and involved in the formation of extracellular matrix in which mineralization can occur. In our experiments, collagen accumulation in the extracellular matrix of pre-osteoblastic cells and hBM-MSCs cultured on CS-*g*-PCL, CS:Gel and TCPS material surfaces was measured using a modified colorimetric assay, as described in previous studies of our group [136, 137]. Sirius red staining, developed by Junqueira et. al in 1979, is one of the most important stains to study collagen networks in different tissues [138]. Sirius red is a large, anionic dye which binds to the [Gly-X-Y]n helical structure of mammalian collagen. It has been reported that Sirius red stains collagen by reacting, via its sulphonic acid groups, with basic groups in the collagen molecule. This dye binds strongly to collagen types I and III and lower to collagen type IV. After Sirius red staining, collagen fibers appeared red in contrast to yellow nuclei, cytoplasms, muscular fibers and red blood cells.

In our experiments, 10^5 MC3T3-E1 pre-osteoblastic cells and 10^5 hBM-MSC cells were seeded on CS-*g*-PCL, CS:Gel materials and TCPS control surfaces. The secretion of collagen was measured in culture medium after 4, 7 and 14 days of culture. At each time point, 100 µl of culture medium was mixed with 1 ml 0.1% Sirius Red Dye (Sigma-Aldrich (St. Louis, MO, USA)) and incubated for 30 min at room temperature. After centrifugation of samples at 15,000g for 15 min, pellets were washed with 0.1 N HCl in order to remove the non-bound dye. Samples were finally centrifuged at 15,000g for 15 min and dissolved in 500 µl 0.5 N NaOH. Absorbance was measured using a Synergy HTX plate reader at 530 nm. The absorbance measurements were normalized with a calibration curve of known concentrations of collagen type I.

2.16 Alizarin red staining

Calcium-rich deposits representing the final stage of mineralization were stained by alizarin red S and quantified by dye extraction. The increased calcium deposits is a late marker of osteogenesis and it is a crucial step towards the formation of calcified extracellular matrix in bone formation. This biological stain was first noted in 1567, when it was observed that when fed to animals, their teeth and bones were stained red. For this purpose, it is commonly used in medical studies involving bone growth, osteoporosis, bone marrow, calcium deposits in the vascular system, cellular signaling, gene expression, tissue engineering and mesenchymal stem cells. Moreover, alizarin red is used to measure calcium carbonate minerals, calcite and aragonite in geology. Free calcium forms precipitate with alizarin, and tissues containing calcium stain red when immersed in alizarin. The alizarin staining works better when performed in basic solution.

In our experiments, calcium deposits in the extracellular matrix of pre-osteoblastic cells cultured on CS-*g*-PCL films and TCPS control were measured using the above colorimetric assay. At each time point (7 and 14 days), cells were fixed with 4% paraformaldehyde for 15 min, rinsed twice with PBS and stained with 300 µL of 2% alizarin red S (pH 4.1) (Sigma-Aldrich (St. Louis, MO, USA)) for 30 min. Then, cells were rinsed three times with H_2O in order to remove the excess stain. Cetylpyridinium chloride (CPC) (Sigma-Aldrich (St. Louis, MO, USA)) was used to quantify the accumulation of calcium deposits by dye extraction. 300 µL of 10% CPC in 10 mM sodium phosphate buffer solution (pH 7.0) were added to each sample and incubated for 1 h under shaking. Absorbance was measured using a Synergy HTX plate reader at 550 nm. Absorbance measurements were normalized to cell number, measured by PrestoBlue® assay, prior to staining.

2.17 In-Cell Enzyme-linked Immunosorbent Assay (ELISA)

Osteopontin is a phosphorylated glycoprotein that appears to be involved in bone mineralization. In our study, the levels of endogenous osteopontin expressed from cells

cultured on CS-*g*-PCL films and TCPS were measured using the in-cell enzyme-linked immunosorbent assay (ELISA). The principle of in-cell ELISA is shown in Figure 2.5. Firstly, 5 x 10^4 cells/well were cultured on the two material surfaces for 10 days. At this time point, cells were fixed with 4% v/v paraformaldehyde for 15 min, before permeabilization with 0.1% v/v and blocking with 2% w/v BSA for 1 h at room temperature. Samples were incubated with anti-mouse primary antibody (1/1000) in 2% BSA/PBS for 2 h at 4 ^{0}C (300 µL) and after washing away the unbound antibody, an anti-rabbit IgG H&L antibody was added on top at 1/1000 dilution for 2 h (300 µL). Then, the enzyme substrate (TMB) (100 µL) (Invitrogen Life Technologies (Carlsbad, CA, USA)) is added and the subsequent reaction produces a color change signal, in proportion to the amount of osteopontin levels. Finally, 100 µL of sulfuric acid stop solution were added and changed the color from blue to yellow. The absorbance was measured using a Synergy HTX plate reader at 450 nm.

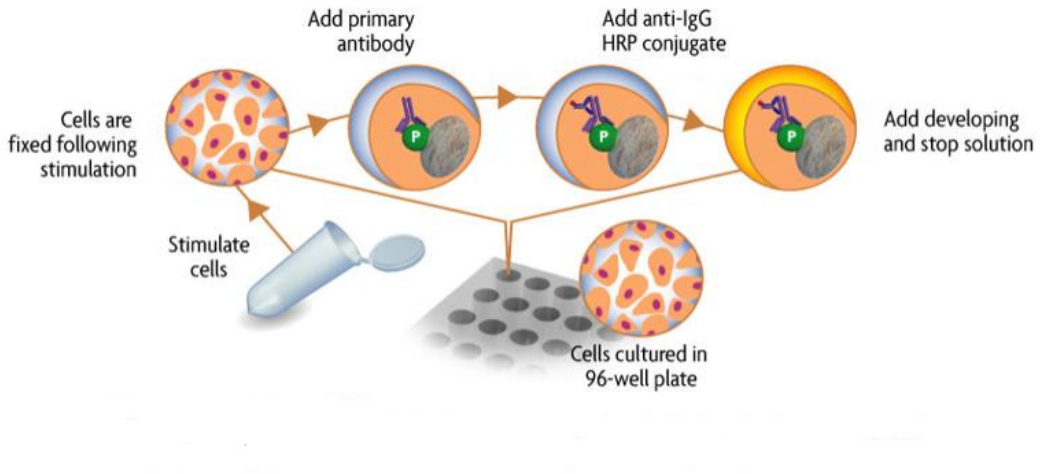

Figure 2.5: Schematic picture showing the main steps of in-cell ELISA
Image from https://www.activemotif.com/catalog/417/suspension-cell-face

2.18 Extraction of total RNA

In order to assess gene expression, total RNA from MC3T3-E1 pre-osteoblastic cells was extracted using TRIzol™ Reagent (Invitrogen Life Technologies (Carlsbad, CA, USA))

according to the manufacturer's protocol. First, 10^5 cells/well were cultured on CS-*g*-PCL and TCPS substrates for 7 and 14 days with the presence of ascorbic acid, β-glycerol phosphate and dexamethasone (50 μg/ml, 0.1 μM and 10 nM, respectively) in culture medium. At each time point, cells were detached from the substrate using trypsin/EDTA and centrifuged at 1500 rpm for 3 min. Then, cell pellets were dissolved in 0.5 mL TRIzol™ Reagent and incubated for 15 min on ice to permit complete dissociation of the nucleoproteins complex. 0.2 mL of chloroform per 1 mL of TRIzol™ Reagent were added to each tube and centrifuged for 15 min at 12,000g at 4 °C. The mixture separates into a lower red phenol-chloroform, an interphase, and a colorless upper aqueous phase. The aqueous phase containing the RNA was transferred to new tubes and 0.5 mL of isopropanol per 1 mL of TRIzol™ Reagent were added. Samples were then incubated on ice and centrifuged for another 15 min at 12,000g at 4 °C. Total RNA precipitate forms a white gel-like pellet at the bottom of the tube. Supernatants were discarded with a micropipettor and pellets were resuspended in 1 mL of 75% ethanol per 1 mL of TRIzol™ Reagent. After centrifugation for 5 minutes at 7500g at 4 °C, pellets were dried for 5-10 min and diluted in 20 μL of RNase-free water. Total RNA quantity and purity were determined by UV spectrometry at 260 and 280 nm using a NanoDrop2000 spectrophotometer (ThermoScientific, USA).

2.19 Semi-quantitative RT-PCR

Polymerase chain reaction (PCR) is a biochemical method for amplifying specific DNA sequences from relatively small amounts of starting material by *in vitro* DNA synthesis. For cDNA synthesis 300 ng of total RNA were reverse transcribed with Superscript II transcriptase (Invitrogen Life Technologies (Carlsbad, CA, USA)) by using random primers (Invitrogen Life Technologies (Carlsbad, CA, USA)) according to the manufacturer's instructions. For PCR, 45 ng of cDNA synthesis reaction were used. The primers used are shown in Table 1. The product size was 149, 164, 158 and 66bp for *Gapdh*, *Alp*, *Colla1* and *Bsp* respectively. The amount of template cDNA and the number of PCR cycles were optimized so that the PCR products could be analyzed within the

exponential phase of the amplification reaction. GAPDH was used as housekeeping gene in order to ensure that the observed differences in the expression levels of each gene in different treatments were not a result of differences in the amount of template cDNA. ImageJ (https://imagej.nih.gov/ij/) was used for band intensity quantification.

Table 1: Oligonucleotide sequences of forward and reverse primers used for semi-quantitative PCR

Gene name	Primers	Product length
Gapdh	F 5'- CCAATGTGTCCGTCGTGGATCT-3' R 5'- GTTGAAGTCGCAGGAGACAACC-3'	149bp
Alp	F 5'-TGCCTACTTGTGTGGCGTGAA-3' R 5'-TCACCCGAGTGGTAGTCACAATG-3'	164bp
Colla1	F 5'-GAGCGGAGAGTACTGGATCG-3' R 5'- GCTTCTTTTCCTTGGGGTTC-3'	158bp
Bsp	F 5'- CCGGCCACGCTACTTTCTT-3' R 5'- TGGACTGGAAACCGTTTCAGA-3'	66bp

2.20 Statistical analysis

Statistical analysis was performed using ANOVA t-test in the GraphPad Prism version 5 software to evaluate significance of the differences between CS-*g*-PCL and TCPS as well as CS:Gel scaffolds and the control substrates (TCPS or 2D CS:Gel). Differences between the experimental time periods were also examined. A p value of <0.05 was considered significant.

3 Results

In this thesis, **two chitosan-based materials were evaluated for their biocompatibility** in terms of cell viability, proliferation, adhesion **as well as their osteogenic differentiation capacity**. In the first one, which was synthesized and physicochemically characterized in the group of Prof. M. Vamvakaki, chitosan was combined with the synthetic biomaterial polycaprolactone for the preparation of chitosan-*graft*-poly(epsilon-caprolactone) (CS-*g*-PCL) copolymer materials. In the second one, which was developed during this thesis, chitosan was combined with the natural biomaterial gelatin for the production of crosslinked chitosan/gelatin (CS:Gel) scaffolds. The CS-*g*-PCL copolymer biomaterial was assessed in the form of films on glass substrates, while CS:Gel in the form of 3D porous scaffolds.

In the following two subsections, we will present the results from the *in vitro* biological response of pre-osteoblastic cells, human bone marrow derived mesenchymal stem cells and human umbilical vein endothelial cells (HUVECs) cultured for appropriate time

periods on both biomaterials, CS-*g*-PCL copolymer films and CS:Gel scaffolds to evaluate their biocompatibility and osteogenic potential.

3.1 *In vitro* biological response of MC3T3-E1 pre-osteoblastic cells on the CS-*g*-PCL material surface

3.1.1 Cell adhesion and morphology using scanning electron microscopy (SEM)

The morphology of MC3T3-E1 pre-osteoblastic cells on the CS-*g*-PCL material surface was investigated by scanning electron microscopy (SEM) on days 2 and 7 after cell seeding, as shown in Figure 3.1.1. The image on day 2 (Fig. 3.1.1 a) shows a few adherent cells on the material surface, but they retain their characteristic osteoblastic morphology, interacting both with the substrate and with each other. Moreover, cells appeared highly elongated in a spindle-like shape.

After 7 days of culture (Fig. 3.1.1 b), pre-osteoblastic cells were extensively proliferated and expanded to form a thick layer on the whole material surface. Cells appeared flattened with wide lamellipodia formation and long cellular extensions of the cell membrane. This morphology is characteristic for cells cultured on a preferable, biocompatible material surface. Moreover, the appearance of granules on the cells indicate the ECM mineralization. The relatively good initial adhesion and the consequent proliferation indicate that the CS-*g*-PCL films may be an ideal substrate for the growth of pre-osteoblastic cells.

CS-*g*-PCL 80/20

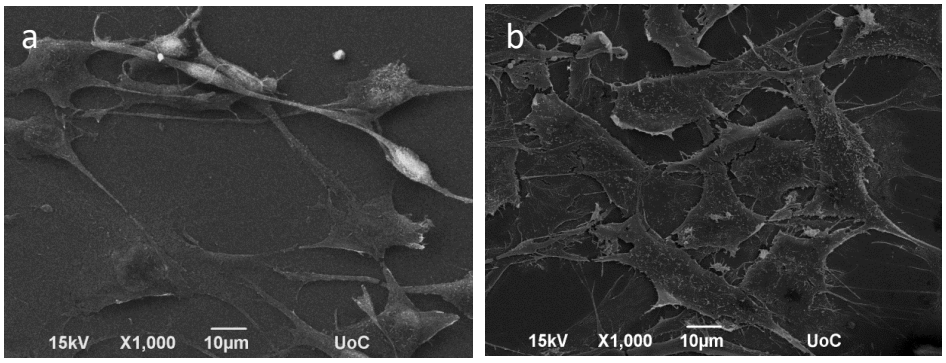

2 days after seeding **7 days after seeding**

Figure 3.1. 1: Scanning electron images showing the morphology of MC3T3-E1 pre-osteoblastic cells on CS-*g*-PCL films, 2 and 7 days after seeding
SEM images illustrating MC3T3 cell adhesion and growth on the copolymer surface. (a) After 2 days of seeding, a few cells were grown on the material surface, but they retain their elongated-fibroblastic morphology. (b) On day 7, cells were extensively proliferated forming a thick layer on the whole material surface. Original magnifications are 1.000x and scale bars represent 10 μm.

3.1.2 Adhesion and morphology using Confocal laser fluorescence microscope (CLFM)

The morphology of the adhered MC3T3-E1 pre-osteoblastic cells cultured on the CS-*g*-PCL material surfaces for 3 days was examined using confocal fluorescence microscopy. The cytoskeletal organization of the cells was visualized via actin (red), vinculin (green) and nucleus (blue) staining (Fig. 3.1.2). Figs. 3.1.2 (c) and (d) depict an overlay of the three stainings. Cells strongly attach on the material surface and form cell-cell interactions. Moreover, they retain their elongated morphology with wide lamellipodia formation and long cellular extensions of the cell membrane. The observed fully spread cell morphology with spindle shape and cytoplasmic extensions signal a strong adhesion profile on the material surface.

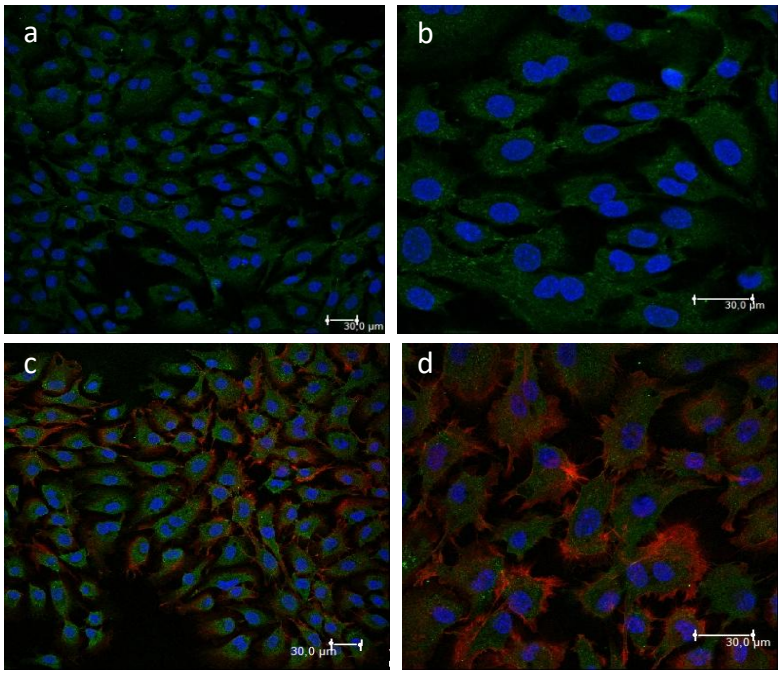

Figure 3.1.2: Confocal fluorescence microscopy images showing the adhesion and morphology of MC3T3-E1 pre-osteoblastic cells on CS-*g*-PCL films, 3 days after seeding
Cytoskeletal organization of cells was visualized via actin (red), vinculin (green) and nucleus (blue) staining. An overlay of the three staining is depicted in (c) and (d) images. Cells strongly attach on the material surface and form cell-cell interactions, covering the whole surface area. Original magnifications are 40x and scale bars represent 30 μm.

3.1.3 Viability and proliferation assay

The viability and proliferation of MC3T3-E1 pre-osteoblastic cells on the CS-g-PCL substrates was quantitatively determined using the colorimetric PrestoBlue® assay, 1,3 and 7 days after cell seeding (Fig. 3.1.3). On day 1, the number of viable cells were similar between CS-*g*-PLC films and TCPS and no significant differences were observed. However, viable cell numbers on the copolymer surface were significantly higher in contrast to TCPS, after 3 and 7 days of culture (Fig. 3.1.3 (a)). At each time point, cell viability was calculated following normalization of absorbance units to cells cultured TCPS (control) and expressed as a percentage to control (100%) (Fig. 3.1.3 (b)). On day 1, the viability of cells cultured on the CS-*g*-PCL films was 80% in contrast to TCPS surfaces and increased to 146% and 127% after 3 and 7 days respectively. This is a promising result indicating that the CS-*g*-PCL films promote the viability and proliferation of pre-osteoblastic cells.

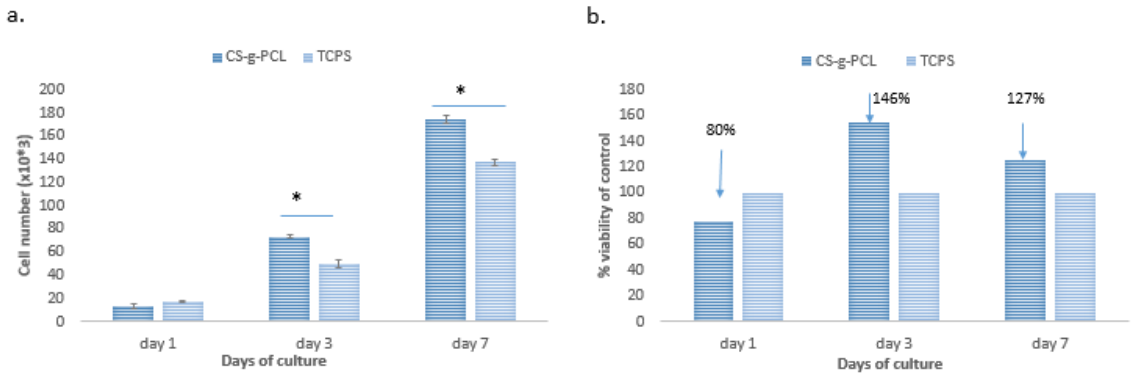

Figure 3.1.3: PrestoBlue® proliferation assay showing the growth of MC3T3-E1 pre-osteoblstic cells cultured on CS-*g*-PCL films and TCPS.

(a) Optical density values of viability are normalized to the cell number according to a calibration curve. The number of cells cultured on CS-*g*-PCL films was similar to TCPS 1 day after seeding but after 3 and 7 days was significantly higher for cells cultured on the CS-*g*-PCL material surface. (b) Cell numbers are calculated in percent of the TCPS control. Error bars represent the average of triplicates ± SE, of two independent experiments (n=6). *p<0.05 *vs.* TCPS.

3.1.4 Alkaline phosphatase activity

In order to examine the potential of MC3T3-E1 pre-osteoblasts cultured on the CS-*g*-PCL films to differentiate into mature osteoblasts in vitro, the alkaline phosphatase (ALP) activity was measured, as an early marker of osteogenesis. For this experiment, cells were cultured in the presence of osteogenic medium. ALP activity of cells cultured on the material surface was normalized to protein concentration as shown on Figure 3.1.4. ALP activity of cells cultured on CS-*g*-PCL was significantly increased in contrast to TCPS, both after 7 and 14 days. In cells cultured on the material surface, ALP activity was higher on day 7 and decreased from day 7 to day 14, following a pattern similar to TCPS.

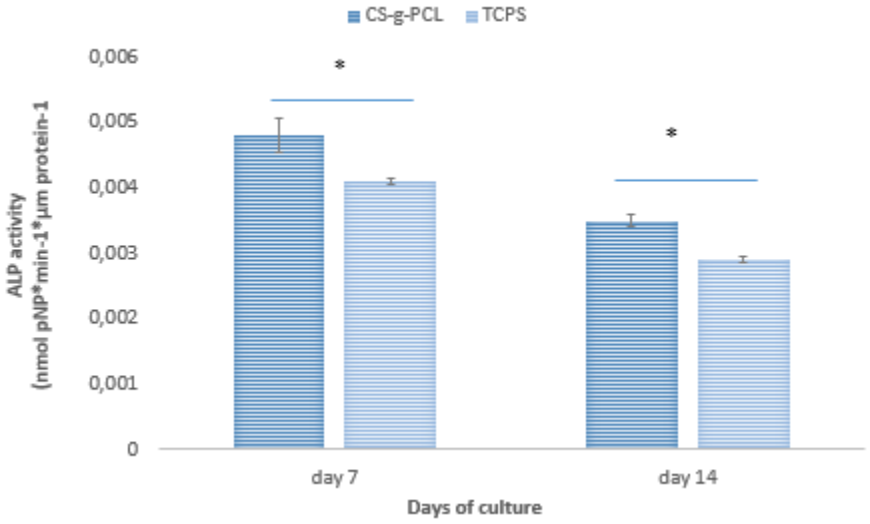

Figure 3.1.4: Alkaline phosphatase (ALP) activity of MC3T3-E1 cells cultured on CS-*g*-PCL films and TCPS for 7 and 14 days.

ALP activity of cells cultured on CS-*g*-PCL was significantly increased in contrast to TCPS, both after 7 and 14 days. Error bars represent the average of triplicates ± SE, of two independent experiments (n=6). *p<0.05 vs. TCPS.

3.1.5 Collagen production

To investigate the effect of the copolymer material on the production of collagen we quantified collagen secreted in the culture supernatant at different time points, in the presence of exogenous ascorbic acid (AA), which is a co-factor in collagen synthesis. It is known that collagen is highly expressed by osteoblasts and involved in the formation of extracellular matrix in which mineralization can occur. Collagen levels of cells cultured on CS-*g*-PCL films and TCPS for 4, 7 and 14 days were measured using the Sirius Red binding assay. As shown is Figure 3.1.5, the copolymer material enhances the production of collagen at all-time points relative to control TCPS. Moreover, collagen levels of cells were lower after 14 days of culture in comparison to previous time points but still comparable to control TCPS.

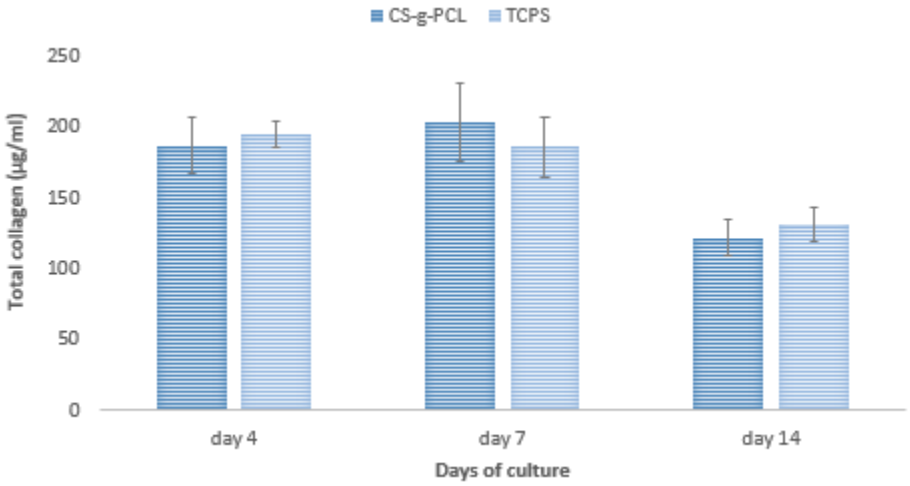

Figure 3.1.5: Levels of collagen in the supernatants of MC3T3-E1 cells cultured on CS-*g*-PCL films and TCPS for 4, 7 and 14 days.
As depicted the copolymer material enhanced the production of collagen at all-time points compared to the TCPS control. Error bars represent the average of triplicates ± SE of two independent experiments (n=6).

3.1.6 Matrix mineralization

Calcium deposits through mineralization is a specific marker of late stages of cell differentiation. As previously described, Alizarin Red is used to stain calcium deposits in the extracellular matrix of pre-osteoblasts after 7 and 14 days of culture in osteogenic medium. In order to normalize calcium deposition to cell number, living cell numbers was measured using the PrestoBlue® assay, prior the Alizarin Red staining. Figure 2.2.6 indicates that the extracted calcium-dye complex by CPC for cells cultured on CS-*g*-PCL films were similar to TCPS after 7 days. Moreover, the matrix mineralization for the copolymer substrate was significantly increased in contrast to TCPS after 14 days of culture.

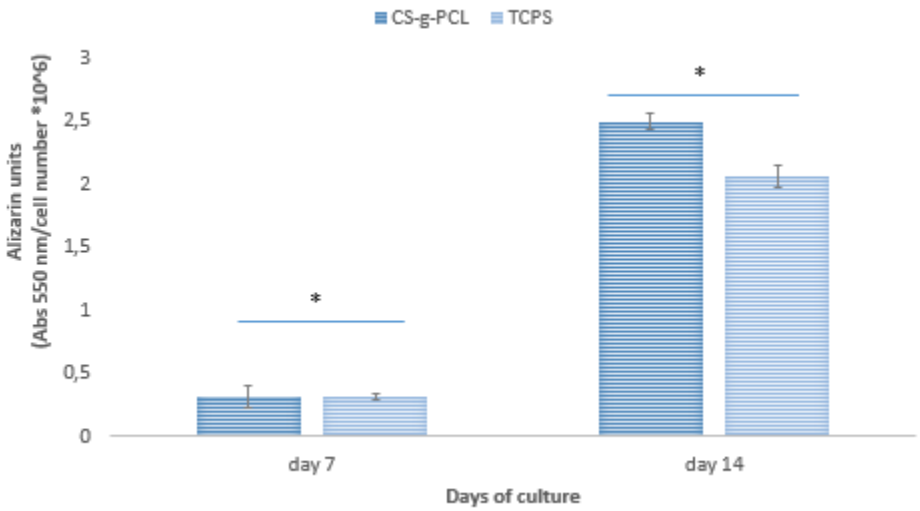

Figure 3.1.6: Calcium biomineralization by Alizarin Red S staining of MC3T3 cells cultured for 7 and 14 days on CS-*g*-PCL and TCPS.

As depicted the matrix mineralization for the copolymer substrate was significantly increased in contrast to TCPS after 14 days of culture. Error bars represent the average of triplicates ± SE, of two independent experiments (n=6). *p<0.05 vs. TCPS.

3.1.7 Endogenous expression of osteopontin

As previously described, osteopontin is a phosphorylated glycoprotein that appears to be involved in bone mineralization. In our study, the endogenous expression of osteopontin of cells cultured on CS-*g*-PCL and TCPS for 4 and 10 days was detected using in-cell enzyme-linked immunosorbent assay (ELISA) and confocal laser fluorescence microscope (CLFM). As shown in Figure 2.2.7 (a) the levels of osteopontin were increased for cells cultured on the material surface in contrast to TCPS both after 4 and 10 days. Moreover, the increase between the two material surfaces 4 days after seeding was significant. This result was also confirmed in the confocal images as depicted in Figure 2.2.7 (b). Endogenous osteopontin was observed in green around the red cell nucleus. The expression of endogenous osteopontin is higher for cells cultured on CS-*g*-PCL films in contrast to TCPS, 10 days after seeding.

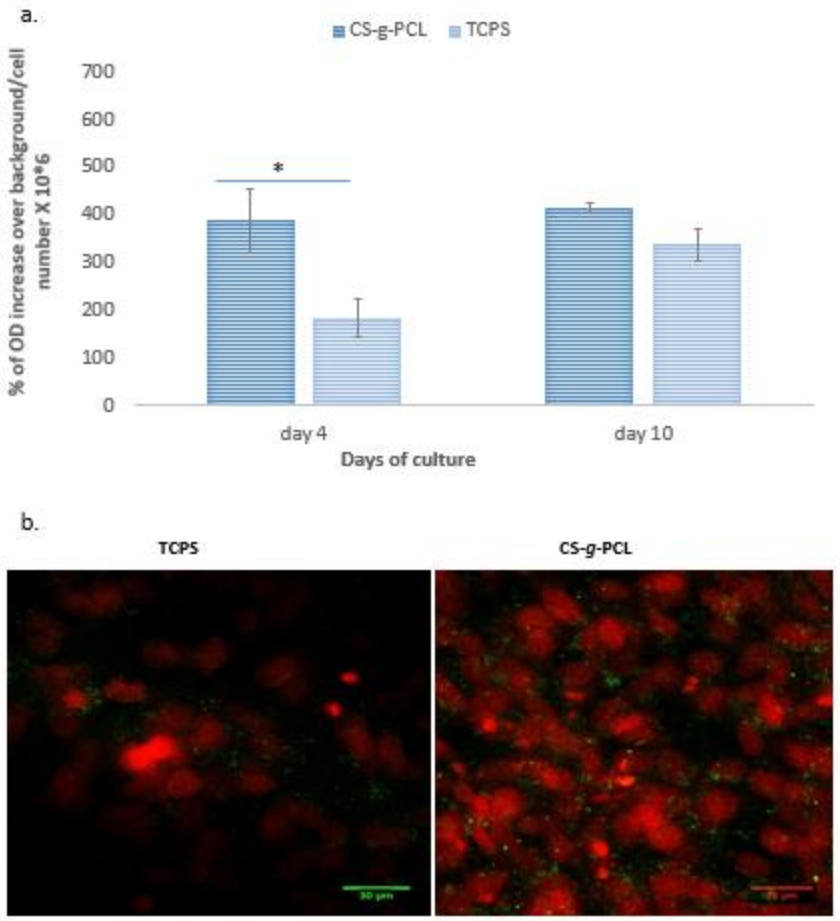

Figure 3.1.7: Endogenous expression of osteopontin on CS-*g*-PCL films and TCPS.
(a) Measurement of endogenous levels of osteopontin of pre-osteoblastic cells cultured on two material surfaces for 4 and 10 days. Osteopontin levels in CS-*g*-PCL films is higher in contrast to TCPS, and the increase was significant on day 4. Error bars represent the average of triplicates ± SE, of two independent experiments (n=6). *p<0.05 vs. TCPS. (b) Confocal images demonstrate the endogenous expression of osteopontin on the two material surfaces, 10 days after seeding. Osteopontin is depicted in green around the red cell nucleus. The expression is higher for cells cultured on CS-*g*-PCL films, in contrast to TCPS, 10 days after seeding. Original magnifications are 40x and scale bars represent 30 μm.

3.1.8 Bone-related gene expression

In our study, the mRNA expressions of *Alp*, *Colla1* and *Bsp* bone-related genes were measured after the MC3T3-E1 cells were cultured on CS-*g*-PCL or TCPS substrates for 4 and 10 days. Data analyzed from semiquantitative RT-PCR (Figure 2.2.8) show that gene expression follows the same pattern for cells cultured on either CS-*g*-PCL or TCPS for 4

and 10 days. Moreover, no statistical differences were found in mRNA levels between the two different material substrates.

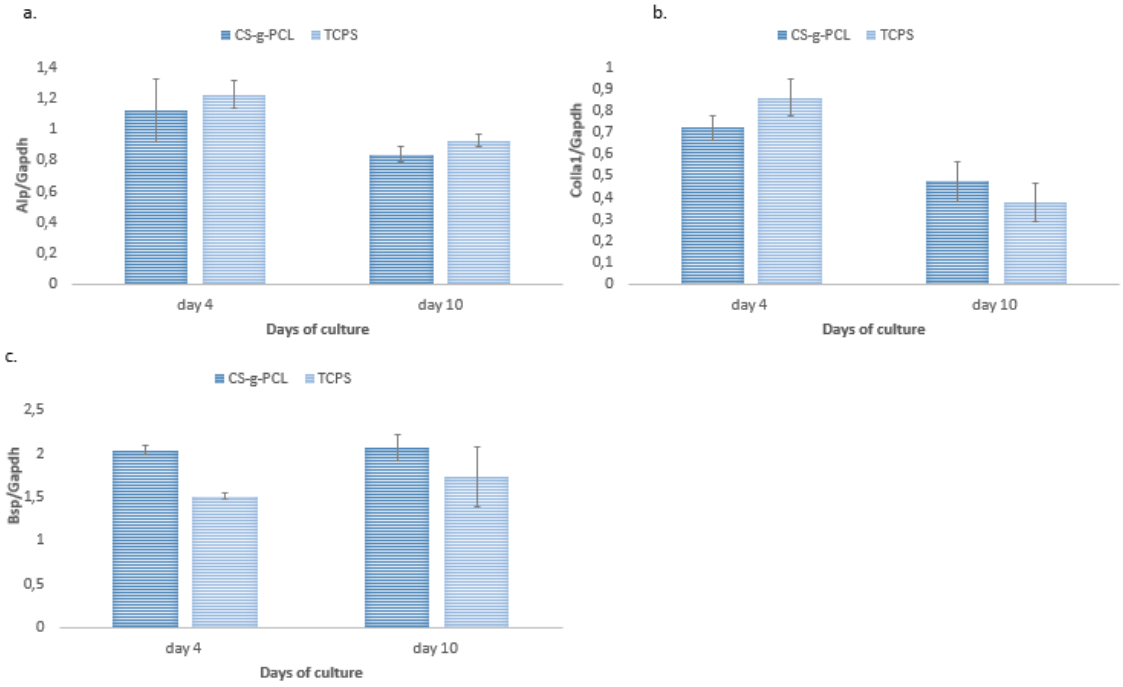

Figure 3.1.8: mRNA expression levels of (a) Alp, (b) Colla1 and (c) Bsp in cells cultured on CS-*g*-PCL and TCPS for 4 and 10 days.
Expression levels were normalized to the *Gapdh* housekeeping gene. Error bars represent the average of triplicates ± SE, of two independent experiments (n=6). **p*<0.05 *vs.* TCPS.

3.2 Development of crosslinked chitosan/gelatin (CS:Gel) scaffolds and their potential to promote osteogenesis

3.2.1 Morphology of CS:Gel scaffolds

We prepared two types of lyophilized 40:60% CS:Gel disc-shaped scaffolds with a diameter 15 mm and a height of 3 mm, the first type was crosslinked with 0.1% v/v

glutaraldehyde, and the second one with 0.1% v/v genipin. The first type results in scaffolds that are white in color in dry state, and change to light yellowish when they become wet, whereas the second scaffold type appears green-blue. Both types are gel-like, soft and elastic when they become wet after neutralization. The morphology of the porous structure of the CS:Gel scaffolds using glutaraldehyde (Figure 3.2.1a) and genipin (Figure 3.2.1b) as crosslinkers was analyzed by scanning electron microscopy (SEM). The interconnecting open pores have a similar structure in both scaffold types, the glutaraldehyde and genipin crosslinked. The pore size of the CS:Gel scaffolds crosslinked with glutaraldehyde were found to range from 40 to 120 µm, whereas the genipin crosslinked scaffolds show a pore size from 70 to 170 µm (Figure 3.2.1.c).

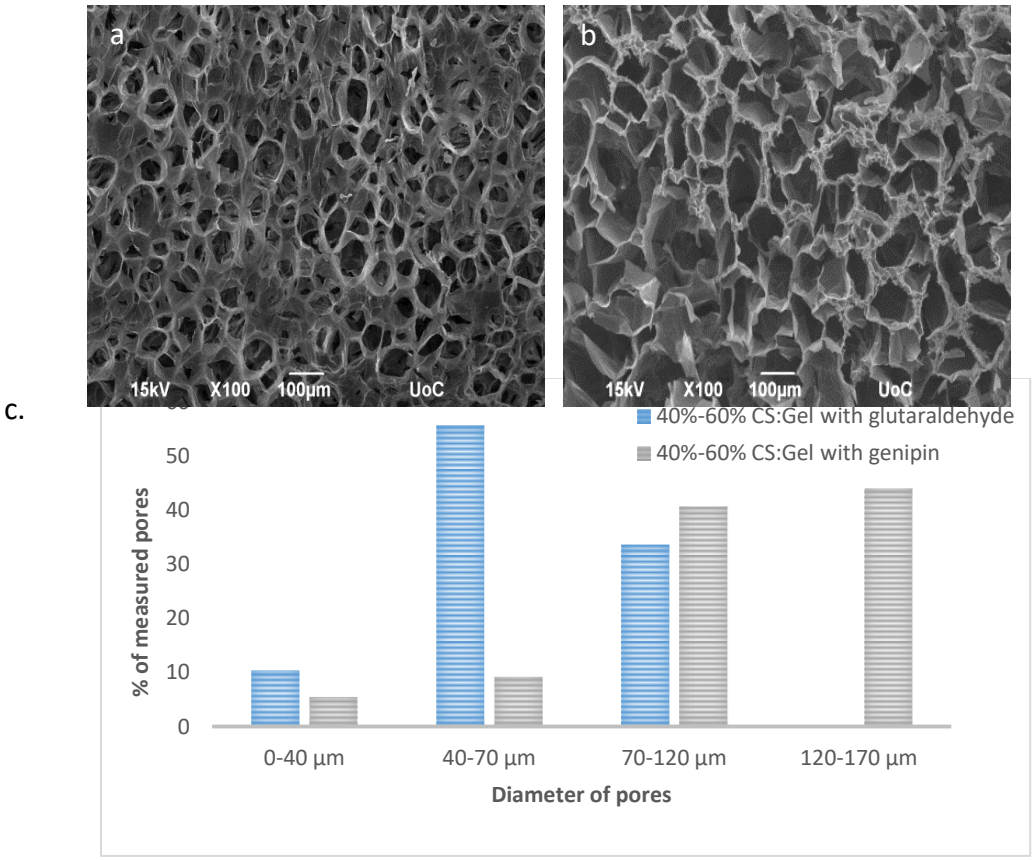

Figure 3.2.1: Scanning electron images showing the morphology of CS:Gel scaffolds
SEM images illustrating the morphology of CS:Gel scaffolds crosslinked with (a) glutaraldehyde and (b) genipin. The interconnecting open pores have a similar structure in both scaffold types. The pore size of the CS:Gel scaffolds crosslinked with glutaraldehyde were found to range from

40 to 120 µm, whereas the genipin crosslinked scaffolds show a pore size from 70 to 170 µm. Original magnifications are 100x and scale bars represent 100 µm.

3.2.2 Swelling of CS:Gel scaffolds

As previously described, the ability of lyophilized CS:Gel scaffolds, crosslinked with glutaraldehyde and genipin, to absorb water was determined by swelling in PBS (pH 7.4)**.** The degree of swelling of the 40-60% CS:Gel scaffolds crosslinked with glutaraldehyde indicates a value of 700% and is significantly higher compared to those crosslinked with genipin, for which we measured a value of 515% (Figure 3.2.2). Water absorption of non-crosslinked scaffolds was not possible to be measured because they dissolved after 12 h in PBS.

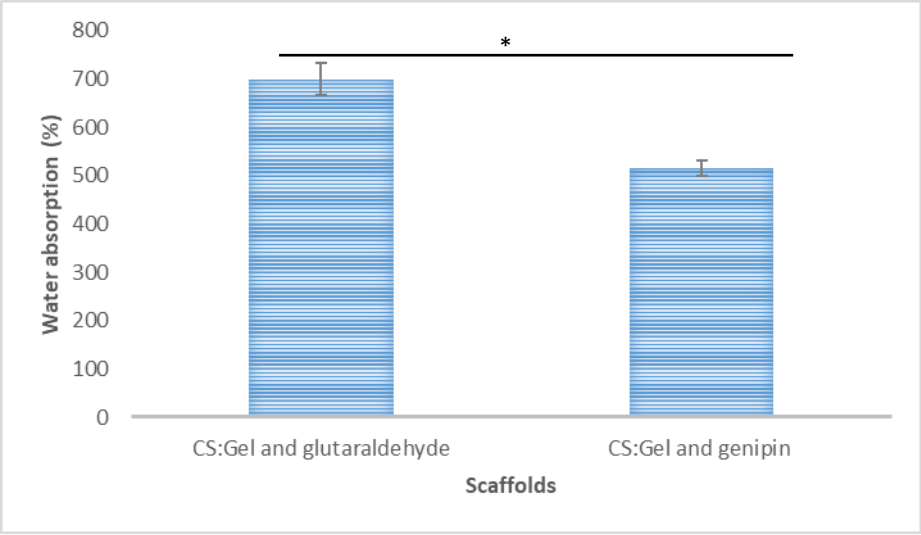

Figure 3.2.2: Degree of swelling of the CS:Gel scaffolds

Percentage of water absorption of 40-60% CS:Gel scaffolds crosslinked with glutaraldehyde and genipin. The degree of swelling of scaffolds crosslinked with glutaraldehyde was significantly higher compared to those crosslinked with genipin. Error bars represent the average of triplicates ± SE, of three independent experiments (n=9). *p<0.05 vs. TCPS.

3.2.3 Infiltration of pre-osteoblasts into the CS:Gel scaffolds

The ability of pre-osteoblastic cells MC3T3-E1 to adhere and infiltrate into the pores of the scaffolds after 3 days in culture was determined by SEM. Representative SEM images in two magnifications show the typical elongated, polygonal morphology of MC3T3-E1 cells cultured on the 40-60% CS:Gel scaffolds using glutaraldehyde (Figures 3.2.3 a and b) and genipin (Figures 3.2.3 c and d) as crosslinkers. However, the glutaraldehyde crosslinked scaffolds demonstrated pronounced cell infiltration into the glutaraldehyde crosslinked scaffolds compared to the genipin counterparts, in which only a poor cell infiltration was observed. Non-adherent small round-shaped pre-osteoblasts were not observed in either scaffold types. Based on the aforementioned results that demonstrate a strong ability of the glutaraldehyde-crosslinked scaffolds to support cell attachment and infiltration into their pores, we performed further *in vitro* biological assessment of glutaraldehyde crosslinked CS:Gel scaffolds.

CS:Gel glutaraldehyde

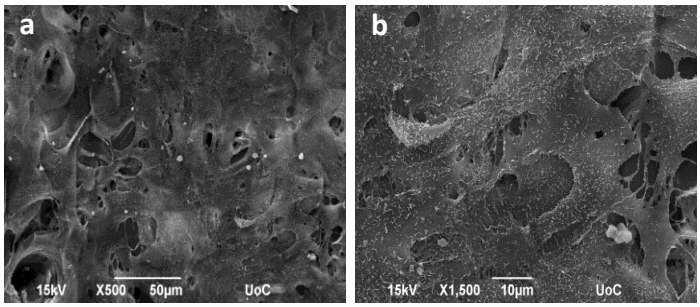

CS:Gel genipin

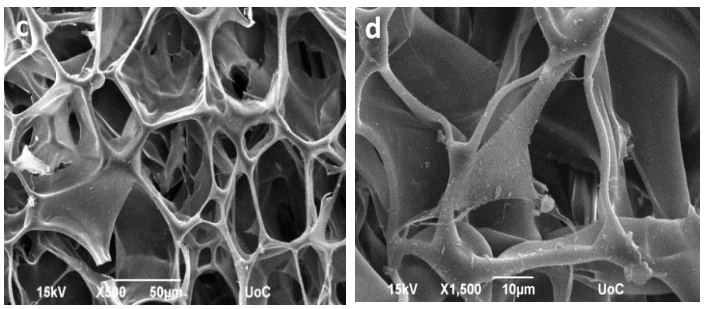

Figure 3.2.3: Scanning electron images showing the morphology of MC3T3-E1 pre-osteoblastic cells on the CS:Gel scaffolds crosslinked with glutaraldehyde and genipin

SEM images illustrating the morphology of MC3T3 pre-osteoblastic cells cultured on the 40%-60% CS:Gel scaffolds using glutaraldehyde (Figure 3.2.3 a and b) or genipin (Figure 3.2.3 c and d) as crosslinker after 4 days in culture. Original magnifications are 500x (a and c) and 1.500x (b and d) and scale bars represent 50 µm and 10 µm, respectively.

3.2.4 Development of different ratios of CS:Gel

We also used SEM to examine the morphology of three different rations (20%-80% CS:Gel, 80%-20% CS:Gel and 60%-40% CS:Gel) of glutaraldehyde crosslinked scaffolds. The morphology of the surface area was different for the three compositions. All scaffolds had open porous structure but the pores of 20%-80% and 60%-40% crosslinked scaffolds appeared to be relative spherical in contrast to flattened non-uniform pores of 80%-20% crosslinked scaffolds (Figure 3.2.4). The adhesion and morphology of MC3T3-E1 pre-osteoblastic cells on the three different material surfaces were also examined (Figure 3.2.5). The results show that cellular appearance and density strongly depended on the substrate. Cells cultured on 20%-80% and 60%-40% CS:Gel scaffolds show the typical, polygonal, elongated morphology and infiltrate into the pores of the material (Figure 3.2.5 a and b). Cells covered the whole surface area and were characterized by wide lamellipodia formation and extensive spreading of the membrane onto the material. However, most of the cells cultured on 80%-20% CS:Gel scaffolds appeared small and round-shaped with under-developed filopodia (Figure 3.2.5 c).

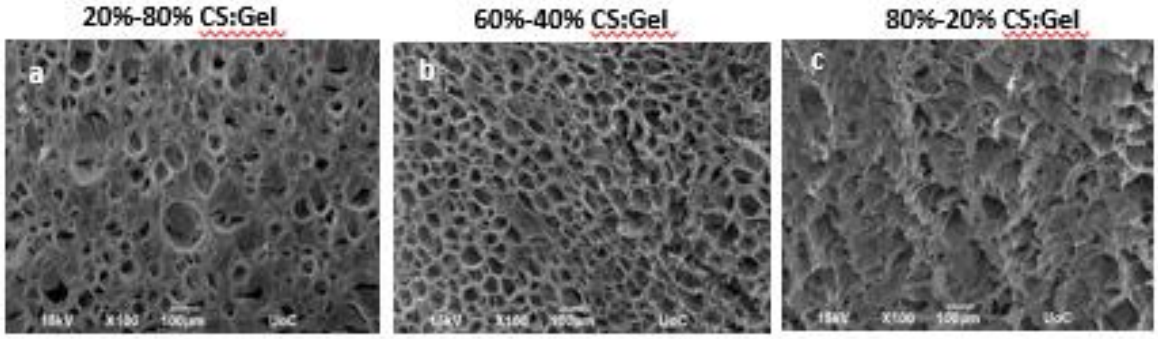

Figure 3.2.4: Scanning electron microscopy (SEM) images showing the morphology of three different ratios of crosslinked CS:Gel scaffolds
(a and b) The pores of 20%-80% and 60%-40% CS:Gel scaffolds were uniform and relative spherical in contrast to (c) flattened non-uniform pores of 80%-20% CS:Gel scaffolds. Original magnifications are x100 and scale bars represent 100 µm.

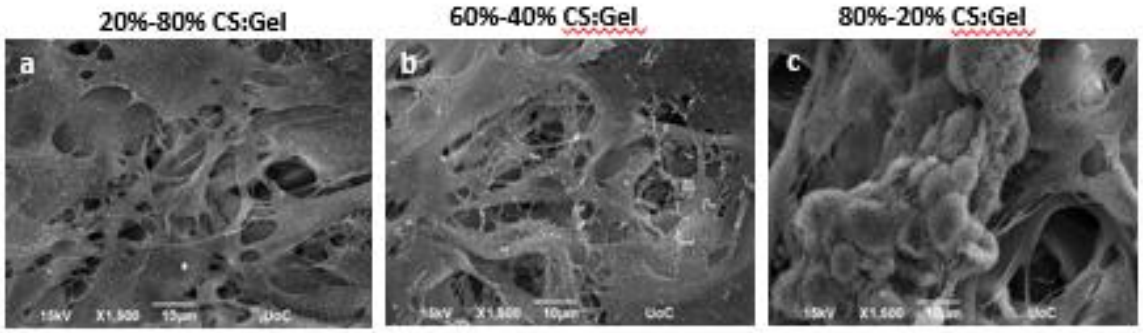

Figure 3.2.5: Scanning electron microscopy (SEM) images showing the morphology of pre-osteoblastic cells on the three different ratios of crosslinked CS:Gel scaffolds
(a and b) Cells cultured on 20%-80% and 60%-40% CS:Gel scaffolds appeared flattened and elongated and they retain their fibroblastic-like morphology in contrast to (c) small, round-shaped morphology of cells cultured on 80%-20% CS:Gel scaffolds. Original magnifications are x1.500 and scale bars represent 10 µm.

3.2.5 Viability of pre-osteoblasts on different ratios of CS:Gel scaffolds

The PrestoBlue assay was used to quantitatively determine the proliferation of viable pre-osteoblastic cells on four different ratios of CS:Gel scaffolds. A comparison of the cellular metabolic activity on the different samples (20%-80% CS:Gel, 80%-20% CS:Gel, 40%-60% CS:Gel and 60%-40% CS:Gel) after 2, 5 and 7 days of culture is depicted in Figure 3.2.6. Pre-osteoblasts displayed similar metabolic activities and no significant

differences between the substrates were observed after 2 days of culture. However, cell density was found significantly higher on 40%-60% CS:Gel scaffolds after 5 and 7 days of culture.

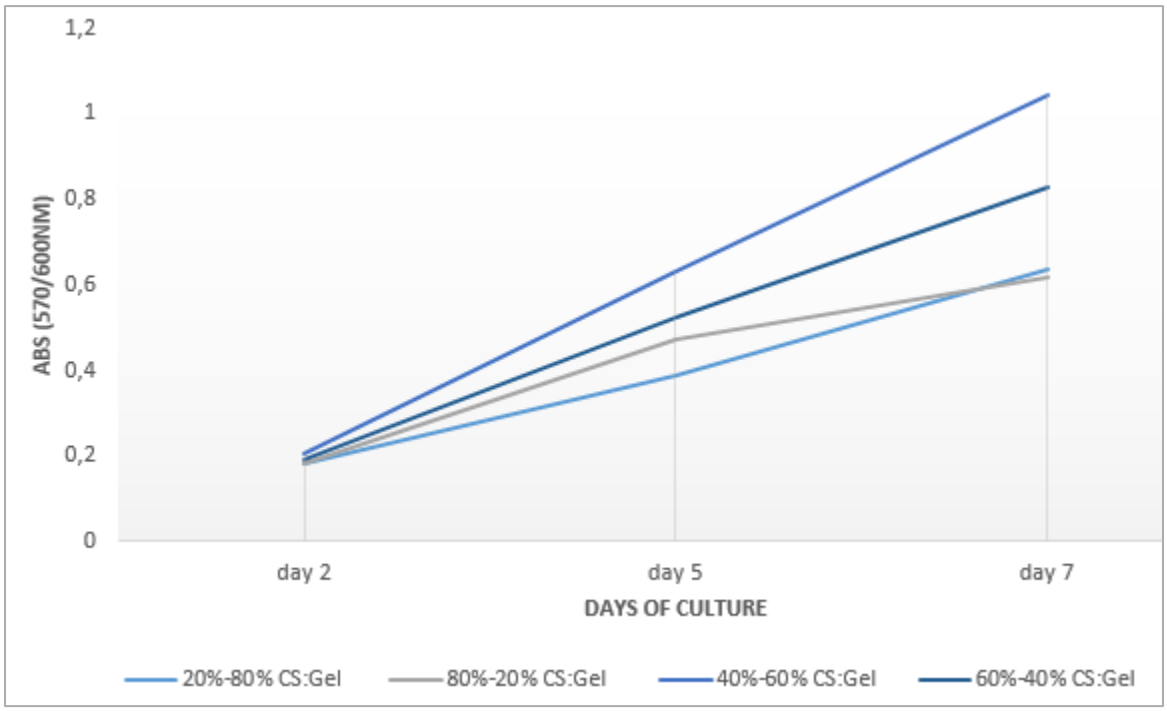

Figure 3.2.6: Metabolic activity of MC3T3-E1 cells on four different CS:Gel scaffolds
Pre-osteoblasts displayed similar metabolic activities and no significant differences between the substrates were observed after 2 days of culture. However, cell density was found significantly higher on 40%-60% CS:Gel scaffolds after 5 and 7 days of culture.

3.2.6 Degradation study of crosslinked CS:Gel scaffolds

For the degradation study, CS:Gel scaffolds crosslinked with two different concentrations (0.1% v/v and 1% v/v) of glutaraldehyde were used. The percentage of weight loss of the CS:Gel scaffolds using 0.1% glutaraldehyde as crosslinker following degradation at 37 °C in PBS for 1, 6, 11, 15 and 21 days was approximately 7, 19, 34, 44

and 48%, respectively. Moreover, the percentage of weight loss of CS:Gel scaffolds using 1% glutaraldehyde as crosslinker at the same days was approximately 5, 7, 14, 17 and 18% respectively (Figure 3.2.6).

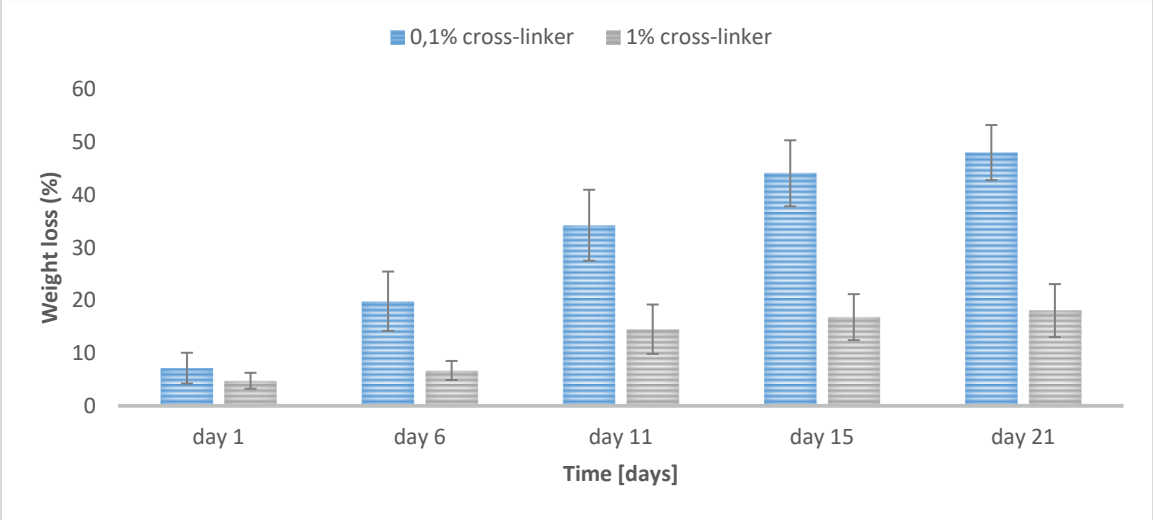

Figure 3.2.7: Percentage of mass loss of 40%-60% CS:Gel scaffolds crosslinked with 0.1% and 1% glutaraldehyde

The weight loss of scaffolds using 0.1% glutaraldehyde as crosslinker was 7, 20, 34, 44,and 48% after 1, 6, 11, 15 and 21 days, respectively. Moreover, the percentage of weight loss of CS:Gel scaffolds using 1% glutaraldehyde as crosslinker after 1, 6, 11, 15 and 21 days was approximately 5, 7, 14, 17 and 18% respectively. Error bars represent the average of triplicates ± SE, of two independent experiments (n=6).

3.2.7 FTIR spectroscopic analysis

FTIR analysis was used for the 40:60% CS:Gel scaffolds crosslinked with two different concentrations (0.1% v/v and 1% v/v) of glutaraldehyde. The peaks for pure chitosan and gelatin are summarized by Thein-Han *et al* [135]. For pure chitosan, the peak at 3450 cm^{-1} denotes the presence of N-H stretching, while 1654 cm^{-1} and 1580 cm^{-1} are

characteristic peaks of amide I and amide II, respectively. Gelatin absorbs strongly at 3200-3500 cm^{-1}, the characteristic peak for N-H stretching and at 1640 cm^{-1} due to C=O stretching. The CS:Gel scaffolds used in the present study retain the characteristic peaks of both chitosan and gelatin (Figure 3.2.8). Moreover, no differences in the FTIR spectra were observed between scaffolds crosslinked with 0.1% and 1% glutaraldehyde.

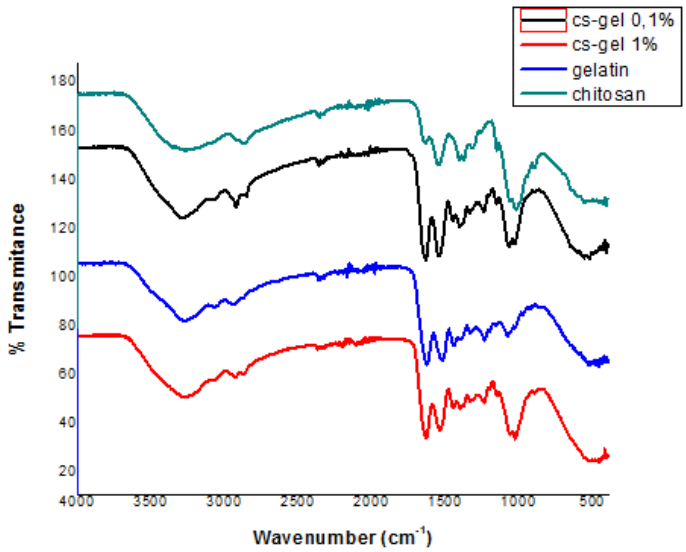

Figure 3.2.8: FTIR analysis of 40:60% CS:Gel scaffolds crosslinked with 0,1% and 1% glutaraldehyde

FTIR analysis of pure chitosan and gelatin was also carried out. Crosslinked CS:Gel scaffolds retain the characteristic peaks of both chitosan and gelatin. Moreover, no differences were observed between the scaffolds crosslinked with 0.1% and 1% glutaraldehyde.

3.2.8 In vitro biological response of MC3T3-E1 pre-osteoblastic cells on the CS:Gel scaffolds crosslinked with 0.1% v/v glutaraldehyde.

Cytoskeletal organization of MC3T3-E1 pre-osteoblastic cells into the pores of the CS:Gel scaffolds crosslinked with glutaraldehyde was visualized via actin and nucleus staining (Figures 3.2.9 a and b). Pre-osteoblastic cells strongly attach into the pores of the scaffolds and form cell-cell interactions, indicating a dense actin cytoskeleton (red)

around the cell nucleus (blue) depicted in both 20x (Figure 3.2.9 a) and 40x (Figure 3.2.9 b) magnifications of the confocal laser fluorescence images.

Cell viability and proliferation of pre-osteoblastic cells was assessed by the PrestoBlue® assay after 2, 4 and 7 days of culture. The viability and proliferation of cells cultured on the 3D CS:Gel scaffolds significantly increased after 7 days in culture compared to 2D CS:Gel surfaces (Figure 3.2.9 c). We investigated the effect of CS:Gel scaffolds on the production of collagen, which is the predominant protein in the extracellular matrix (ECM), by quantifying the secreted collagen in the supernatant produced by the pre-osteoblastic cells. Figure 3.2.9 d demonstrates that CS:Gel scaffolds significantly enhance collagen production at all-time points compared to the TCPS control surface, and thus support ECM formation.

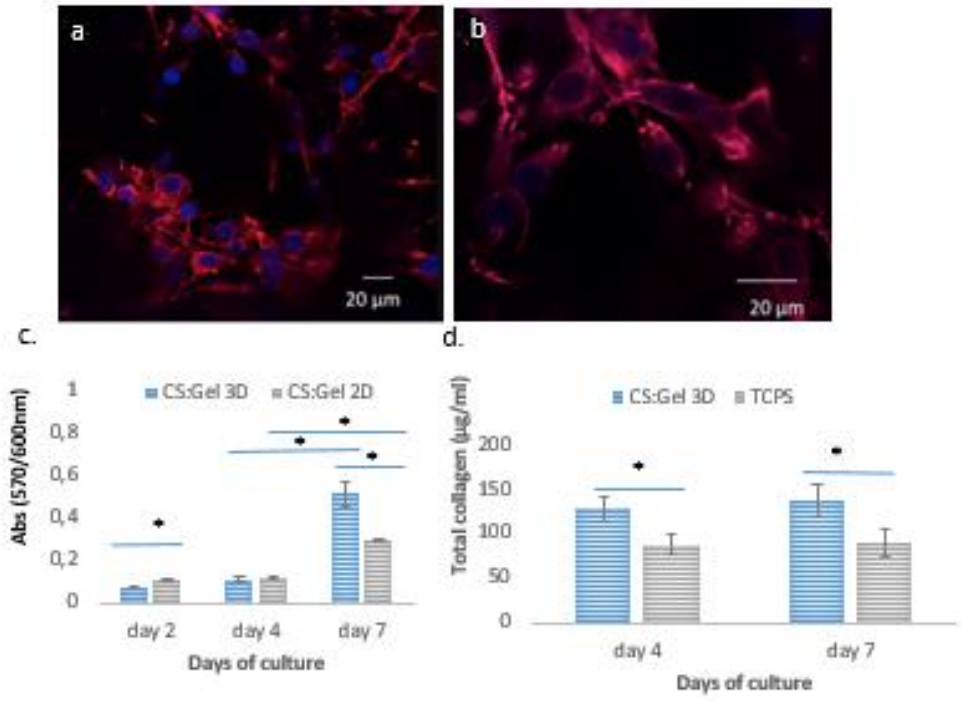

Figure 3.2.9: *In vitro* biological repsonse of MC3T3-E1 cells cultured on the 40%-60% CS:Gel scaffolds crosslinked with 0.1% v/v glutaraldehyde
(a and b) Confocal laser fluorescence images showing the cytoskeletal organization with dense actin distribution (in red) of pre-osteoblastic cells within CS:Gel scaffolds crosslinked with glutaraldehyde at a magnification of 20x (a) and 40x (b); Cell nuclei are shown in blue. (c)

Viability and proliferation of cells after 2, 4 and 7 days of culture using 2D CS:Gel surface as control substrate. (d) Levels of collagen produced from cells cultured on 3D and TCPS for 4 and 7 days. Bars represent 20 μm. Error bars represent the average of triplicates ± SE, of three independent experiments (n=9). *p<0.05 vs. 2D CS:Gel or TCPS.

3.2.9 In vitro biological response of MC3T3-E1 pre-osteoblastic cells on the CS:Gel scaffolds crosslinked with 1% v/v glutaraldehyde.

As previously described, 40%-60% CS:Gel scaffolds crosslinked with 0.1% glutaraldehyde promote the adhesion, proliferation and ECM formation of pre-osteoblastic cells. The same results were observed when the concentration of glutaraldehyde was increased from 0.1% to 1%. Representative SEM images in two magnifications show the typical elongated, fibroblastic-like morphology of MC3T3-E1 cells cultured on the material surface for 4 days. Cells covered the whole surface area and non-adherent small round-shaped cells were not observed (Figure 3.2.10 a and b). Moreover, the viability and proliferation of cells cultured on 3D scaffolds for 2 and 7 days, was significantly increased compared to 2D matrices (Figure 3.2.10 c). The amount of collagen secreted by the cells cultured on 3D CS:Gel scaffolds was significantly increased compared to TCPS, after 4 and 7 days in culture.

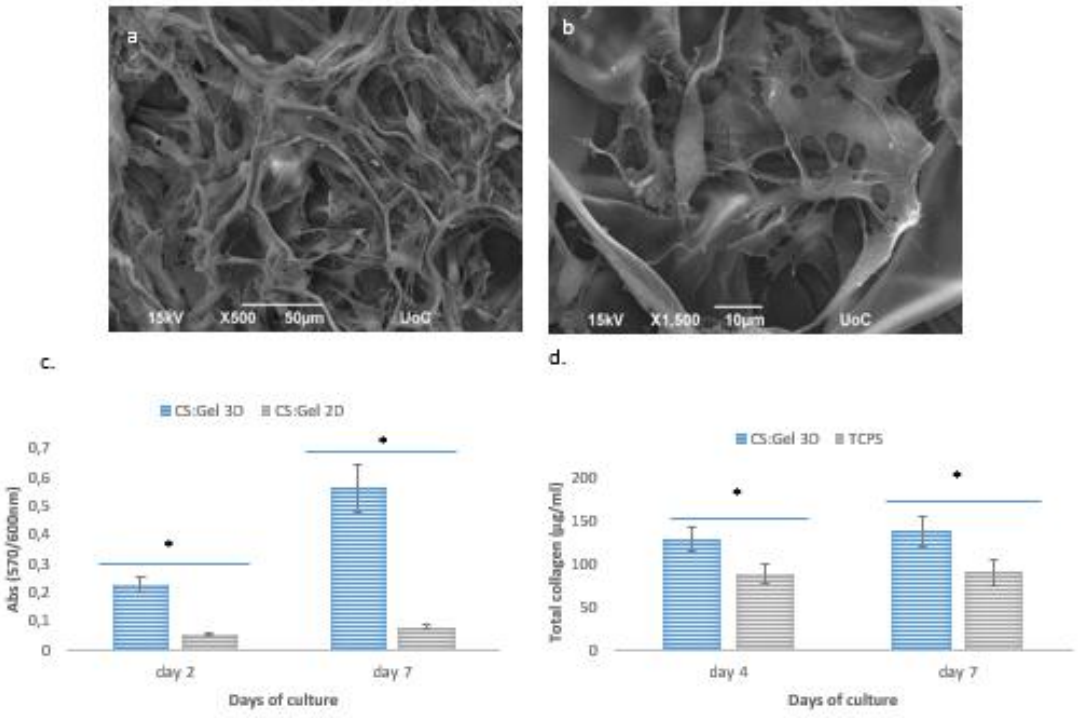

Figure 3.2.10: *In vitro* biological response of MC3T3-E1 cells cultured on 40%-60% CS:Gel scaffolds crosslinked with 1% v/v glutaraldehyde

(a and b) SEM images illustrating the morphology of cells cultured on the material surface for 4 days. (c) Viability and proliferation of cells after 4 and 7 days in culture using 2D CS:Gel surface as control substrate. (d) Levels of collagen produced from the cells cultured on 3D CS:Gel and TCPS surfaces for 4 and 7 days. Bars represent (a) 50 and (b) 10µm, respectively. Error bars represent the average of triplicates ± SE, of two independent experiments (n=6). **p*<0.05 *vs.* 2D CS:Gel or TCPS.

3.2.10 Characterization of hBM-MSCs

As previously described, the isolation and characterization of hBM-MSCs were performed by the group of Prof. Pontikoglou and Prof. Papadaki at the Medical School. These cells were isolated from the bone marrow of healthy individuals and were immunophenotypically analyzed for the expression of cell surface markers using flow cytometry. The results showed that these cultures comprised a homogeneous cell population positive for CD90, CD105, CD73 surface antigens and negative for the hematopoietic markers CD45 and CD34 (Figure 3.2.11 a) corroborating the mesenchymal origin of the cells [139]. Moreover, consistent with the established

biological properties of MSC, P2 cells demonstrated spindle-like morphology and the ability to undergo osteogenic (Figures 3.2.11 b) and adipocytic differentiation (Figure 3.2.11 c), as evidenced by the respective cytochemical detection of mineralized matrix and lipid droplets.

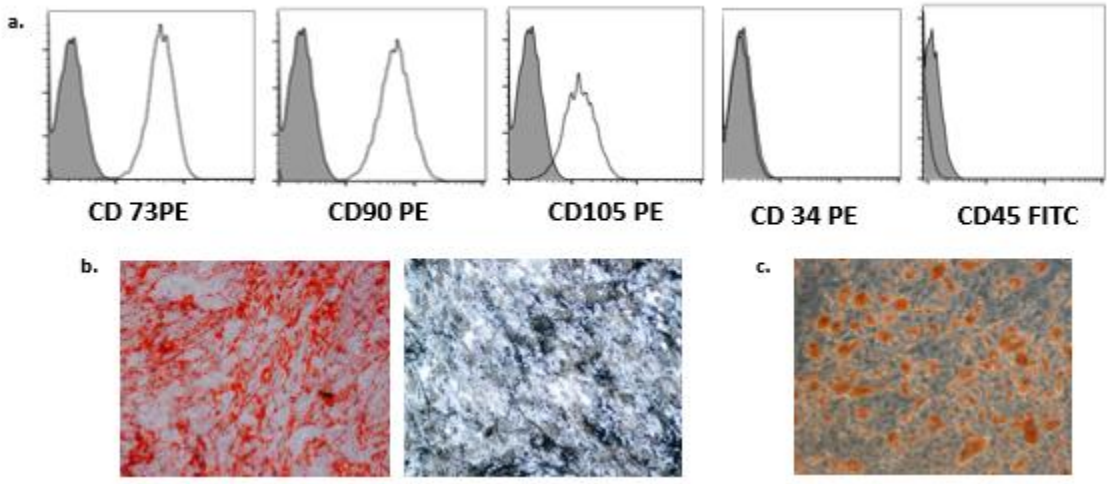

Figure 3.2.11: Characterization of the hBM-MSCs
(a)Flow cytometric analysis of cell surface markers of BM-MSCs showing representative histograms and their respective controls. Trypsinized cells at cells P2 were labelled with PE- or FITC-conjugated monoclonal antibodies (white histograms, dotted line) or corresponding isotypic controls (gray histograms, solid line). (b) Representative images of osteogenic differentiation, showing mineralization visualized by von Kossa staining (left) and Alizarin Red staining (right) at 21 days. (c) Representative image of adipogenic differentiation in which the lipid droplet formation was visualized by Oil Red O staining at 14 days.

3.2.11 In vitro biological response of BM-MSCs on CS:Gel scaffolds crosslinked with 0.1% v/v glutaraldehyde

The ability of glutaraldehyde crosslinked CS:Gel scaffolds to promote the adhesion, proliferation and ECM formation of BM-MSCs was also examined. SEM images illustrate the typical elongated, fibroblastic-like morphology of cells cultured on the material surface for 4 days. Cells covered the whole surface area and non-adherent small round-shaped cells were not observed (Figure 3.2.12 a and b). Moreover, the viability and proliferation of cells cultured on 3D scaffolds for 4 and 8 days, was significantly

increased compared to TCPS. No differences were observed between the two material surfaces after 12 days of culture. (Figure 3.2.12 c). The amount of collagen secreted by cells cultured on 3D CS:Gel scaffolds was significantly increased, compared to TCPS, after 14 days in culture (Figure 3.2.12 d).

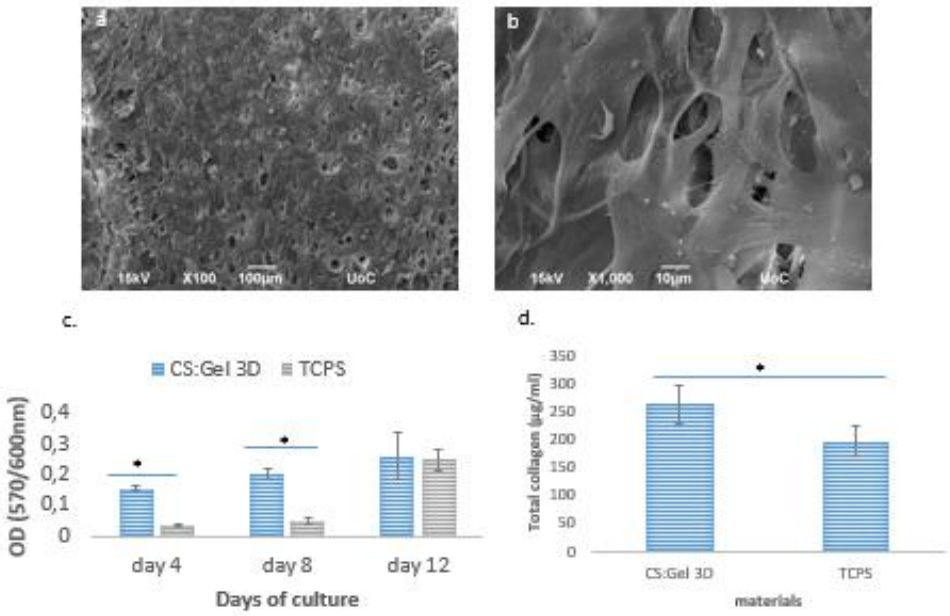

Figure 3.2.12: In vitro biological response of BM-MSCs cultured on 40%-60% CS:Gel scaffolds crosslinked with 0.1% v/v glutaraldehyde
(a and b) SEM images illustrating the morphology of cells cultured on the material surface for 4 days. (c) Viability and proliferation of cells after 4, 8 and 12 days in culture using TCPS surface as the control substrate. (d) Levels of collagen produced from cells cultured on 3D CS:Gel and TCPS surfaces for 14 days. Bars represent (a) 100 and (b) 10µm, respectively. Error bars represent the average of triplicates ± SE, of two independent experiments (n=6). *p<0.05 vs. TCPS.

3.2.12 Co-culture of BM-MSCs and HUVECs on CS:Gel scaffolds crosslinked with 0.1% glutaraldehyde

The morphology of monocultured and co-cultured cells on CS:Gel scaffolds crosslinked with glutaraldehyde was visualized using confocal laser fluorescence microscope (CLFM). Anti-CD31 antibody was used to stain HUVECs (red), and DAPI (blue) was used for nucleus staining of both BM-MSCs and HUVECs (Figure 3.2.13 a-c). HUVECs adhered and spread well on the pores of the scaffold exhibiting a cobblestone-like morphology

(Figure 3.2.13 b). Moreover, results showed that both BM-MSCs and HUVECs adhere well on the material surface (Figure 3.2.13 c). Viability and proliferation of monocultures and co-cultures at three different ratios (1:1 BM-MSCs/HUVECS, 1:5 BM-MSCs/HUVECs, 5:1 BM-MSCs/HUVECs) was also examined by using the PrestoBlue® assay. The viability and proliferation of BM-MSCs was increased when they were co-cultured with HUVECs both after 5 and 10 days of culture (Figure 3.2.13 d).

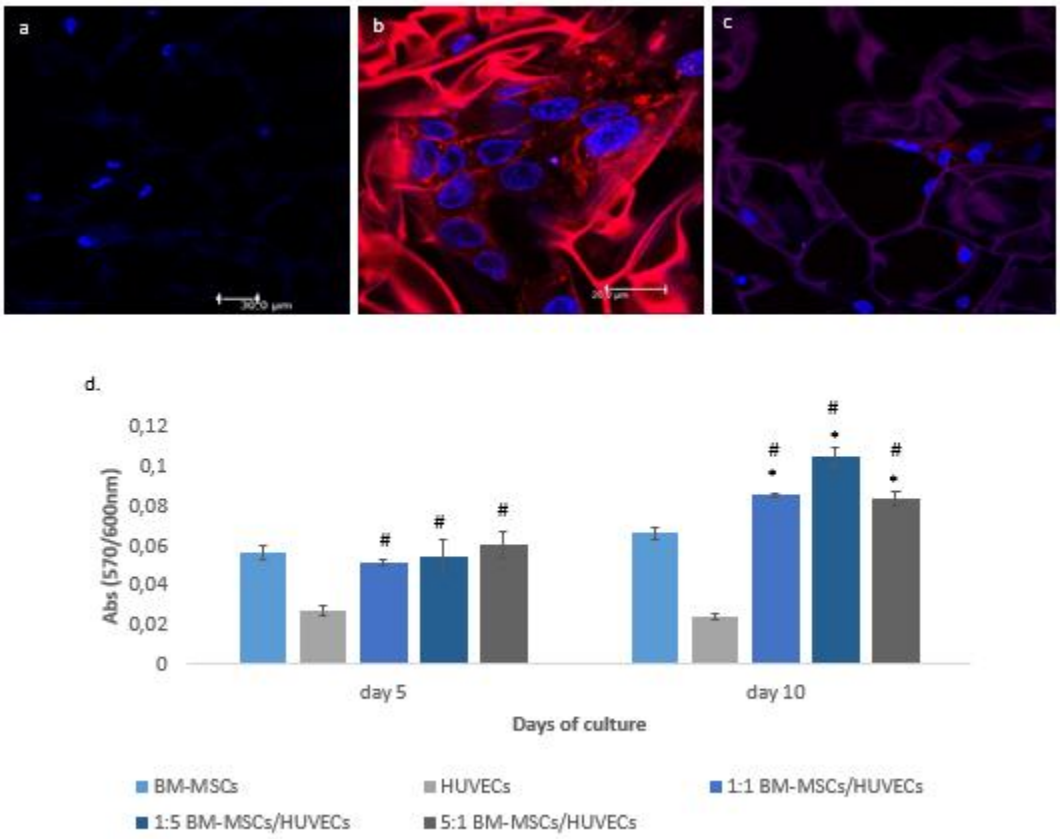

Figure 3.2.13: Co-culture of BM-MSCs and HUVECs on 40%-60% CS:Gel scaffolds crosslinked with 0.1% v/v glutaraldehyde.
(a-c) Confocal laser fluorescence images showing the morphology of monocultures (a and b, BM-MSCs and HUVECs respectively) and co-cultures (c) on the material surface after 5 days of culture. Original magnifications are x20 (a and c) and x40 (b). (d) Viability and proliferation of monocultures and co-cultures, 5 and 10 days after seeding. Error bars represent the average of triplicates ± SE, of two independent experiments (n=6). * p<0.05 vs. BM-MSCs, # p<0.05 vs. HUVECs.

4 Discussion

In the present thesis, two chitosan-based biomaterials were evaluated for their biocompatibility in terms of cell viability and proliferation, adhesion as well as osteogenic differentiation capacity. In the first biomaterial, **CS-*g*-PCL copolymer**, chitosan was combined with the synthetic biomaterial polycaprolactone, and in the second one, **CS:Gel**, chitosan was combined with the natural biomaterial gelatin. The CS-

g-PCL biomaterial was assessed in the form of films on glass substrates, while CS:Gel in the form of 3D porous scaffolds.

In the following two subsections, we will discuss the *in vitro* biological response of cells cultured on both biomaterials, CS-*g*-PCL copolymer films and CS:Gel porous scaffolds, under the prism of the literature.

4.1 *In vitro* biological response of MC3T3-E1 pre-osteoblastic cells on the CS-*g*-PCL material surface

The development of biomaterials for bone tissue engineering aims to provide favorable substrates for osteoblastic and mesenchymal stem cells to facilitate their functions such as cellular viability, proliferation, migration and differentiation towards tissue regeneration [68]. Ceramics were widely used as bone implants due to their stability and strength, but their bioactivity and compatibility are under exploration. On the other hand, many studies indicate the enhancement of osteogenesis both *in vitro* and *in vivo* with the use of biodegradable materials [99, 140]. Moreover, biocompatibility is another basic requirement for scaffolds for their use in tissue engineering applications [141]. All these factors determine the material selection for the fabrication of the suitable scaffolds. Chitosan, is a common natural polymer which is derived from chitin, the second most abundant polymer in nature. Chitosan has been extensively employed in tissue engineering applications due to its advantageous properties, derived from the diverse number of amino groups [142]. Many studies have shown that following blending or graft polymerization of chitosan with other polymers, the biological, mechanical and degradation characteristics are enhanced [143]. In this direction, PCL is a suitable synthetic polymer for blending with chitosan due to its low melting point and good tensile properties [144]. Young *et al*. have shown that CS-PCL blended membranes is a good biomaterial to fabricate bioengineered corneal endothelium and facilitate in this way the corneal endothelial cell (CEC) transplantation *in vivo* [145]. Moreover, Prasad *et al*. indicate that the adhesion, viability, and proliferation of human

keratinocytes (HaCaT) and mouse fibroblasts (L-929) cultured on electrospun chitosan/PCL blends were enhanced and proposed the use of these blends as appropriate biomaterials for skin tissue engineering [146].

Previous studies of our group have focused on the synthesis of a novel chitosan-graft-poly(ε-caprolactone) (CS-*g*-PCL) copolymer, in which PCL was chemically modified and grafted onto a chitosan backbone. This copolymer was used as a matrix for the development of Wharton's Jelly mesenchymal stem cells from three different donors and the results showed excellent cellular response [147]. In addition, the evaluation of the immunomodulatory potential of the copolymer material, by analyzing the differentiation of primary bone marrow derived macrophages (BMDM), suggests that CS-*g*-PCL promotes the anti-inflammatory activity and the transition of M1 to M2 macrophages. This immunomodulation is crucial for the prediction of the fate of a developed biomaterial in tissue engineering [148].

Based on the previous study, the aim of this study was to evaluate the *in vitro* biological response of MC3T3-E1 pre-osteoblastic cells on the CS-*g*-PCL surfaces. These cells, which can be easily obtained and cultured, have the capacity to differentiate into osteoblasts and osteocytes *in vitro* [149]. First, the adhesion of the cells on CS-*g*-PCL surfaces after 2 and 7 days of culture was examined by SEM analysis (Figure 3.1.1). Cells reached confluence on day 7 and retain their characteristic fibroblastic phenotype with a highly elongated spindle-like shape. This result is in accordance with previous studies in which CS-PCL blends promote the adhesion of bone marrow mesenchymal stem cells, fibroblasts, keratinocytes and corneal endothelial cells [142, 146, 150, 151]. Initial cell adhesion is a critical step in tissue engineering because it mediates subsequent events such as proliferation [152]. In our study, the viability and proliferation of the cells was examined using the colorimetric assay, PrestoBlue®. Figure 3.1.3 shows that the viability and proliferation of the MC3T3-E1 cells cultured on copolymeric material containing 80% wt chitosan was significantly increased compared to TCPS, after 3 and 7 days of culture. On the other hand, Ying et al. demonstrated that Bone Marrow Mesenchymal Stem Cells (BMMSCs) cultured on electrospun PCL-CS nanofibrous membrane showed

higher viability and proliferation as the concentration of PCL increased from 50% to 75% [142].

Our study on the *in vitro* assessment of pre-osteoblastic cells shows that the CS-*g*-PCL copolymer material supports the viability and proliferation as well as the differentiation of pre-osteoblastic cells. This was confirmed by a significant increase in the ALP activity for cells cultured on CS-*g*-PCL surfaces in contrast to TCPS (Figure 3.1.4). The increased levels of extracellular collagen at early stages of culture were also measured (Figure 3.1.5), indicating a healthy extracellular matrix formation on the copolymer surface, which is essential for tissue regeneration. In addition, the increased expression of osteopontin (Figure 3.1.7) as well as calcium deposits (Figure 3.1.6) for the cells cultured on CS-*g*-PCL films indicate that the copolymer material promotes the mineralized matrix formation. Young et al. showed that bovine corneal endothelial cells cultured on CS-PCL 75:25 blend membrane exhibited the highest production of collagen type IV, in contrast to CS-PCL 85-15 and CS-PCL 90-10 [145]. Finally, He *et al.* showed that a CS-PCL 30-70 composition favors the differentiation of bone marrow mesenchymal stem cells (BMSCs), compared to the CS-PCL 50-50 and CS-PCL 0-100 blends [142]. Finally, the expression of specific genes of osteogenesis was measured using semiquantitative RT-PCR. Figure 3.1.8 show that gene expression follow the same pattern and no statistical differences were observed for cells cultured in either CS-g-PCL or TCPS for 4 and 10 days. This may be explained by the small differences in gene expressions that couldn't be detected with semiquantitative RT-PCR. Real time PCR is necessary to detect these small differences in expressions of bone-related genes.

In conclusion, this study described the *in vivo* biological response of pre-osteoblastic cells on CS-*g*-PCL copolymer surfaces. Cells cultured on the material surface retain their characteristic fibroblastic morphology, interacting both with the substrate and with each other. The viability and proliferation of the cells cultured on the CS-*g*-PCL surfaces for 3 and 7 days was significantly increased compared to TCPS. Moreover, the increased levels of specific osteogenic markers of the cells cultured on the copolymer substrates indicate that the CS-*g*-PCL copolymer promotes the differentiation of pre-osteoblastic

cells into mature osteoblasts, demonstrating the potential of the graft copolymer for scaffold fabrication in bone tissue engineering applications.

4.2 Development of crosslinked chitosan/gelatin (CS:Gel) scaffolds and their potential to promote osteogenesis

Reconstruction of the maxillofacial complex and rehabilitation of mastigatory function following trauma, pathological processes or congenital deformities remains a clinical challenge. Natural materials are widely used as biomaterial scaffolds due to low toxicity, low chronic inflammatory response and their ability to enhance cell viability, proliferation and differentiation of cells [153]. Chitosan is a low cost biopolymer that has been used for various tissue engineering applications [111, 154]. In turn, gelatin was combined with chitosan as it enhances the mechanical and biological properties of chitosan [143, 155]. Gelatin exhibits important characteristics for tissue engineering such as biocompatibility, biodegradability, low antigenicity and high tensile strength [6]. Moreover, the freeze drying technique was used to produce porous scaffolds with interconnecting pores [3].

In the present study, 40:60% CS:Gel scaffolds were synthesized by crosslinking with two different crosslinker reagents, either the chemical compound glutaraldehyde or the natural genipin, which is extracted from gardenia fruits and is not cytotoxic for mammalian cells [118]. Both scaffold types, crosslinked with glutaraldehyde and genipin, indicate homogenous interconnecting spherical pores with a mean pore size in the range of 70-120 µm and 70-170 µm, respectively. The microstructure of the scaffolds including pore size of 70-110 µm and open porosity of 85-90% with interconnected channels allowing cells to migrate into the 3D structure and obtain nutrition from the culture medium have been reported to favor bone tissue engineering [156]. Moreover, the adhesion and proliferation of human bone marrow mesenchymal stem cells cultured on 3D hybrid scaffolds with 100 µm pore size has been reported to increase, compared to higher pore sizes [132].

The control of the mechanical properties of scaffolds affecting cell response is a critical parameter in tissue engineering [143]. The rheological analysis indicates no differences in dynamic storage between the two 40:60% CS:Gel scaffold types, crosslinked with glutaraldehyde and genipin. Both show a typical gel-like behavior with frequency independence of their storage modulus. Based on the enhanced pre-osteoblastic cell infiltration into the glutaraldehyde crosslinked 40:60% CS:Gel scaffolds compared to the genipin crosslinked counterparts observed by SEM (Figure 3.2.3), we performed the evaluation of the *in vitro* biological response in terms of cell morphology, viability and proliferation in pre-osteoblastic cells MC3T3-E1 and human BM-MSCs. Cells cultured on both scaffolds crosslinked with glutaraldehyde and genipin retain their characteristic fibroblast-like morphology and adhere by large attachment areas exhibiting numerous philopodia formations. However, scaffolds using glutaraldehyde as crosslinker demonstrate a higher cell infiltration within the pores compared to genipin crosslinked scaffolds. Chiono et al. reported that adhesion and proliferation of neuroblastoma cells were poor for various compositions of CS:Gel scaffolds using genipin as a crosslinker [130]. Although glutaraldehyde is not a natural crosslinking agent compared to genipin, we did not observe cytotoxicity in cultures of the MC3T3-E1 pre-osteoblastic cell line. In addition, other cell types such as fibroblasts and human umbilical vein endothelial cells (HUVECs) cultured on chitosan/gelatin scaffolds crosslinked with 0.25% v/v glutaraldehyde showed enhanced metabolic activity [154]. The behavior of a material towards the adhesion and proliferation of cells is affected by the cell line, as the mechanisms of adhesion and proliferation are cell-specific [130].

The water uptake ability of scaffolds is essential for tissue engineering applications [157] as it facilitates the transport of nutrients and metabolites through materials and the prevention of infections during wound healing through absorbing inflammation liquids [158]. High degrees of swelling increase the pore size and total porosity and subsequently maximize the internal surface area/volume ratio allowing the scaffolds to favor cell attachment and infiltration into the pores and thus enhance tissue growth. Water absorption increases as the concentration of the hydrophilic compound in a

composite scaffold increases [143]. Our results demonstrated a higher swelling degree for the glutaraldehyde crosslinked scaffolds compared to the genipin crosslinked ones and are in accordance with a previous study [159]. Cell response onto a material surface begins with adhesion, followed by migration, which is obtained by filopodia and lamellipodia and finally proliferation [160]. The basic advantage of 3D matrices is the high specific area provided for cell-cell and cell-matrix adhesion as well as support for cell traction [154]. In this study, pre-osteoblastic cells attached on 2D and 3D CS:Gel substrates, however, cell viability and proliferation after 7 days in culture was superior onto the 3D CS:Gel scaffolds. Similarly, the viability and proliferation of hBM-MSCs cultured on CS:Gel scaffolds for 4, 8 and 12 days was significantly increased in comparison to the TCPS control substrate, which is in line with previous studies, suggesting that different factors may affect the cell behavior. These factors include stiffness, surface topography and hydrophilicity and affect the biological processes of cells such as viability, proliferation, migration and differentiation [161, 162]. 3D cultures exhibit different stiffness compared to 2D, despite their identical chemical composition directly affecting the adhesion of cells [163]. The secretion of collagen in the extracellular matrix of cells is a marker usually examined in osteogenesis. It takes place in the intermediate phase of osteoblast differentiation and contributes to the formation of extracellular matrix, in which mineralization can occur [164]. The increased collagen levels, secreted by pre-osteoblasts cultured on the glutaraldehyde crosslinked CS:Gel scaffolds suggest that they provide an ideal microenvironment for cell differentiation.

Mesenchymal stem cells (MSCs) are multipotent adult cells that reside in the perivascular niche of the bone marrow and have the ability to self-renew and differentiate into multiple lineages, including osteogenic, adipogenic and chondrogenic. The localization of MSCs around blood vessels has prompted the investigation of cross-talk between MSCs and vascular cells for a variety of tissue engineering applications [165]. Many studies have shown that the co-culture of MSCs and vascular cells such as endothelial cells (ECs) enhance the osteogenic and angiogenic properties of tissue engineering constructs, because ECs express several factors such as BMP-2 that induce

osteogenic differentiation both *in vitro* and *in vivo* [166, 167]. This result was also confirmed in our study, where the viability and proliferation of hBM-MSCs was increased when they were co-cultured with endothelial cells both after 5 and 10 days of culture (Figure 3.2.13 d).

5 Conclusions

Chitosan is an important natural, biocompatible and biodegradable material in tissue engineering applications as it evokes minimal foreign body response and fibrous encapsulation as well as it promotes the wound healing. Based on these properties of chitosan, the objective of this thesis was to combine chitosan with other synthetic or natural polymers and examine their potential to promote osteogenesis.

In the first part of this thesis, a CS-*g*-PCL copolymer was used as a potential biomaterial for the adhesion, proliferation and differentiation of MC3T3-E1 pre-osteoblastic cells. These copolymers were synthesized and characterized by the research group of Prof.

Vamvakaki. Our results indicated that CS-*g*-PCL material surfaces enhance the adhesion, viability and proliferation of cells. Moreover, alkaline phosphatase activity, calcium deposits and intracellular osteopontin levels were higher for cells cultured on copolymer materials compared to TCPS substrates. Additionally, the expression levels of alkaline phosphatase (*alp*), collagen type I (*collaI*) and bone sialoprotein (*bsp*) genes were found to be similar for cells cultured both on CS-*g*-PCL and TCPS substrates. Based on these results, the CS-*g*-PCL copolymer elicit good biological response and due to its mechanical properties which are similar to cancellous bone, it may be a suitable biomaterial for bone regeneration.

In the second part of this thesis, chitosan was combined with the natural biomaterial gelatin for the production of chitosan/gelatin (CS:Gel) scaffolds. These scaffolds were fabricated by chemical crosslinking using either glutaraldehyde or genipin and were tested for their capacity to promote osteogenic response. Our results suggested that CS:Gel scaffolds crosslinked with both glutaraldehyde and genipin, elicit a similar structure morphology with a small difference in the pore size ranging between 40-120 μm and 70-170 μm, respectively. We continued our study with the glutaraldehyde crosslinked CS:Gel scaffolds due to their more efficient cell adhesion and infiltration. Among the four different ratios of CS:Gel scaffolds (80%-20% CS:Gel, 20%-80% CS:Gel, 40%-60% CS:Gel and 60%-40% CS:Gel), the viability and proliferation was significantly increased for cells cultured on 40%-60% CS:Gel scaffolds. Moreover, 40%-60% CS:Gel scaffolds crosslinked with two different concentrations of glutaraldehyde (0,1% v/v and 1% v/v) promote the adhesion, proliferation and extracellular matrix formation of MC3T3-E1 pre-osteoblastic cells. The results also showed that the degradation rate of 40%-60% CS:Gel scaffolds crosslinked with 0,1% v/v and 1% v/v glutaraldehyde was 48% and 18% of weight loss after 21 days, respectively. We also found that human bone marrow mesenchymal stem cells (BM-MSCs) cultured on glutaraldehyde crosslinked CS:Gel scaffolds were able to grow, proliferate and secrete collagen in their culture medium. Finally, co-culture of BM-MSCs with human umbilical vein cells (HUVECs) on

CS:Gel scaffolds resulted in increased proliferation rates for both cell types comparing to monocultures.

The above results show the potential of both chitosan-based materials to support new tissue formation and thus provide a promising strategy for cancellous bone tissue engineering applications.

6 Outlook and future work

As previously described, in the present thesis, two chitosan-based biomaterials were used to evaluate the viability, proliferation and differentiation of cells. In the first biomaterial, CS-*g*-PCL copolymer, the synthetic biomaterial polycaprolactone, is chemically grafted onto a chitosan backbone. Our results indicated that the CS-*g*-PCL material surfaces promote the in vitro biological response of MC3T3-E1 pre-osteoblastic cells. Therefore, it is suggested that CS-*g*-PCL copolymers may be useful as biodegradable and osteoconductive materials for load bearing grafts in bone defects. Based on these results, the *in vitro* and *in vivo* biological response of human bone-marrow mesenchymal stem cells (hBM-MSCs) cultured on 3D fabricated CS-*g*-PCL scaffolds could be the subject of future work that would provide a better insight into the cell-material interactions in three dimensions.

In the second biomaterial, CS:Gel, chitosan was chemically crosslinked with gelatin. Our results indicated that 40%-60% CS:Gel scaffolds enhance the viability, proliferation and extracellular matrix formation of MC3T3-E1 pre-osteoblastic cells and hBM-MSCs. Moreover, co-culture of BM-MSCs with human umbilical vein cells (HUVECs) on CS:Gel scaffolds resulted in increased proliferation rates for both cell types compared to the monocultures, which supports the notion that the developed CS:Gel scaffolds provide a suitable matrix for vascularized bone grafts, a prerequisite for the reconstruction of long

bones. For this, a thorough investigation of the interactions of both cell types within the scaffold is needed. Based on these results, the addition of hydroxyapatite (HA) on CS:Gel scaffolds may enhance their osteogenic potential as they mimic the chemical composition of bones (Appendix). HA is not only bioactive but also osteoconductive, non-toxic and non-immunogenic and its structure is crystallographically similar to that of bone mineral. Moreover, previous studies reported that nano-hydroxyapatite (nHA) precipitates may have higher solubility and therefore affect the biological responses [168].

7 Appendix

Hydroxyapatite (HA) is the major inorganic component of bone. It is an osteoconductive, non-toxic and non-inflammatory biomaterial, which promotes the proliferation and differentiation of osteoblastic cells. In this chapter, we present the combination of the natural biomaterials, chitosan and gelatin with nano-hydroxyapatite (nHA, nanopowder

<200 nm particle size) in order to better mimic the chemical composition of bones, their physicochemical characterization and biocompatibility assessment in terms of pre-osteoblastic cell viability and proliferation up to 7 days in culture.

7.1.1 Preparation of Chitosan/Gelatin/nanoHydroxyapatite (CS:Gel:nHA) scaffolds

The scaffolds were prepared by dissolving 4% w/v chitosan (CS) in a 1% v/v acetic acid and 4% w/v gelatin (Gel) in ultrapure demineralized water at 50 °C, according to Jun Ji *et. al* [168]. Moreover, 10% rod-like nano-hydroxyapatite (nHA) was dissolved in ultrapure demineralized water in room temperature. The solutions were poured together with the ratio of 5:2:3 CS:Gel:nHA respectively and stirred for 2 h at 50 °C. 400 µl/well of the above mixture were then casted into the wells of a 24 well plate, transferred to freeze at -20 °C overnight and lyophilized for 24 h at -40 °C. Lyophilized scaffolds were crosslinked with 0.1% v/v glutaraldehyde and lyophilized for another 24 h at -40 °C. Finally, scaffolds were neutralized by using 0.1 N NaOH, rinsed thoroughly with ultrapure water until pH was neutral and finally with PBS overnight prior their placing in a vented oven for 24 h at 37 °C.

7.1.2 Characterization of CS:Gel:nHA scaffolds

For the morphological characterization of the scaffolds, scanning electron microscopy was performed by using a JEOL JSM-6390 LV instrument in high vacuum after sputtering with a 20 nm thick layer of gold. Energy-dispersive X-ray spectroscopy (EDS) analysis was performed on JEOL JSM 6390 LV. A piece of CS:Gel:nHA scaffold was placed on carbon tape coated stub. The sample was then platinum coated for 1 min at 20 mA.

The Fourier transform infrared spectroscopy analysis (FTIR) of CS:Gel:nHA scaffolds was recorded using a Nicolet 6700 optical spectrometer within the region 400–4000 cm^{-1}. The spectral data were collected and the numerical values were transferred to Origin software for graphical representation.

The thermal stability of scaffolds was investigated by thermogravimetric analysis (TGA) using a Perkin Elmer Pyris Diamond TG/DTA instrument. Approximately 10-15 mg of the samples were placed in a platinum holder and were heated under constant nitrogen flow from room temperature up to 500 ^{o}C with a heating rate of 10 ^{o}C/min.

X-ray diffraction (XRD) analysis was performed to examine the crystallinity of the prepared CS:Gel:nHA scaffolds. XRD patterns were obtained on a PANanalytical X´pert Pro MPD powder diffractometer at 40 kV and 45 mA using CuKa radiation (λ =1.5418°).

Finally, the ability of lyophilized CS:Gel:nHA scaffolds to absorb water was determined by swelling them in phosphate buffer saline (PBS, pH 7.4). The dry samples were weighted and they were placed in PBS for 30 minutes. The excess of water was removed with filter paper and their weight was measured immediately. The percentage water uptake was examined using the following formula:

$W= W_1-W_0/W_0$,

where W_o is the weight of dried scaffolds, while W_1 is the weight of wet scaffolds after 30 min in PBS. The values were expressed as the mean +/- standard error (n=6).

7.1.3 Cell viability and proliferation

The viability of MC3T3-E1 pre-osteoblastic cells on CS:Gel:nHA scaffolds was determined by means of the PrestoBlue® assay. At each time point, at day 2, 5, and 7 in culture, 400 µl PrestoBlue® reagent diluted in α-MEM (1:10) was added directly to each well and incubated at 37 °C for 60 min. The supernatants of the samples were transferred to another 24-well plate and the absorbance was measured at 570 nm and 600 nm in a spectrophotometer (Synergy HTX Multi-Mode Microplate Reader, BioTek, Bad Friedrichshall, Germany). The seeded scaffolds were rinsed twice with PBS and placed in fresh culture medium. Tissue culture polystyrene (TCPS) was used as control. All samples were analyzed in triplicates of two independent experiments.

7.2.1 Morphology and swelling degree of CS:Gel:nHA scaffolds

The scaffolds were soft and elastic after neutralization in an aqueous solution in contrast to the inelastic and stiff as-prepared lyophilized counterparts. The morphology of CS:Gel:nHA scaffolds using glutaraldehyde (Fig.7.2.1 a and b) as crosslinker was observed by means of scanning electron microscopy (SEM). The pores of scaffolds appeared to be relatively spherical and flattened. The pore size of the scaffolds was mainly between 70 to 120 µm (a and b). Moreover, the water absorption was significantly lower in CS:Gel:nHA scaffolds compared to CS:Gel scaffolds (c). Water absorption of non-crosslinked scaffolds was not measured because scaffolds were dissolved in PBS after 12 h.

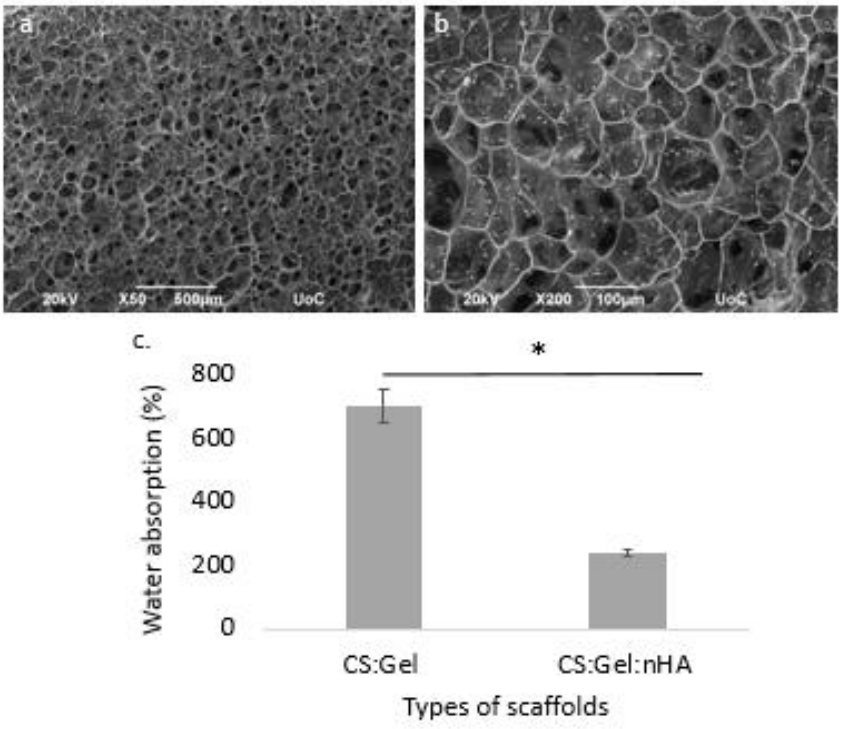

Figure 7.2.1: Morphology and swelling degree of CS:Gel:nHA scaffolds
(a and b) SEM images illustrating the morphology of CS:Gel:nHA scaffolds crosslinked with glutaraldehyde. The pores of scaffolds appeared to be spherical and interconnected with a mean pore size between 70-120 µm. (c) Percentage of water absorption of CS:Gel:nHA scaffolds crosslinked with glutaraldehyde. The swelling degree of the CS:Gel:nHA scaffolds was

significantly lower compared to the one of the CS:Gel scaffolds. Error bars represent the average of triplicates ± SE, of two independent experiments (n=6). *p<0.05 vs. TCPS.

7.2.2 Characterization of CS:Gel:nHA scaffolds

The EDS spectrum of nHA confirmed the presence of calcium, phosphate and oxygen peaks of nHA (Fig. 7.2.2 a).

FT-IR spectrum of nHA showed a peak at 3571 cm^{-1}, which corresponds to –OH stretching. The band at 1045 cm^{-1} corresponds to c3 of phosphate mode while the band at 571 cm^{-1} corresponds to c4 of phosphate. Comparing the FT-IR spectrum of CS:Gel (FT-IR spectrum was described in 3.2.7 section) with CS:Gel:nHA (Fig. 7.2.2 b) , suggests that characteristic bands of nHA, chitosan and gelatin are present in the composite scaffolds.

XRD spectrum of nHA shows diffraction peak at 25.7, 32.2, 32.9, 46.8 and 49.5. The XRD of CS:Gel:nHA scaffolds (Fig. 7.2.3 a) scaffold showed peaks at 32.2 attributed to the presence of nHA in the composite scaffold, which was absent in CS:Gel scaffolds, and this is in accordance with a previous report of Peter et al. [169].

The TGA data of CS:Gel:nHA scaffolds show after the water evaporation a relative sharp degradation step of the organic components starting at 250 ^{o}C and ending at approximately 450 ^{o}C, with a maximum decomposition rate at 400 ^{o}C and a weight loss of ~ 50 %. At temperatures higher than 450 ^{o}C, there is a slight decrease of the weight and a remaining weight of ~ 50% corresponding to the inorganic part of the nHA compound (Fig. 7.2.3 b).

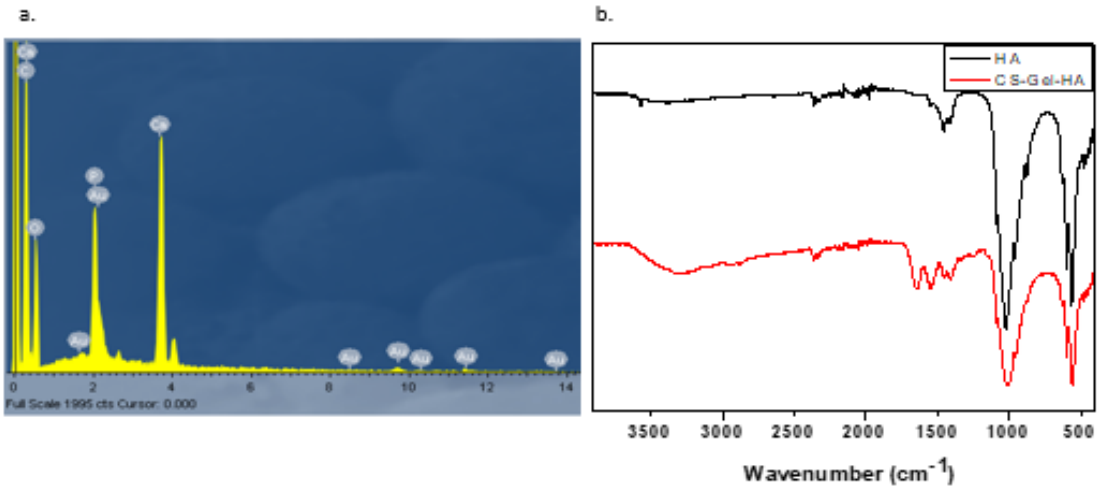

Figure 7.2.2: EDS and FTIR analysis of CS:Gel:nHA scaffolds

(a) EDS analysis of CS:Gel:nHA scaffolds confirmed the presence of calcium, phosphate and oxygen peaks of nHA. (b) FTIR analysis CS:Gel:nHA scaffolds suggests that the characteristic bands of nHA, chitosan and gelatin are present in the composite scaffolds.

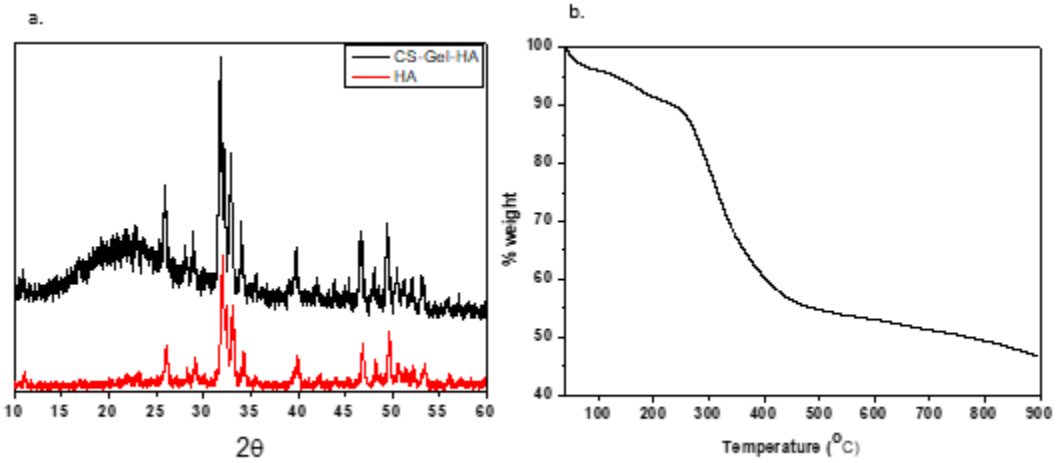

Figure 7.2.3: XRD and TGA analysis of CS:Gel:nHA scaffolds

(a) XRD analysis of CS:Gel:nHA scaffolds confirmed the presence of HA in scaffolds with the characteristic peak around 32° (2θ). (b) TGA analysis shows a sharp degradation step of the organic compounds between 250 and 450 ^{o}C, and a remaining weight of 50% corresponding to the inorganic nHA compound.

7.2.3 Viability and proliferation of pre-osteoblatsic cells on CS:Gel:nHA scaffolds

The viability and proliferation of pre-osteoblastic cells on CS:Gel:nHA scaffolds was assessed by the PrestoBlue® assay after 2, 5 and 7 days of culture. The viability and proliferation of cells cultured on the CS:Gel:nHA scaffolds was significantly increased compared to TCPS, after 2 days in culture. No significant differences were observed between the two material surfaces after 5 and 7 days of culture (Figure 7.2.4).

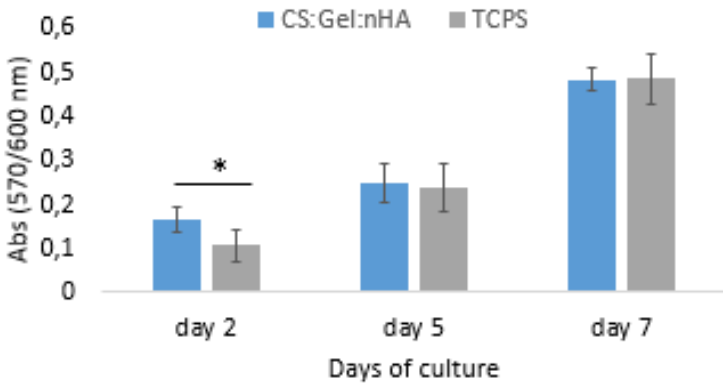

Figure 7.2.4: Viability and proliferation of pre-osteoblastic cells on CS:Gel:nHA and TCPS substrates.
Viability and proliferation of cells on CS:Gel:nHA and TCPS surfaces after 2, 5 and 7 days of culture. The viability and proliferation of cells cultured on CS:Gel:nHA scaffolds was significantly increased compared to TCPS, after 2 days of culture. Error bars represent the average of triplicates ± SE, of two independent experiments (n=6), *p<0.05 vs. TCPS.

7.3 Conclusions

Hydroxyapatite (HA) is an important component of human bone and bone tissue engineering scaffolds. This non-toxic, osteoconductive and anti-inflammatory biomaterial was combined with chitosan and gelatin in order to better mimic the chemical composition of bones. CS:Gel:nHA scaffolds with a mean pore size between 70-120 µm, were successfully fabricated by freeze-drying. EDS, FTIR and XRD analysis confirm the presence of HA in 3D porous scaffolds. The ability of scaffolds to absorb water was decreased after the addition of HA. The viability and proliferation of MC3T3-E1 pre-osteoblastic cells on CS:Gel:nHA scaffolds were significantly increased compared

to TCPS substrates after 2 days of culture. Previous studies demonstrated that the presence of nHA improves both the biological and mechanical properties of CS:Gel scaffolds [168]. Thus, the addition of nHA to CS:Gel scaffolds can constitute a promising scaffold for tissue engineering applications. However, additional experiments are needed in order to examine the ability of these scaffolds to promote the differentiation of cells both *in vitro* and *in vivo*.

8 References

1. Fratzl, P., *Bone fracture: When the cracks begin to show.* Nat Mater, 2008. **7**(8): p. 610-2.
2. Sarasam, A. and S.V. Madihally, *Characterization of chitosan-polycaprolactone blends for tissue engineering applications.* Biomaterials, 2005. **26**(27): p. 5500-8.
3. Mao, J.S., et al., *Structure and properties of bilayer chitosan-gelatin scaffolds.* Biomaterials, 2003. **24**(6): p. 1067-74.
4. Tseng, H.J., et al., *Characterization of chitosan-gelatin scaffolds for dermal tissue engineering.* J Tissue Eng Regen Med, 2013. **7**(1): p. 20-31.
5. Wang, P.Y., et al., *Dynamic compression modulates chondrocyte proliferation and matrix biosynthesis in chitosan/gelatin scaffolds.* J Biomed Mater Res B Appl Biomater, 2009. **91**(1): p. 143-52.
6. Miranda, S.C., et al., *Three-dimensional culture of rat BMMSCs in a porous chitosan-gelatin scaffold: A promising association for bone tissue engineering in oral reconstruction.* Arch Oral Biol, 2011. **56**(1): p. 1-15.
7. Clarke, B., *Normal bone anatomy and physiology.* Clin J Am Soc Nephrol, 2008. **3 Suppl 3**: p. S131-9.
8. Taichman, R.S., *Blood and bone: two tissues whose fates are intertwined to create the hematopoietic stem-cell niche.* Blood, 2005. **105**(7): p. 2631-9.
9. Wolf, G. *Function of the Bone Protein Osteocalcin Definitive Evidence, Nutrition Reviews Volume 54, Issue 10*. Nutrition Reviews, 1996. **54**, 332-333.
10. Boskey, A.L., *Bone composition: relationship to bone fragility and antiosteoporotic drug effects.* Bonekey Rep, 2013. **2**: p. 447.
11. Gdyczynski, C.M., et al., *On estimating the directionality distribution in pedicle trabecular bone from micro-CT images.* Physiol Meas, 2014. **35**(12): p. 2415-28.
12. Eriksen, E.F., *Normal and pathological remodeling of human trabecular bone: three dimensional reconstruction of the remodeling sequence in normals and in metabolic bone disease.* Endocr Rev, 1986. **7**(4): p. 379-408.
13. Zimmerman, D., et al., *Impaired bone formation in transgenic mice resulting from altered integrin function in osteoblasts.* Dev Biol, 2000. **220**(1): p. 2-15.
14. Rey, C., et al., *Bone mineral: update on chemical composition and structure.* Osteoporos Int, 2009. **20**(6): p. 1013-21.
15. Brodsky, B. and A.V. Persikov, *Molecular structure of the collagen triple helix.* Adv Protein Chem, 2005. **70**: p. 301-39.
16. Termine, J.D., *Non-collagen proteins in bone.* Ciba Found Symp, 1988. **136**: p. 178-202.
17. Grof, J., et al., *Non-collagen proteins of stapedial bone matrix in perilymph of otosclerotic patients.* Acta Otolaryngol, 1985. **99**(5-6): p. 557-63.
18. Brighton, C.T. and R.M. Hunt, *Histochemical localization of calcium in the fracture callus with potassium pyroantimonate. Possible role of chondrocyte mitochondrial calcium in callus calcification.* J Bone Joint Surg Am, 1986. **68**(5): p. 703-15.
19. Cremers, S. and A. Farooki *Biochemical markers of bone turnover in osteonecrosis of the jaw in patients with osteoporosis and advanced cancer involving the bone Annals of the New York Academy of Sciences Volume 1218, Issue 1*. Annals of the New York Academy of Sciences, 2011. **1218**, 80-87.
20. Burr, D.B., *Targeted and nontargeted remodeling.* Bone, 2002. **30**(1): p. 2-4.

21. Rucci, N., *Molecular biology of bone remodelling.* Clin Cases Miner Bone Metab, 2008. **5**(1): p. 49-56.
22. Bruzzaniti, A. and R. Baron, *Molecular regulation of osteoclast activity.* Rev Endocr Metab Disord, 2006. **7**(1-2): p. 123-39.
23. Marquis, M.E., et al., *Bone cells-biomaterials interactions.* Front Biosci (Landmark Ed), 2009. **14**: p. 1023-67.
24. Caetano-Lopes, J., H. Canhao, and J.E. Fonseca, *Osteoblasts and bone formation.* Acta Reumatol Port, 2007. **32**(2): p. 103-10.
25. Lew, K.S., et al., *Macroporous bioceramics: a remarkable material for bone regeneration.* J Biomater Appl, 2012. **27**(3): p. 345-58.
26. Mackie, E.J., *Osteoblasts: novel roles in orchestration of skeletal architecture.* Int J Biochem Cell Biol, 2003. **35**(9): p. 1301-5.
27. Harada, S. and G.A. Rodan, *Control of osteoblast function and regulation of bone mass.* Nature, 2003. **423**(6937): p. 349-55.
28. Raggatt, L.J. and N.C. Partridge, *Cellular and molecular mechanisms of bone remodeling.* J Biol Chem, 2010. **285**(33): p. 25103-8.
29. Aarden, E.M., E.H. Burger, and P.J. Nijweide, *Function of osteocytes in bone.* J Cell Biochem, 1994. **55**(3): p. 287-99.
30. Buenzli, P.R. and N.A. Sims, *Quantifying the osteocyte network in the human skeleton.* Bone, 2015. **75**: p. 144-50.
31. Matic, I., et al., *Quiescent Bone Lining Cells Are a Major Source of Osteoblasts During Adulthood.* Stem Cells, 2016. **34**(12): p. 2930-2942.
32. Yamashita, T., N. Takahashi, and N. Udagawa, *New roles of osteoblasts involved in osteoclast differentiation.* World J Orthop, 2012. **3**(11): p. 175-81.
33. Sila-Asna, M., et al., *Osteoblast differentiation and bone formation gene expression in strontium-inducing bone marrow mesenchymal stem cell.* Kobe J Med Sci, 2007. **53**(1-2): p. 25-35.
34. Arboleya, L. and S. Castaneda, *Osteoimmunology: the study of the relationship between the immune system and bone tissue.* Reumatol Clin, 2013. **9**(5): p. 303-15.
35. Lazner, F., et al., *Osteopetrosis and osteoporosis: two sides of the same coin.* Hum Mol Genet, 1999. **8**(10): p. 1839-46.
36. Golub, E.E., et al., *The role of alkaline phosphatase in cartilage mineralization.* Bone Miner, 1992. **17**(2): p. 273-8.
37. Orimo, H., *The mechanism of mineralization and the role of alkaline phosphatase in health and disease.* J Nippon Med Sch, 2010. **77**(1): p. 4-12.
38. Siffert, R.S., *The role of alkaline phosphatase in osteogenesis.* J Exp Med, 1951. **93**(5): p. 415-26.
39. Shoulders, M.D. and R.T. Raines, *Collagen structure and stability.* Annu Rev Biochem, 2009. **78**: p. 929-58.
40. Ricard-Blum, S. and F. Ruggiero, *The collagen superfamily: from the extracellular matrix to the cell membrane.* Pathol Biol (Paris), 2005. **53**(7): p. 430-42.
41. Sakamoto, A., et al., *A comparative study of fibrous dysplasia and osteofibrous dysplasia with regard to expressions of c-fos and c-jun products and bone matrix proteins: a clinicopathologic review and immunohistochemical study of c-fos, c-jun, type I collagen, osteonectin, osteopontin, and osteocalcin.* Hum Pathol, 1999. **30**(12): p. 1418-26.
42. Ireton, J.E., J.G. Unger, and R.J. Rohrich, *The role of wound healing and its everyday application in plastic surgery: a practical perspective and systematic review.* Plast Reconstr Surg Glob Open, 2013. **1**(1).

43. Lund, S.A., C.M. Giachelli, and M. Scatena, *The role of osteopontin in inflammatory processes.* J Cell Commun Signal, 2009. **3**(3-4): p. 311-22.
44. Denhardt, D.T. and X. Guo, *Osteopontin: a protein with diverse functions.* FASEB J, 1993. **7**(15): p. 1475-82.
45. Kerr, J.M., et al., *The human bone sialoprotein gene (IBSP): genomic localization and characterization.* Genomics, 1993. **17**(2): p. 408-15.
46. Harris, N.L., et al., *Functional analysis of bone sialoprotein: identification of the hydroxyapatite-nucleating and cell-binding domains by recombinant peptide expression and site-directed mutagenesis.* Bone, 2000. **27**(6): p. 795-802.
47. Malaval, L., et al., *Bone sialoprotein plays a functional role in bone formation and osteoclastogenesis.* J Exp Med, 2008. **205**(5): p. 1145-53.
48. Ogata, Y., *Bone sialoprotein and its transcriptional regulatory mechanism.* J Periodontal Res, 2008. **43**(2): p. 127-35.
49. Kalfas, I.H., *Principles of bone healing.* Neurosurg Focus, 2001. **10**(4): p. E1.
50. Marsell, R. and T.A. Einhorn, *The biology of fracture healing.* Injury, 2011. **42**(6): p. 551-5.
51. Yamagiwa, H. and N. Endo, *[Bone fracture and the healing mechanisms. Histological aspect of fracture healing. Primary and secondary healing].* Clin Calcium, 2009. **19**(5): p. 627-33.
52. Egermann, M., et al., *Effect of BMP-2 gene transfer on bone healing in sheep.* Gene Ther, 2006. **13**(17): p. 1290-9.
53. Bigham, A.S., et al., *Xenogenic demineralized bone matrix and fresh autogenous cortical bone effects on experimental bone healing: radiological, histopathological and biomechanical evaluation.* J Orthop Traumatol, 2008. **9**(2): p. 73-80.
54. Bansal, M.R., S.B. Bhagat, and D.D. Shukla, *Bovine cancellous xenograft in the treatment of tibial plateau fractures in elderly patients.* Int Orthop, 2009. **33**(3): p. 779-84.
55. Kinnane, N., *Burden of bone disease.* Eur J Oncol Nurs, 2007. **11 Suppl 2**: p. S28-31.
56. Gaston, M.S. and A.H. Simpson, *Inhibition of fracture healing.* J Bone Joint Surg Br, 2007. **89**(12): p. 1553-60.
57. Starr, A.J., *Fracture repair: successful advances, persistent problems, and the psychological burden of trauma.* J Bone Joint Surg Am, 2008. **90 Suppl 1**: p. 132-7.
58. Einhorn, T.A., *The cell and molecular biology of fracture healing.* Clin Orthop Relat Res, 1998(355 Suppl): p. S7-21.
59. Gomez-Barrena, E., et al., *Bone regeneration: stem cell therapies and clinical studies in orthopaedics and traumatology.* J Cell Mol Med, 2011. **15**(6): p. 1266-86.
60. Arvidson, K., et al. *Bone regeneration and stem cells Journal of Cellular and Molecular Medicine Volume 15, Issue 4*. Journal of Cellular and Molecular Medicine, 2011. **15**, 718-746.
61. Babhulkar, S., K. Pande, and S. Babhulkar, *Nonunion of the diaphysis of long bones.* Clin Orthop Relat Res, 2005(431): p. 50-6.
62. Gomez-Barrena, E., et al., *Bone fracture healing: cell therapy in delayed unions and nonunions.* Bone, 2015. **70**: p. 93-101.
63. Liu, J. and D.G. Kerns, *Mechanisms of guided bone regeneration: a review.* Open Dent J, 2014. **8**: p. 56-65.
64. Hobby, B. and M.A. Lee, *Managing atrophic nonunion in the geriatric population: incidence, distribution, and causes.* Orthop Clin North Am, 2013. **44**(2): p. 251-6.
65. Vats, A., et al., *Scaffolds and biomaterials for tissue engineering: a review of clinical applications.* Clin Otolaryngol Allied Sci, 2003. **28**(3): p. 165-72.

66. Griffith, L.G. and M.A. Swartz, *Capturing complex 3D tissue physiology in vitro.* Nat Rev Mol Cell Biol, 2006. **7**(3): p. 211-24.
67. Antoni, D., et al., *Three-dimensional cell culture: a breakthrough in vivo.* Int J Mol Sci, 2015. **16**(3): p. 5517-27.
68. Howard, D., et al., *Tissue engineering: strategies, stem cells and scaffolds.* J Anat, 2008. **213**(1): p. 66-72.
69. Brochhausen, C., et al., *[Tissue engineering of cartilage and bone : growth factors and signaling molecules].* Orthopade, 2009. **38**(11): p. 1053-62.
70. Bernstein, H.S. and D. Srivastava, *Stem cell therapy for cardiac disease.* Pediatr Res, 2012. **71**(4 Pt 2): p. 491-9.
71. Hoffman, L.M. and M.K. Carpenter, *Characterization and culture of human embryonic stem cells.* Nat Biotechnol, 2005. **23**(6): p. 699-708.
72. Naderi, H., M.M. Matin, and A.R. Bahrami, *Review paper: critical issues in tissue engineering: biomaterials, cell sources, angiogenesis, and drug delivery systems.* J Biomater Appl, 2011. **26**(4): p. 383-417.
73. Qayyum, A.A., et al., *Adipose-derived mesenchymal stromal cells for chronic myocardial ischemia (MyStromalCell Trial): study design.* Regen Med, 2012. **7**(3): p. 421-8.
74. Weber, B., S.M. Zeisberger, and S.P. Hoerstrup, *Prenatally harvested cells for cardiovascular tissue engineering: fabrication of autologous implants prior to birth.* Placenta, 2011. **32 Suppl 4**: p. S316-9.
75. Jin, H.J., et al., *Comparative analysis of human mesenchymal stem cells from bone marrow, adipose tissue, and umbilical cord blood as sources of cell therapy.* Int J Mol Sci, 2013. **14**(9): p. 17986-8001.
76. Colnot, C., *Cell sources for bone tissue engineering: insights from basic science.* Tissue Eng Part B Rev, 2011. **17**(6): p. 449-57.
77. Phinney, D.G. and D.J. Prockop, *Concise review: mesenchymal stem/multipotent stromal cells: the state of transdifferentiation and modes of tissue repair--current views.* Stem Cells, 2007. **25**(11): p. 2896-902.
78. Farini, A., et al., *Clinical applications of mesenchymal stem cells in chronic diseases.* Stem Cells Int, 2014. **2014**: p. 306573.
79. Kim, N. and S.G. Cho, *Clinical applications of mesenchymal stem cells.* Korean J Intern Med, 2013. **28**(4): p. 387-402.
80. Sant, S., et al., *Biomimetic Gradient Hydrogels for Tissue Engineering.* Can J Chem Eng, 2010. **88**(6): p. 899-911.
81. Even-Ram, S. and K.M. Yamada, *Cell migration in 3D matrix.* Curr Opin Cell Biol, 2005. **17**(5): p. 524-32.
82. Kanczler, J.M. and R.O. Oreffo, *Osteogenesis and angiogenesis: the potential for engineering bone.* Eur Cell Mater, 2008. **15**: p. 100-14.
83. Tayalia, P. and D.J. Mooney, *Controlled growth factor delivery for tissue engineering.* Adv Mater, 2009. **21**(32-33): p. 3269-85.
84. Gothard, D., et al., *Tissue engineered bone using select growth factors: A comprehensive review of animal studies and clinical translation studies in man.* Eur Cell Mater, 2014. **28**: p. 166-207; discussion 207-8.
85. Dutta, R.C. and A.K. Dutta, *Cell-interactive 3D-scaffold; advances and applications.* Biotechnol Adv, 2009. **27**(4): p. 334-9.
86. Lu, P., V.M. Weaver, and Z. Werb, *The extracellular matrix: a dynamic niche in cancer progression.* J Cell Biol, 2012. **196**(4): p. 395-406.

87. Chan, B.P. and K.W. Leong, *Scaffolding in tissue engineering: general approaches and tissue-specific considerations.* Eur Spine J, 2008. **17 Suppl 4**: p. 467-79.
88. Berger, J., et al., *Structure and interactions in covalently and ionically crosslinked chitosan hydrogels for biomedical applications.* Eur J Pharm Biopharm, 2004. **57**(1): p. 19-34.
89. Szczepanska, J., et al., *Protective effect of chitosan oligosaccharide lactate against DNA double-strand breaks induced by a model methacrylate dental adhesive.* Med Sci Monit, 2011. **17**(8): p. BR201-208.
90. Phelps, E.A. and A.J. Garcia, *Update on therapeutic vascularization strategies.* Regen Med, 2009. **4**(1): p. 65-80.
91. Ko, H.C., B.K. Milthorpe, and C.D. McFarland, *Engineering thick tissues--the vascularisation problem.* Eur Cell Mater, 2007. **14**: p. 1-18; discussion 18-9.
92. O'Brien, F.J., et al., *The effect of pore size on cell adhesion in collagen-GAG scaffolds.* Biomaterials, 2005. **26**(4): p. 433-41.
93. Ansaloni, L., et al., *Hernia repair with porcine small-intestinal submucosa.* Hernia, 2007. **11**(4): p. 321-6.
94. Hench, L.L., *Biomaterials: a forecast for the future.* Biomaterials, 1998. **19**(16): p. 1419-23.
95. Gotman, I., *Characteristics of metals used in implants.* J Endourol, 1997. **11**(6): p. 383-9.
96. Polo-Corrales, L., M. Latorre-Esteves, and J.E. Ramirez-Vick, *Scaffold design for bone regeneration.* J Nanosci Nanotechnol, 2014. **14**(1): p. 15-56.
97. Ulery, B.D., L.S. Nair, and C.T. Laurencin, *Biomedical Applications of Biodegradable Polymers.* J Polym Sci B Polym Phys, 2011. **49**(12): p. 832-864.
98. Xynos, I.D., et al., *Bioglass 45S5 stimulates osteoblast turnover and enhances bone formation In vitro: implications and applications for bone tissue engineering.* Calcif Tissue Int, 2000. **67**(4): p. 321-9.
99. Amini, A.R., C.T. Laurencin, and S.P. Nukavarapu, *Bone tissue engineering: recent advances and challenges.* Crit Rev Biomed Eng, 2012. **40**(5): p. 363-408.
100. Hench, L.L. and J.M. Polak, *Third-generation biomedical materials.* Science, 2002. **295**(5557): p. 1014-7.
101. Jaeger, W. *Principles of polymer engineering. Van N. G. MCCRUM, C. P. BUCKLEY und C. B. BUCKNALL. ISBN 0-19-856155-5. Oxford Oxford University Press 1988. XII, 391 S., geb. Volume 42, Issue 1*. Acta Polymerica, 1991. **42**, 52-52.
102. Liu, X. and P.X. Ma, *Polymeric scaffolds for bone tissue engineering.* Ann Biomed Eng, 2004. **32**(3): p. 477-86.
103. Langer, R. and D.A. Tirrell, *Designing materials for biology and medicine.* Nature, 2004. **428**(6982): p. 487-92.
104. Weigel, T., G. Schinkel, and A. Lendlein, *Design and preparation of polymeric scaffolds for tissue engineering.* Expert Rev Med Devices, 2006. **3**(6): p. 835-51.
105. Ge, Z., Z. Jin, and T. Cao, *Manufacture of degradable polymeric scaffolds for bone regeneration.* Biomed Mater, 2008. **3**(2): p. 022001.
106. Wang, F., et al., *Degradable/non-degradable polymer composites for in-situ tissue engineering small diameter vascular prosthesis application.* Biomed Mater Eng, 2014. **24**(6): p. 2127-33.
107. Gunatillake, P.A. and R. Adhikari, *Biodegradable synthetic polymers for tissue engineering.* Eur Cell Mater, 2003. **5**: p. 1-16; discussion 16.
108. Rinaudo, M. *Chitin and Chitosan ? Properties and Applications ChemInform Volume 38, Issue 27*. ChemInform, 2007. **38**, no.

109. Venkatesan, J. and S.K. Kim, *Chitosan composites for bone tissue engineering--an overview.* Mar Drugs, 2010. **8**(8): p. 2252-66.
110. Miranda, S.C.C.C., et al., *Three-dimensional culture of rat BMMSCs in a porous chitosan-gelatin scaffold: A promising association for bone tissue engineering in oral reconstruction.* Archives of Oral Biology, 2011. **56**(1): p. 1-15.
111. Di Martino, A., M. Sittinger, and M.V. Risbud, *Chitosan: a versatile biopolymer for orthopaedic tissue-engineering.* Biomaterials, 2005. **26**(30): p. 5983-90.
112. Cheung, R.C., et al., *Chitosan: An Update on Potential Biomedical and Pharmaceutical Applications.* Mar Drugs, 2015. **13**(8): p. 5156-86.
113. Lopez-Garcia, J., et al., *HaCaT Keratinocytes Response on Antimicrobial Atelocollagen Substrates: Extent of Cytotoxicity, Cell Viability and Proliferation.* J Funct Biomater, 2014. **5**(2): p. 43-57.
114. Nwe, N., T. Furuike, and H. Tamura, *Isolation and characterization of chitin and chitosan from marine origin.* Adv Food Nutr Res, 2014. **72**: p. 1-15.
115. Sritanaudomchai, H., et al. *Characterization and multilineage differentiation of embryonic stem cells derived from a buffalo parthenogenetic embryo Molecular Reproduction and Development Volume 74, Issue 10*. Molecular Reproduction and Development, 2007. **74**, 1295-1302.
116. Xia, W., et al. *Tissue engineering of cartilage with the use of chitosan-gelatin complex scaffolds Journal of Biomedical Materials Research Part B: Applied Biomaterials Volume 71B, Issue 2*. Journal of Biomedical Materials Research Part B: Applied Biomaterials, 2004. **71B**, 373-380.
117. Ueno, H., T. Mori, and T. Fujinaga, *Topical formulations and wound healing applications of chitosan.* Adv Drug Deliv Rev, 2001. **52**(2): p. 105-15.
118. Muzzarelli, R.A., et al., *Biochemistry, histology and clinical uses of chitins and chitosans in wound healing.* EXS, 1999. **87**: p. 251-64.
119. Heber, D., *Herbal preparations for obesity: are they useful?* Prim Care, 2003. **30**(2): p. 441-63.
120. Djagny, V.B., Z. Wang, and S. Xu, *Gelatin: a valuable protein for food and pharmaceutical industries: review.* Crit Rev Food Sci Nutr, 2001. **41**(6): p. 481-92.
121. Wang, H.M., et al., *Novel biodegradable porous scaffold applied to skin regeneration.* PLoS One, 2013. **8**(6): p. e56330.
122. Ma, P.X. and R. Langer, *Fabrication of biodegradable polymer foams for cell transplantation and tissue engineering.* Methods Mol Med, 1999. **18**: p. 47-56.
123. Lu, T., Y. Li, and T. Chen, *Techniques for fabrication and construction of three-dimensional scaffolds for tissue engineering.* Int J Nanomedicine, 2013. **8**: p. 337-50.
124. Loh, Q.L. and C. Choong, *Three-dimensional scaffolds for tissue engineering applications: role of porosity and pore size.* Tissue Eng Part B Rev, 2013. **19**(6): p. 485-502.
125. Nam, Y.S. and T.G. Park, *Porous biodegradable polymeric scaffolds prepared by thermally induced phase separation.* J Biomed Mater Res, 1999. **47**(1): p. 8-17.
126. Autissier, A., et al., *Fabrication of porous polysaccharide-based scaffolds using a combined freeze-drying/cross-linking process.* Acta Biomater, 2010. **6**(9): p. 3640-8.
127. Burke, R.F. and R.V. Decareau, *Recent Advances in the Freeze-Drying of Food Products.* Adv Food Res, 1964. **13**: p. 1-88.
128. Stevens, B., et al. *A review of materials, fabrication methods, and strategies used to enhance bone regeneration in engineered bone tissues Journal of Biomedical Materials Research Part B: Applied Biomaterials Volume 85B, Issue 2*. Journal of Biomedical Materials Research Part B: Applied Biomaterials, 2008. **85B**, 573-582.

129. Chatzinikolaidou, M., et al., *Wharton's jelly Mesenchymal Stem Cell response on chitosan-graft-poly (epsilon-caprolactone) copolymer for myocardium tissue engineering.* Curr Pharm Des, 2014. **20**(12): p. 2030-9.
130. Chiono, V., et al., *Genipin-crosslinked chitosan/gelatin blends for biomedical applications.* J Mater Sci Mater Med, 2008. **19**(2): p. 889-98.
131. Delorme, B. and P. Charbord, *Culture and characterization of human bone marrow mesenchymal stem cells.* Methods Mol Med, 2007. **140**: p. 67-81.
132. Chatzinikolaidou, M., et al., *Recombinant human bone morphogenetic protein 2 (rhBMP-2) immobilized on laser-fabricated 3D scaffolds enhance osteogenesis.* Colloids Surf B Biointerfaces, 2017. **149**: p. 233-242.
133. Sotiropoulou, P.A., et al., *Characterization of the optimal culture conditions for clinical scale production of human mesenchymal stem cells.* Stem Cells, 2006. **24**(2): p. 462-71.
134. Alsberg, E., H.A. von Recum, and M.J. Mahoney, *Environmental cues to guide stem cell fate decision for tissue engineering applications.* Expert Opin Biol Ther, 2006. **6**(9): p. 847-66.
135. Kaigler, D., et al., *Endothelial cell modulation of bone marrow stromal cell osteogenic potential.* FASEB J, 2005. **19**(6): p. 665-7.
136. Hadjicharalambous, C., et al., *Effects of NSAIDs on the osteogenic differentiation of human adipose tissue-derived stromal cells.* J Pharm Pharmacol, 2016. **68**(11): p. 1403-1408.
137. Hadjicharalambous, C., et al., *Proliferation and osteogenic response of MC3T3-E1 pre-osteoblastic cells on porous zirconia ceramics stabilized with magnesia or yttria.* J Biomed Mater Res A, 2015. **103**(11): p. 3612-24.
138. Lattouf, R., et al., *Picrosirius red staining: a useful tool to appraise collagen networks in normal and pathological tissues.* J Histochem Cytochem, 2014. **62**(10): p. 751-8.
139. Batsali, A.K., et al., *Differential expression of cell cycle and WNT pathway-related genes accounts for differences in the growth and differentiation potential of Wharton's jelly and bone marrow-derived mesenchymal stem cells.* Stem Cell Res Ther, 2017. **8**(1): p. 102.
140. Drosse, I., et al., *Tissue engineering for bone defect healing: an update on a multi-component approach.* Injury, 2008. **39 Suppl 2**: p. S9-20.
141. Stevens, M.M., *Biomaterials for bone tissue engineering.* Materials Today, 2008. **11**(5): p. 18-25.
142. He, Y., et al., *Osteogenic induction of bone marrow mesenchymal cells on electrospun polycaprolactone/chitosan nanofibrous membrane.* Dent Mater J, 2017. **36**(3): p. 325-332.
143. Thein-Han, W.W., et al., *Chitosan-gelatin scaffolds for tissue engineering: physico-chemical properties and biological response of buffalo embryonic stem cells and transfectant of GFP-buffalo embryonic stem cells.* Acta Biomater, 2009. **5**(9): p. 3453-66.
144. Madihally, S.V. and H.W. Matthew, *Porous chitosan scaffolds for tissue engineering.* Biomaterials, 1999. **20**(12): p. 1133-42.
145. Young, T.H., et al., *Fabrication of a bioengineered corneal endothelial cell sheet using chitosan/polycaprolactone blend membranes.* Colloids Surf B Biointerfaces, 2014. **116**: p. 403-10.
146. Prasad, T., et al., *Characterization and in vitro evaluation of electrospun chitosan/polycaprolactone blend fibrous mat for skin tissue engineering.* J Mater Sci Mater Med, 2015. **26**(1): p. 5352.

147. Chatzinikolaidou, M., et al., *Wharton's Jelly Mesenchymal Stem Cell Response on Chitosan-graft-poly (epsilon -caprolactone) Copolymer for Myocardium Tissue Engineering.* Current Pharmaceutical Design, 2014. **20**(12): p. 2030-2039.
148. Papadimitriou, L., et al., *Immunomodulatory Potential of Chitosan-graft-poly(ε-caprolactone) Copolymers toward the Polarization of Bone-Marrow-Derived Macrophages.* ACS Biomaterials Science & Engineering, 2017. **3**(7): p. 1341-1349.
149. Thibault, R.A., A.G. Mikos, and F.K. Kasper, *Scaffold/Extracellular matrix hybrid constructs for bone-tissue engineering.* Adv Healthc Mater, 2013. **2**(1): p. 13-24.
150. Bai, M.Y., et al., *The effect of active ingredient-containing chitosan/polycaprolactone nonwoven mat on wound healing: in vitro and in vivo studies.* J Biomed Mater Res A, 2014. **102**(7): p. 2324-33.
151. Wang, T.J., et al., *The phenotypic response of bovine corneal endothelial cells on chitosan/polycaprolactone blends.* Colloids Surf B Biointerfaces, 2012. **90**: p. 236-43.
152. Anselme, K., *Osteoblast adhesion on biomaterials.* Biomaterials, 2000. **21**(7): p. 667-81.
153. Ma, P.X., *Biomimetic materials for tissue engineering.* Adv Drug Deliv Rev, 2008. **60**(2): p. 184-98.
154. Huang, Y., et al., *In vitro characterization of chitosan-gelatin scaffolds for tissue engineering.* Biomaterials, 2005. **26**(36): p. 7616-27.
155. Lawrence, B.J. and S.V. Madihally, *Cell colonization in degradable 3D porous matrices.* Cell Adh Migr, 2008. **2**(1): p. 9-16.
156. Danilevicius, P., et al., *Burr-like, laser-made 3D microscaffolds for tissue spheroid encagement.* Biointerphases, 2015. **10**(2): p. 021011.
157. Skarmoutsou, A., et al., *Nanomechanical properties of hybrid coatings for bone tissue engineering.* J Mech Behav Biomed Mater, 2013. **25**: p. 48-62.
158. Liu, Y., et al., *The Properties of Chitosan-Gelatin Scaffolds by Once or Twice Vacuum Freeze-Drying Methods.* Polymer-Plastics Technology and Engineering, 2013. **52**(11): p. 1154-1159.
159. Tseng, H.J., et al., *Characterization of chitosan-gelatin scaffolds for dermal tissue engineering.* Journal of Tissue Engineering and Regenerative Medicine, 2013. **7**(1): p. 20-31.
160. Hadjicharalambous, C., et al., *Porous alumina, zirconia and alumina/zirconia for bone repair: fabrication, mechanical and in vitro biological response.* Biomed Mater, 2015. **10**(2): p. 025012.
161. Tan, J.L., et al., *Cells lying on a bed of microneedles: An approach to isolate mechanical force.* Proceedings of the National Academy of Sciences of the United States of America, 2003. **100**(4): p. 1484-1489.
162. Cuy, J.L., et al., *Adhesive protein interactions with chitosan: Consequences for valve endothelial cell growth on tissue-engineering materials.* Journal of Biomedical Materials Research Part A, 2003. **67a**(2): p. 538-547.
163. Huang, Y., M. Siewe, and S.V. Madihally, *Effect of spatial architecture on cellular colonization.* Biotechnol Bioeng, 2006. **93**(1): p. 64-75.
164. Hadjicharalambous, C., et al., *Proliferation and osteogenic response of MC3T3-E1 pre-osteoblastic cells on porous zirconia ceramics stabilized with magnesia or yttria.* J Biomed Mater Res A, 2015.
165. Dahlin, R.L., et al., *Flow perfusion co-culture of human mesenchymal stem cells and endothelial cells on biodegradable polymer scaffolds.* Ann Biomed Eng, 2014. **42**(7): p. 1381-90.

166. Kang, Y., et al., *Osteogenic and angiogenic potentials of monocultured and co-cultured human-bone-marrow-derived mesenchymal stem cells and human-umbilical-vein endothelial cells on three-dimensional porous beta-tricalcium phosphate scaffold.* Acta Biomater, 2013. **9**(1): p. 4906-15.
167. Saleh, F.A., M. Whyte, and P.G. Genever, *Effects of endothelial cells on human mesenchymal stem cell activity in a three-dimensional in vitro model.* Eur Cell Mater, 2011. **22**: p. 242-57; discussion 257.
168. Ji, J., et al., *Sphere-shaped nano-hydroxyapatite/chitosan/gelatin 3D porous scaffolds increase proliferation and osteogenic differentiation of human induced pluripotent stem cells from gingival fibroblasts.* Biomed Mater, 2015. **10**(4): p. 045005.
169. Peter, M., et al., *Preparation and characterization of chitosan–gelatin/nanohydroxyapatite composite scaffolds for tissue engineering applications.* Carbohydrate Polymers, 2010. **80**(3): p. 687-694.